BROWN BOVERI REVIEW

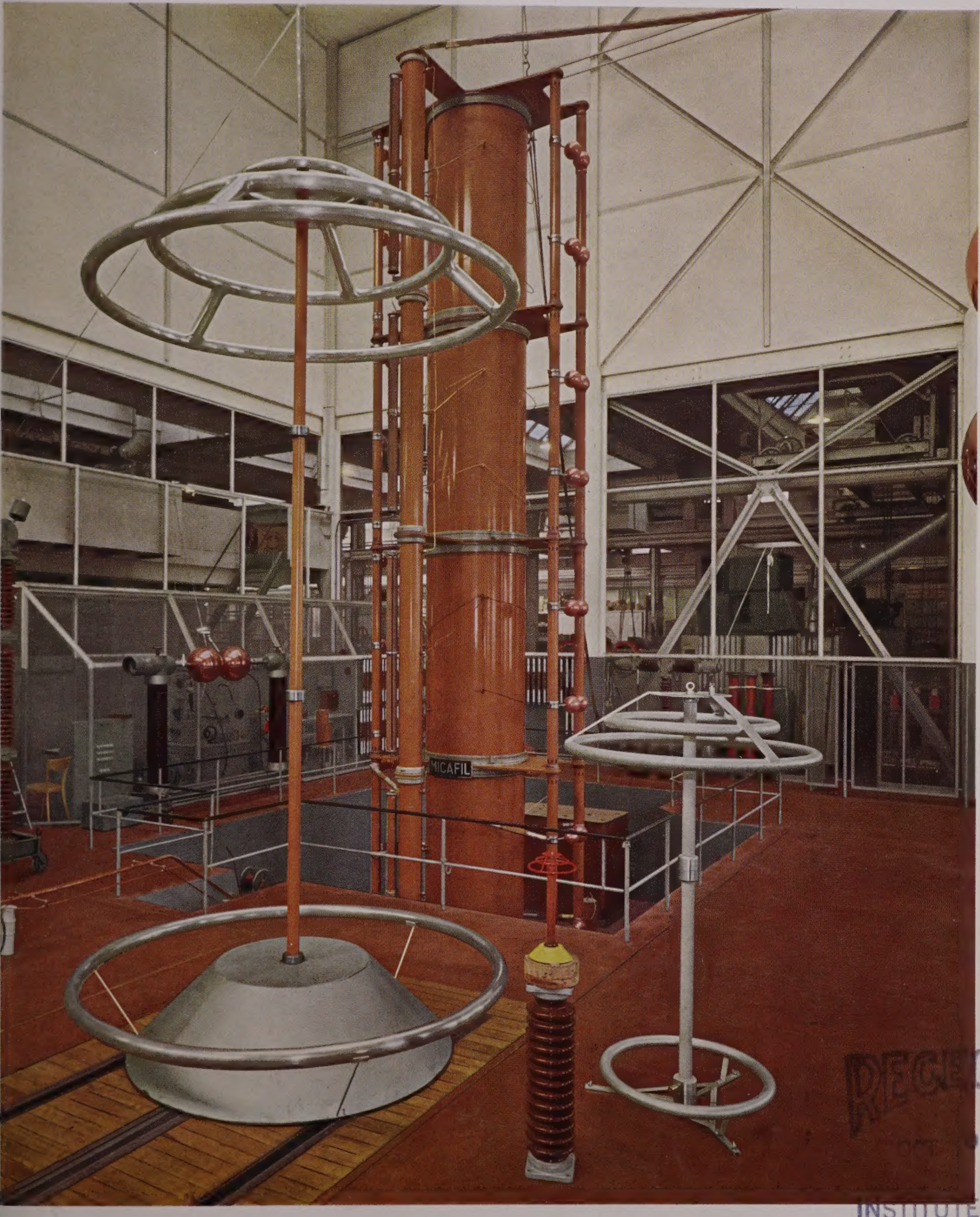
The newly developed screened ohmic voltage dividers for 2·3, 0·2 and 0·9 MV, standing in front of the 3·6-MV impulse generator

RECEIVED
OCT 1960
INSTITUTE OF THE
AERONAUTICAL SCIENCES

OVERI REV. VOL. 47 No. 4 p. 193—280 BADEN, APRIL 1960

Printed in Switzerland

THE BROWN BOVERI REVIEW

ISSUED BY BROWN, BOVERI & COMPANY, LIMITED, BADEN (SWITZERLAND)

VOL. 47 APRIL 1960 No. 4

The Brown Boveri Review appears monthly — Reproduction of articles or illustrations is permitted subject to full acknowledgement

CONTENTS:

	Page
P. Baltensperger: The Shape and Magnitude of Overvoltages when Interrupting Small Inductive and Capacitive Currents in H.V. Systems	195
M. Christoffel: The Effect of Switching Surges on Transformers, Reactors and Instrument Transformers	225
B. Gänger: Permissible Switching Overvoltages and Dielectric Tests	231
A. Ašner: Progress in the Measurement of Very High, Rapidly Changing Impulse Voltages	239
F. Deutsch: Measuring the Active Power Losses of Large Reactors	268

THE SHAPE AND MAGNITUDE OF OVERVOLTAGES WHEN INTERRUPTING SMALL INDUCTIVE AND CAPACITIVE CURRENTS IN H.V. SYSTEMS

621.316.5.015.3

The interruption of small inductive and capacitive currents gives rise to voltage surges of low to medium frequency. Though these are usually well below the insulation level for the installation, they may equal it in very rare cases. But sometimes restriking occurs, in which case the voltage amplitudes, disregarding damped transients, are of the same order of magnitude as the medium-frequency surges. The total change in voltage during a restrike is divided between the two parts of the system on either side of the breaker, in the ratio of their surge impedance or other characteristic impedance. The rate at which the voltage collapses during restriking is always less than that of a standard 1/50 impulse.

QUALITATIVELY the phenomena occurring when small inductive or capacitive currents are switched in high-voltage circuits are for the most part well known.[1] For example, it has been firmly established that restriking during the interruption of a capacitive current may possibly cause the voltage to swing violently upwards. Likewise, the complicated voltage transient produced by disconnecting a transformer at no-load is also well known. This voltage increases with a medium frequency as the breaker contacts open, but collapses when a restrike takes place and, after this sequence has been repeated several times, decays at a damped medium frequency to the recovery voltage (at the service frequency). Moreover, restriking in particular and its effects on the elements of the system have not been fully investigated before. The object of the present article is to analyse qualitatively and as quantitatively as possible the shapes of the voltage wave when making or breaking small inductive and capacitive currents. It should then be possible to assess the voltage stress on the various elements of the system, above all transformers, and to determine the admissible overvoltages produced by switching, and what test voltages are necessary for the particular element to be adequately tested.

Analysis of the Voltage Wave

A. General Description of the Transient Recovery Voltage when Interrupting Single-Phase Circuits

1. Transformers at No-Load or with Inductive Load [2]

Remarks will be confined to establishing a number of important and, in some cases, new facts. Fig. 1 shows the single-pole diagram of the circuit.

---

[1] See bibliography on page 224.

[2] See [1–6, 8, 19, 20] of the bibliography.

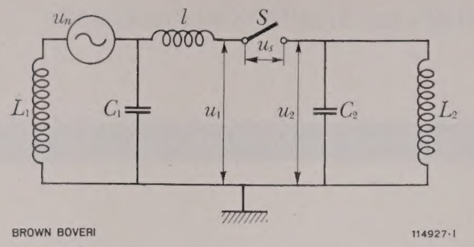

Fig. 1. – Single-pole diagram of an inductive circuit

L_1, L_2 = Inductances of the live and disconnected systems

C_1, C_2 = Capacitances of the live and disconnected systems (transformer)
For transformers insert 1/3 of the phase capacitance

l = Inductance of the line between live side and transformer to be disconnected

S = Circuit-breaker

u_n = Driving service-frequency voltage

u_1 = Voltage to earth of live breaker terminal

u_2 = Voltage to earth of disconnected breaker terminal

$u_s = u_1 - u_2$ = Voltage between breaker contacts

If, on interrupting the circuit, the current is chopped at the momentary value i_a, the circuits (L_1, C_1) and (L_2, C_2) oscillate independently, provided the breaker does not have a resistor in parallel with the break. If restriking does not occur in the breaker, the overvoltages to earth on either side of the breaker can be estimated as follows:

The disconnected part (L_2, C_2) contains the energy $i_a^2 \frac{L_2}{2} + u_a^2 \frac{C_2}{2}$ (for notation see Fig. 2). In the assumed undamped resonant circuit this energy has completely changed to the capacitive energy $u_{2max}^2 \frac{C_2}{2}$ by the time the maximum voltage $u_{2\,max}$ is attained. From this we can deduce the theoretical maximum overvoltage between the breaker terminal and earth. On the disconnected side it amounts to

$$u_{2\,max} = \sqrt{u_a^2 + \frac{L_2}{C_2}\, i_a^2} \tag{1}$$

Analogously, the maximum voltage between breaker terminal and earth on the live side is

$$u_{1\,max} = \sqrt{u_a^2 + \frac{L_1}{C_1}\, i_a^2} \tag{2}$$

The transient voltage on the live side decays with a damped oscillation to the service-frequency input voltage u_n; that on the disconnected side to zero. The gap between the breaker contacts experiences the difference between these two voltages. In most cases $u_{2\,max}$ is greater than $u_{1\,max}$ and it is quite sufficient to consider $u_{2\,max}$ alone, and use the approximate value

$$u_{2\,max} \sim i_a \sqrt{\frac{L_2}{C_2}} \tag{3}$$

In infinitely powerful systems, where $\sqrt{L_1/C_1}$ is very small indeed, no overvoltage is experienced on the live side in such cases, in contrast to "weak" systems in which, for example, the power is supplied by a single transformer of low rating and capacitance over a short transmission line. Numerical values of typical tests are contained in Table I, e.g. under the headings Stadsforsen and Rothenbrunnen. The shape of the three voltage waves u_1, u_2 and u_s is depicted in Fig. 2. The initial rate of change of the voltage, after the current was chopped, is

$\left(\frac{\mathrm{d}u_2}{\mathrm{d}t}\right)_{t=0} = \frac{i_a}{C_2}$, on the disconnected side and

$\left(\frac{\mathrm{d}u_1}{\mathrm{d}t}\right)_{t=0} = \frac{i_a}{C_1}$ on the live side.

Moreover it is established that the voltage across the breaker and the voltage at the transformer terminals differ by the system voltage u_n, i.e.

$$u_T = u_s \pm u_n$$

In practice the extreme values given by equations (1) and (2) are seldom attained because the gap between the opening breaker contacts limits the voltage. The result is repeated restriking. Fig. 3 shows a characteristic trace of the restriking voltage between the breaker contacts.

The voltages u_α to u_δ rising with the medium frequency, provided they were not interrupted by the restrikes $R_\alpha - R_\delta$, would decay at the same natural frequencies, or at the same frequency as the damped oscillation $u_\varkappa$. In Fig. 1 these natural frequencies are

$$f_1 = \frac{1}{2\pi\sqrt{L_1 C_1}} \qquad f_2 = \frac{1}{2\pi\sqrt{L_2 C_2}} \tag{4}$$

In h.v. systems the above frequencies f_1 and f_2 vary roughly between 200 and 5000 c/s, the frequency f_2 being, if anything, nearer the lower limit.

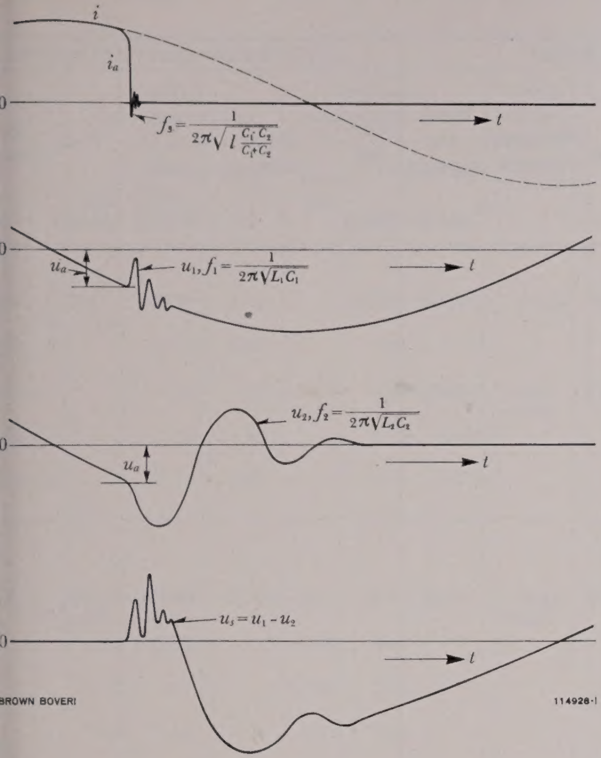

Fig. 2. – Interruption of a low inductive current without restriking. Curves of voltage and current

i = Current
i_a = Chopping current
u_1 = Voltage to earth of live side
u_2 = Voltage to earth of disconnected side
u_s = Voltage between breaker contacts
f_1, f_2, f_3 = Natural frequencies
u_a = Momentary value of service-frequency voltage when the current breaks
t = Time

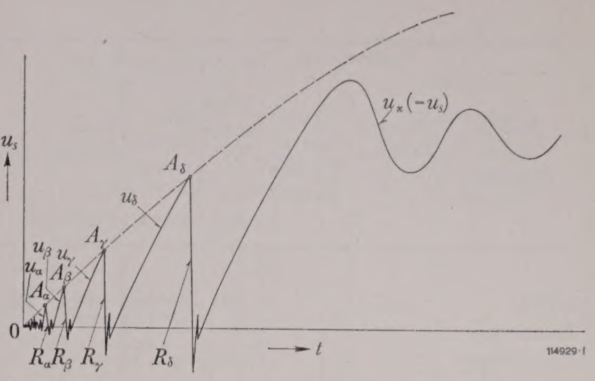

Fig. 3. – Characteristic breaker voltage when interrupting a low inductive current

u_α–u_δ = Medium-frequency voltage increases
A_α–A_δ = Voltage peaks immediately before restriking. These points determine the voltage characteristic of the breaker
R_α–R_δ = Restrikes
$u_\varkappa$ = Damped medium-frequency oscillation
u_s = Voltage between breaker contacts
t = Time

When the arc restrikes across the breaker, the capacitances C_1 and C_2 mutually discharge through lengths of line of inductance l, practically no current flowing in L_1 and L_2. Since l is frequently small, e.g. of the order of magnitude of 10^{-5} to 10^{-4} H, this discharge usually takes place in the form of a damped high-frequency oscillation like the one shown in Fig. 3. The prevailing natural frequency is then given by

$$f_3 = \frac{1}{2\pi\sqrt{l \cdot \frac{C_1 \cdot C_2}{C_1 + C_2}}} \tag{5}$$

and its value may be, for example, 100 kc/s. Further typical voltage waves are illustrated in Fig. 9, 10 and 11. Thus, when a low inductive current is interrupted, the voltage may take three possible waveforms in a wide variety of combinations, namely medium-frequency rise, restrikes and medium-frequency decay damped after a few periods. Special attention will be devoted to restriking in part 3 of this chapter.

To calculate the medium frequencies f_1 and f_2, larger values should be substituted for the transformer capacitances C_1 and C_2 than for the high-frequency oscillation f_3. Supposing C_1^* and C_2^* are the transformer capacitances per phase to earth, then, in accordance with well-known considerations, the capacitances governing the medium-frequency oscillations amount to one-third of C_1^* and C_2^*; i.e. $C_1 = C_1^*/3$, and $C_2 = C_2^*/3$. With a 100-MVA transformer, for instance, C_1^* can be about 10^{-8} F, therefore C_1 is of the order of 3×10^{-9} F. On the other hand, with a rapid rate of change of the voltage (f_3), the input capacitance of the transformer winding must be taken into account. In the above example this is of the order of 8×10^{-10} F.

Numerous measurements from testing stations and h.v. systems are available to show the magnitude of the overvoltages [1, 3–6, 19, 20]. But so far nobody has yet succeeded in establishing simple laws or

TABLE I

Overvoltages when transformers are disconnected at no-load

System data					Breaker				Transformers disconnected				
System Place (Country)	Neutral earthing [2]	With line on live side (length)	Frequency c/s (Hz)	Short-circuit power MVA	Rated voltage kV	Type	Parallel resistor	Breaking capacity MVA	Rating MVA	Shunt reactors	Impedance voltage ε in %	Ratio kV/kV	Servi volta kV
ATEL[1] Bottmingen (Switzerland)	a.s.c.		50	750/200	150	DCF		2500	23·3		10	167/ 45...56	150
						DCVF	non-linear	3500					
KglV Stadsforsen (Sweden)	solid	no	50	110	220	DCVF	non-linear	5000	60	3×9·8 kV	21·4 for 9·8/ 220 kV	9·8/ 132/220	220
		yes (72 km)											
	a.s.c.	no											
		yes (72 km)											
	solid	no								1 × 9·8 kV 10 MVA			
		yes (72 km)											
	a.s.c.	no											
		yes (72 km)											
	un-earthed	no											
		yes (72 km)											
	a.s.c.	no								Transformer alone			
		yes (72 km)											
	un-earthed	no											
		yes (72 km)											
EVS Wendlingen (Germany)	spark gap with resistor	yes (35 km)	50		110	DCVF	non-linear	2500	100	fed from regulating transformer 110 kV ±22 %		10·5/ 110/220	9 11 12
PE Lehrte (Germany)	solid	yes (176 km)	50		220	DCVF	non-linear	5000	100	1×10 kV 8 MVA		220/ 110/10	224 220

---

[1] For full names see end of Table III on page 212.

[2] A. S. C. = arc suppression coil.

tions	Overvoltages						Body responsible for measurement	Graphical representation of overvoltage factor min. arith. mean max. prim. sec. live side	Circuit *S* = Test breaker *K* = Shunt reactor *G* = Generator *T* = Transformer
	Mean overvoltage factor			Maximum overvoltage factor					
uence	Live side	Transformer		Live side	Transformer				
		prim.	sec.		prim.	sec.			
-∞–0		2·00	2·10		2·90	2·95	FKH[1]	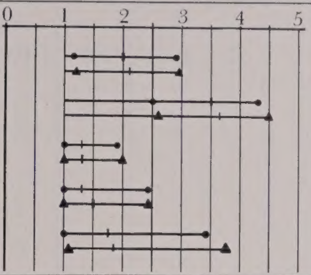	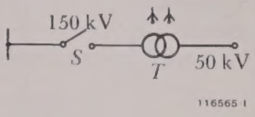
0·3 s–0		3·50	3·65		4·30	4·50			
-∞–0		1·30	1·30		1·90	2·00			
-5 s–0		1·30	1·50		2·43	2·44			
0·3 s–0		1·75	1·85		3·42	3·75			
-∞–0	1·40	1·60		1·70	2·00		EdF	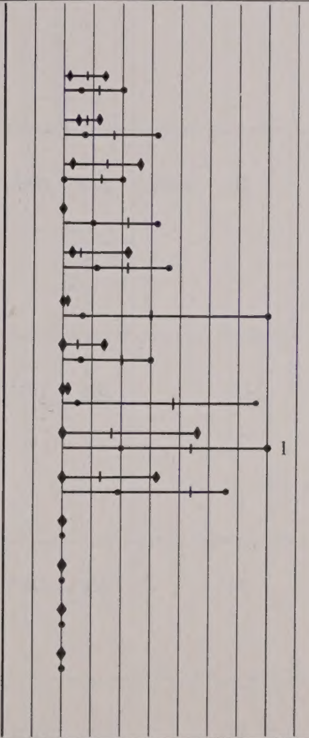	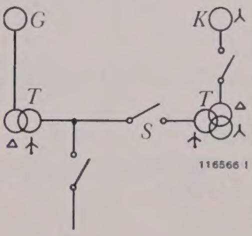
	1·40	1·85		1·60	2·60				
	1·75	1·65		2·30	2·00				
	1·00	2·10		1·00	2·60				
	1·30	2·10		2·10	2·80				
	1·05	2·50		1·05	4·50				
	1·25	2·00		1·70	2·50				
	1·05	2·90		1·05	4·30				
	1·85	3·20		3·30	4·50				
	1·65	3·20		2·60	3·80				
	1·00	1·00		1·00	1·00				
	1·00	1·00		1·00	1·00				
	1·00	1·00		1·00	1·00				
	1·00	1·00		1·00	1·00				
-∞–0		1·25	1·25		1·70	1·55	StGH	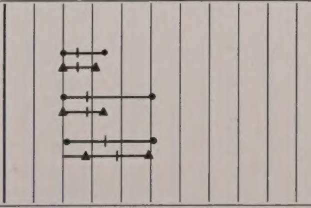	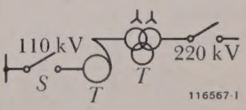
		1·42	1·42		2·51	1·68			
		1·73	1·94		2·57	2·47			
-∞–0	1·00	1·40		1·10	1·90		StGH	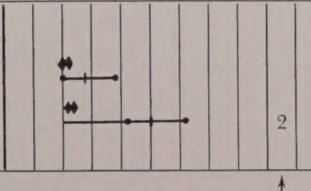	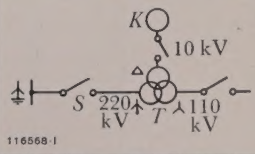
	1·1	2·5		1·2	3·1				

ures in the arrowed column indicate sparkover once or twice by lightning arresters.

Overvoltages when transformers are disconnected at no-load

System data					Breaker				Transformers disconnected				
System Place (Country)	Neutral earthing [2]	With line on live side (length)	Frequency c/s (Hz)	Short-circuit power MVA	Rated voltage kV	Type	Parallel resistor	Breaking capacity MVA	Rating MVA	Shunt reactors	Impedance voltage ε in %	Ratio kV/kV	Serv volt k
RWE[1] Rommerskirchen (Germany)	solid		50	2000	220	DHVF	non-linear	8000	660			220/ 380/30	24
										1×30 kV 50 MVA			24
										2×30 kV 50 MVA			23
										3×30 kV 50 MVA			23
										3×30 kV 50 MVA			24
										+340 km line with transf. at far end			23
RWE Hoheneck (Germany)	solid		50	4000	220	DHVF	non-linear	8000	660			220/ 380/30	23
										1×30 kV 50 MVA			23
										2×30 kV 50 MVA			23
KglV Harspranget (Sweden)	solid		50		380	DCVF	non-linear	8000	3× 115			16 / $\frac{370}{\sqrt{3}}$	43
										1×16 kV 40 MVA			40
										2×16 kV 40 MVA			39
BW Aschaffenburg (Germany)	solid un-earthed		50		220	DCVF	non-linear	6000	100		11·7	220/ 110/20	24
KZ Rothenbrunnen (Switzerland)	solid		50		220	DCVF	non-linear	5000	125	with cables		220/ 150/14	25
													19
													22
										without cables			19
													25
													22
					150	DCVF	non-linear	4500		with cables			14
													14

[1] For full names see end of Table III on page 212.

[2] A.S.C. = arc suppression coil.

ions	Overvoltages						Body respon- sible for measure- ment	Graphical representation of overvoltage factor min. arith. mean max. prim. ●——+——● sec. ▲——+——▲ live side ♦——+——♦	Circuit *S* = Test breaker *K* = Shunt reactor *G* = Generator *T* = Transformer
	Mean overvoltage factor			Maximum overvoltage factor					
ence	Live side	Transformer		Live side	Transformer				
		prim.	sec.		prim.	sec.			
∞–0		1·0	1·0		1·0	1·0	StGH	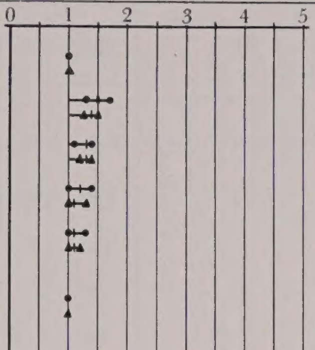	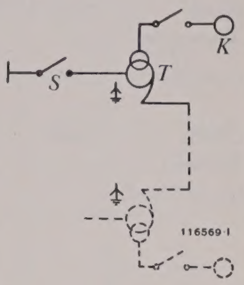
		1·5	1·4		1·7	1·5			
		1·3	1·3		1·4	1·4			
		1·2	1·1		1·4	1·3			
		1·1	1·1		1·3	1·2			
		1·0	1·0		1·0	1·0			
∞–0		1·0	1·0		1·0	1·0	StGH	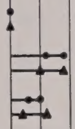	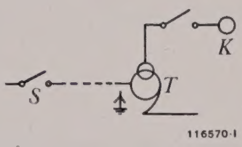
		—	—		1·9	1·9			
		—	—		1·5	1·6			
∞–0	1·10	1·37		1·10	1·70		KglV	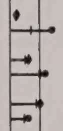	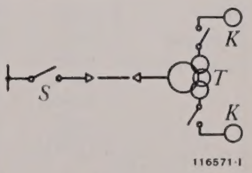
	1·28	1·50		1·30	1·60				
	1·45	1·23		1·50	1·30				
∞–0	1·07	1·47	—	1·3	2·1	—	StGH	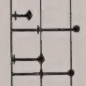	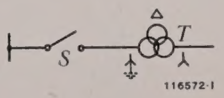
	1·03	1·50	—	1·5	2·0	—			
∞–0	1·0	1·22	1·22	1·0	1·5	1·5	FKH	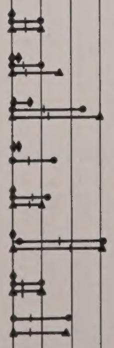	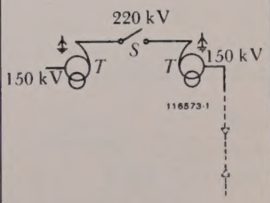
	1·0	1·18	1·24	1·1	1·5	1·8			
1s–0	1·03	1·53	1·62	1·3	2·20	2·5			
∞–0	1·01	1·28	—	1·1	1·7	—			
	1·0	1·33	1·28	1·0	1·6	1·5			
1s–0	1·0	1·80	1·98	1·0	2·54	2·52			
∞–0	1·0	1·17	1·16	1·0	1·5	1·5			
1s–0	—	1·30	1·28	—	1·95	1·9			

Overvoltages when transformers are disconnected at no-load

System data					Breaker				Transformers disconnected				
System Place (Country)	Neutral earthing [2]	With line on live side (length)	Frequency c/s (Hz)	Short-circuit power MVA	Rated voltage kV	Type	Parallel resistor	Breaking capacity MVA	Rating MVA	Shunt reactors	Impedance voltage ε in %	Ratio kV/kV	Servi voltag kV
PE[1] Bierde (Germany)	unearthed	yes (107 km)	50		110	DCVF	non-linear	4000	100			10/ 110/220	110
										1 × 10 kV 8 MVA			105
GBBM Mettlen (Switzerland)	solid		50		220	DCVF	non-linear	5000	100			150/220	244
													248
													247
													244
													191
													258
													189
													255
SBB Vernayaz (Switzerland)	single-phase, mid-point earthed with 13200 Ω		$16^2/_3$		150	DC(V)F	non-linear	1500	13·8			15/ 66/132	127
										third reactor with generator 3000 kW cos φ = 0·8			131
							without resistor			third reactor at no-load			126
					80	DC(V)F	non-linear	750					66
							without resistor						65
							non-linear			third reactor with generator 3000 kW cos φ = 0·8			63
EdF Fontenay (France)	single-pole test		50		250	DCSF	non-linear	5000	23	third reactor loaded with auto-transf.		10·5/ $\frac{96}{\sqrt{3}}/\frac{231}{\sqrt{3}}$	130
	one side solidly earthed												

---

[1] For full names see end of Table III on p. 212.

[2] A.S.C. = arc suppression coil.

tions	Overvoltages						Body responsible for measurement	Graphical representation of overvoltage factor 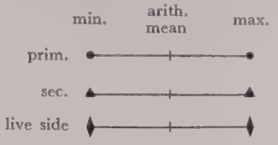	Circuit *S* = Test breaker *K* = Shunt reactor *G* = Generator *T* = Transformer
	Mean overvoltage factor			Maximum overvoltage factor					
uence	Live side	Transformer		Live side	Transformer				
		prim.	sec.		prim.	sec.			
∞–0	1·1	1·6	—	1·5	2·1	—	StGH	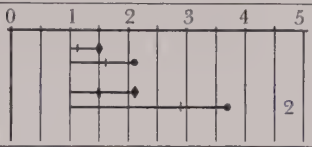	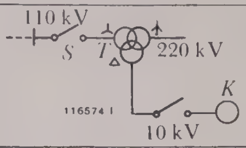
	1·5	2·9	—	2·1	3·7	—			
∞–0	1·0	1·08	1·05	1·0	1·3	1·4	FKH	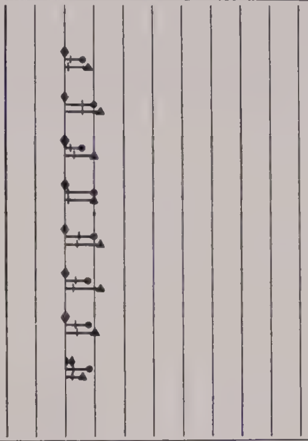	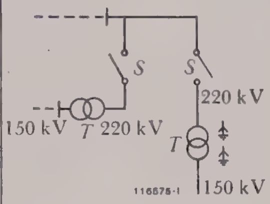 S S 220 kV 150 kV T 220 kV T 116575·I 150 kV
	1·0	1·29	1·29	1·0	1·5	1·6			
	1·0	1·09	1·15	1·0	1·3	1·5			
.1s–0	1·0	1·05	1·04	1·0	1·5	1·5			
∞ 0	1·0	1·23	1·20	1·0	1·5	1·6			
	1·0	1·18	1·14	1·0	1·4	1·6			
	1·0	1·17	1·19	1·0	1·4	1·5			
	1·01	1·14	1·11	1·1	1·4	1·3			
∞–0		2·17	2·24		3·1	3·0	BB	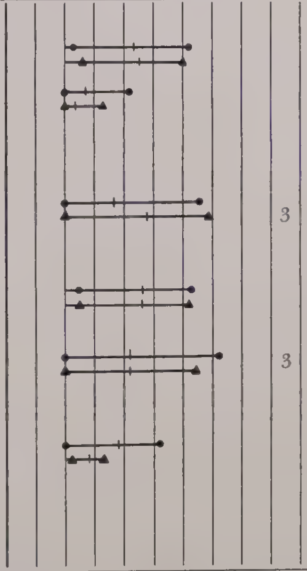	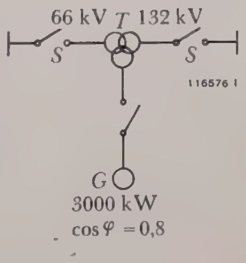 66 kV T 132 kV S S 116576 I G 3000 kW cos φ = 0,8
		1·33	1·18		2·1	1·64			
		1·84	2·4		3·28	3·45			
		2·32	2·31		3·15	3·1			
		2·1	2·1		3·6	3·23			
		1·9	1·4		2·6	1·63			
∞ 0		1·22	1·13		1·25	1·2	EdF	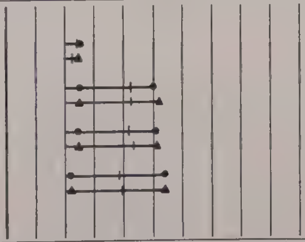	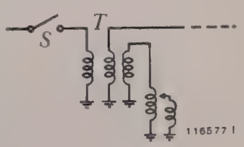
		2·12	2·14		2·5	2·6			
		2·11	2·17		2·55	2·55			
		1·93	1·99		2·70	2·70			

ures in the arrowed column indicate sparkover once or twice by lightning arresters.

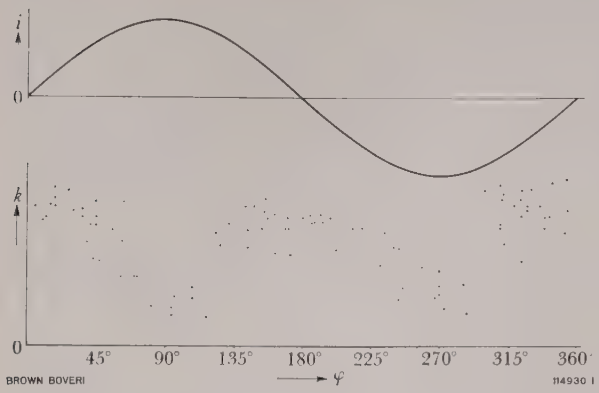

Fig. 4. – Measured overvoltages as a function of the moment of contact separation relative to the phase angle of the current

Interruption of 14 A (purely inductive) at 8 kV, by an airblast circuit-breaker

φ = Phase angle of service-frequency current at moment of contact separation

k = Maximum overvoltage factor per interruption (each point represents one measurement)

i = Service-frequency current

even accurate data for calculation, from which the overvoltage could be reliably predicted. One certain fact is that the overvoltages are on the one hand limited by the electric strength of the break (voltage characteristic) and, on the other, that on the live side they cannot be higher than given by formula (2), or on the disconnected side higher than given by formula (1), i.e. they are limited by the system. Nevertheless, the many practical measurements indicate that the overvoltages are in most cases insignificant. Roughly 90% of all overvoltage factors are below 2·5. Table I shows the results of numerous tests performed in power systems with Brown Boveri airblast circuit-breakers. Factors of 3 or more are extremely rare, either because no higher values were possible due to system parameters, i.e. because, for example, $i_a\sqrt{L_2/C_2}$ in equation (1) was small; or, on account of the wide diversity of the overvoltages in a particular installation, higher values only occurred exceptionally.

As a matter of fact, the *diversity of the overvoltages* and their actual magnitude could possibly be restricted still further. In Fig. 4 the surges caused by an airblast breaker are plotted in relation to the moment of contact separation relative to the phase angle of the interrupted sinusoidal current.

When separation took place at the peak of the current wave, or slightly before, the overvoltage was small. Practical evaluation of this result is, however, rather difficult because, firstly, each pole of a triple-pole breaker had to be tripped with a synchronous control unit of its own. Secondly, the current of a transformer is distorted and, for instance, when interrupted shortly after making, does not follow normal laws. Moreover, the nature of the distortion is different for every voltage step. Therefore, with a synchronous tripping device it is practically impossible to strike the most favourable moment exactly every time.

A detailed account of *current chopping* and the mathematical connection with overvoltages has already appeared elsewhere [8]. The current can be chopped in inductive, capacitive and even purely ohmic circuits. Whether chopping will take place, and the magnitude of the current at which it is chopped, depend on the system conditions and the circuit-breaker. Up to now the currents measured have had a peak value of 20 A at the most for a single chamber of an airblast breaker. With a resistance of, say, 1000 Ω in series with the breaker it has been possible to eliminate chopping and the accompanying overvoltages.

2. Lines or Cables at No-Load, and Capacitor Banks

The simplest diagrams of the circuits concerned are shown in Fig. 5.

The phenomena produced by interrupting lines or cables at no-load are very similar to those experienced when capacitor banks are disconnected. The current and voltage curves are reproduced in Fig. 6, in which ‘a’ depicts an interruption without restriking, ‘b’ with restriking, and ‘c’ without restriking but with current chopping.

With perhaps the exception of ‘c’ these phenomena are all well known. If, as in ‘c’ for instance, the current is chopped before it reaches its natural zero, the voltage on the disconnected side does not remain at the service-frequency peak value, but at a lower momentary value u_a of the driving voltage. In an infinitely powerful system, the voltage $u_n - u_a$ across the breaker is less than in the classical case. But if the supply system is not so powerful, the chopping

Fig. 5. – Single-pole circuits for line-dropping (a) and capacitor switching (b)

u_n = System voltage
u_1, u_2, u_s = Voltages as in Fig. 1
L_1, C_1 = Inductance and capacitance of supply system
S = Circuit-breaker
Z = Line or cable at no-load
C = Capacitance of capacitor
l = Inductance of line between live side and element to be disconnected

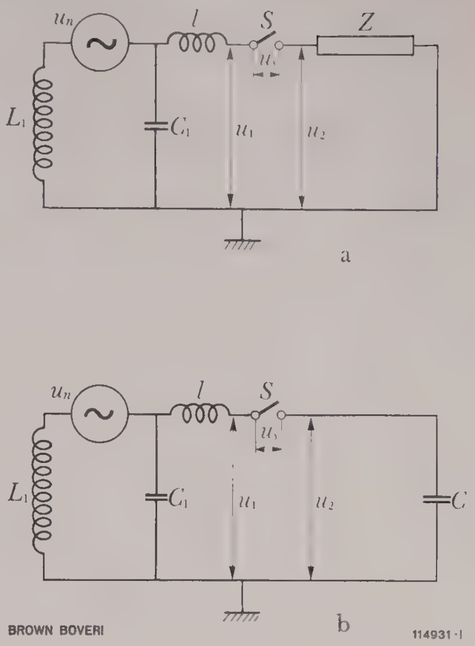

current i_a creates an oscillation with an over-voltage, whose value may theoretically be that given by (2), i.e. the voltage u_s across the breaker can rise to the value

$$u_s = u_a + u_0 + \lambda_1 \cdot \sqrt{u_a^2 + \frac{L_1}{C_1}\, i_a^2} \qquad (6)$$

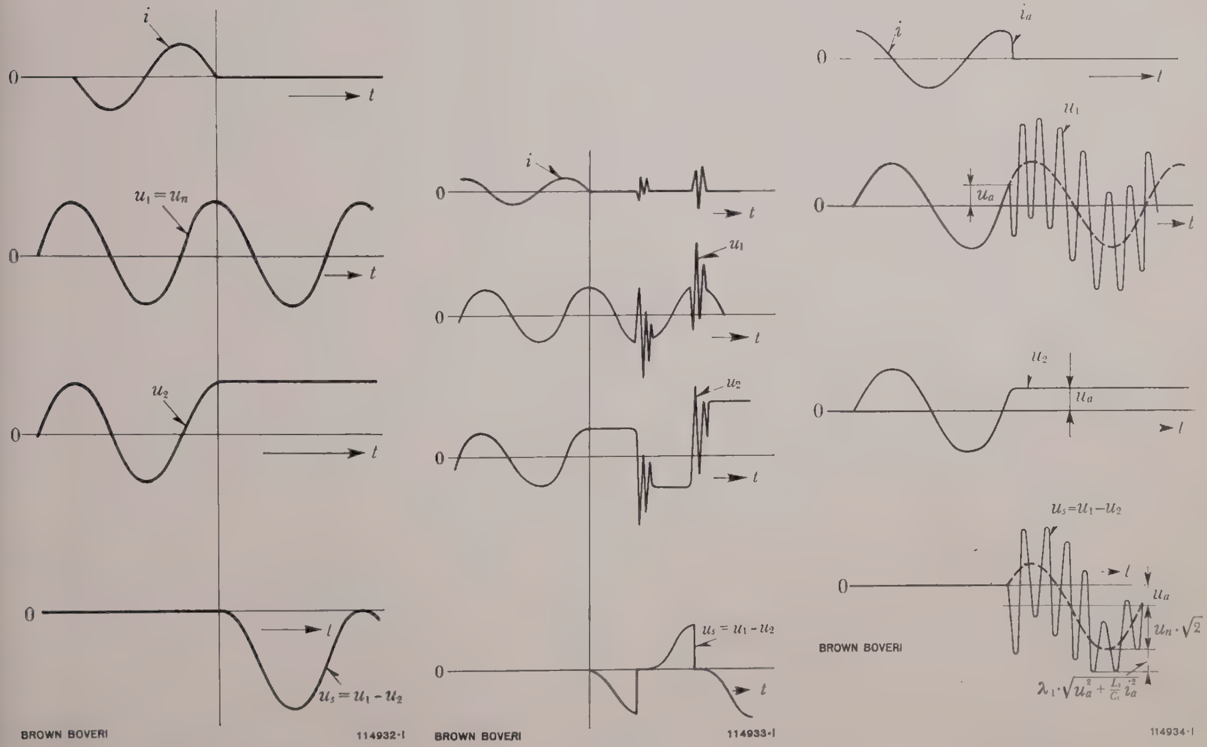

a: Without restriking b: With restriking c: With current chopping

Fig. 6. – Interruption of a capacitive current (line or cable at no-load; capacitor bank) — Curves of voltage and current

i = Current
i_a = Chopping current
u_n = System voltage = $u_0 \cos \omega t$
u_0 = Voltage to earth on live side
u_2 = Voltage to earth on disconnected side
u_s = Voltage between breaker terminals
λ_1 = Damping coefficient < 1
t = Time

For other notation, see formula (2) on page 196

TABLE II

Overvoltages during line-dropping tests in h.v. systems

System data				Breaker				Feeding transformers	Line at no-load		
System Place (Country)	Neutral earthing [2]	Frequency c/s (Hz)	Short-circuit power MVA	Rated voltage kV	Type	Parallel resistor	Breaking capacity MVA		Service voltage kV	Length km	No-load current A
BPA[1] Coulee Dam (USA)	solid	60	6800	220	DCVF	non-linear	6000		$235/\sqrt{3}$	160	62
											115
											156
KglV Stadsforsen (Sweden)	solid	50	320	220	DCVF	non-linear	5000	50 MVA 9·8/230 kV + 55 MVA 9·8/230 kV	220	72	27
	a.s.c.										36
	solid									480	190
	a.s.c.										
PE Lehrte (Germany)	solid	50		220	DCVF	non-linear	5000		225	176	65
	a.s.c.								215		
	unearthed							100 MVA 10/110/220 kV	224		
	a.s.c.										
RWE Rommers-kirchen (Germany)	solid	50	2000	380	DHVF	non-linear	12000	660 MVA auto-transformer 220/380/30 kV	425	340	337
			6000						415		
KglV Harsprånget (Sweden)	solid	50		380	DCVF	non-linear	8000	3 × 115 MVA $\frac{16/380}{\sqrt{3}}$ kV with shunt reactors 16kV...40MVA	300	476	324
									410		450
									490		524
									540		600
									300	+ inductive load	310
									410		328
									410		245
									410		124

---

[1] For full names see end of Table III on page 212.

[2] A.S.C. = arc suppression coil.

Overvoltages ean age factor Line side	Maximum overvoltage factor Live side	Line side	Body responsible for measurement	Graphical representation of overvoltage factor min. arith. mean max. line side ▲—+—▲ live side ●—+—●	Circuit *S* = Test breaker *K* = Shunt reactor *G* = Generator *T* = Transformer
1·00		1·00	—	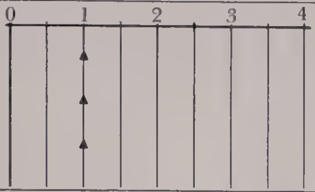	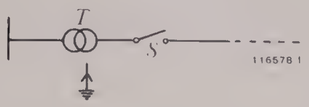
1·00		1·00			
1·00		1·00			
1·10	1·00	1·10	EdF	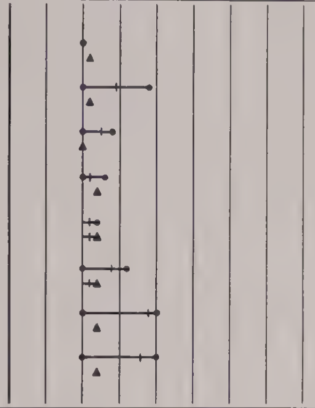	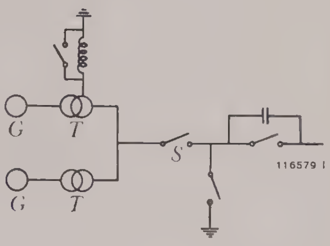
1·10	1·90	1·10			
1·00	1·40	1·00			
1·20	1·30	1·20			
1·10	1·20	1·20			
1·10	1·60	1·20			
1·20	2·00	1·20			
1·20	2·00	1·20			
1·0	1·1	1·1	StGH	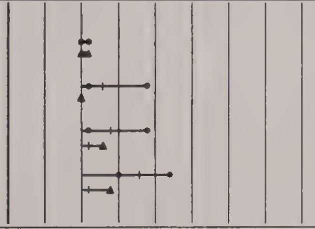	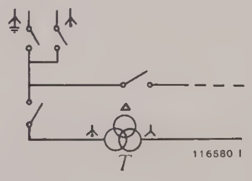
1·0	1·9	1·0			
1·1	1·9	1·3			
1·1	2·2	1·4			
1·0	1·3	1·2	StGH	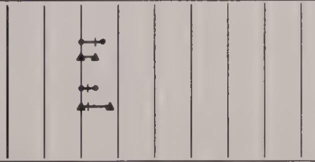	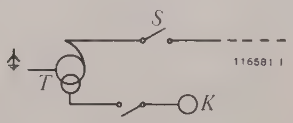
1·1	1·2	1·4			
1·20	1·10	1·20	KglV	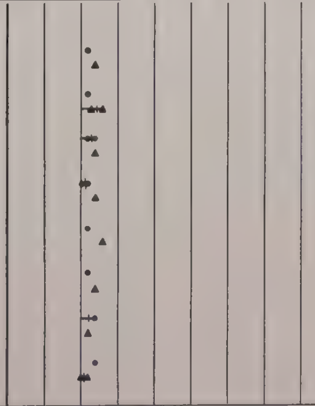	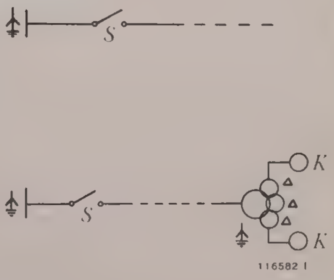
1·24	1·10	1·30			
1·20	1·20	1·20			
1·20	1·10	1·20			
1·30	1·10	1·30			
1·20	1·10	1·20			
1·10	1·20	1·10			
1·03	1·20	1·10			

TABLE II (cont.)

Overvoltages during line-dropping tests in h.v. systems

System data				Breaker					Line at no-load		
System Place (Country)	Neutral earthing [2]	Frequency c/s (Hz)	Short-circuit power MVA	Rated voltage kV	Type	Parallel resistor	Breaking capacity MVA	Feeding transformers	Service voltage kV	Length km	No-load current A
BW [1] Aschaffenburg (Germany)	solid	50		220	DCVF	non-linear	6000	100 MVA 220/110/20 kV	235	52	20·3
	unearthed										
	solid								245	132	55·7
	unearthed								232		
	solid								236	192	78
	unearthed								239		
	solid								238	250	114
	unearthed								237		
KZ Rothenbrunnen (Switzerland)	solid	50		150	DCVF	non-linear	4500	16·5 MVA 10/156·6 kV	134	90	20
									162		24
								System 150 kV	151		26
								16·5 MVA 10/156·6 kV	135	14	3·3
									164		4·1
								System 150 kV	150		4·2
PE Bierde (Germany)	a.s.c.	50		110	DCVF	non-linear	4000	2 × 100 MVA 10/110/220 kV 1 × 100 MVA 10/110/220 kV	111	107	21·9
	unearthed										
	a.s.c.										
GBBM Mettlen (Switzerland)	solid	50		220	DCVF	non-linear	5000	100 MVA 150/220 kV	219	105	65
									249		66
									227		59
MK Avegno (Switzerland)	solid	50		220	DCVF	non-linear	5000	64 MVA	220	54	20
									250		24
									218	160	57
									253		66

---

[1] For full names see end of Table III on page 212.

[2] A.S.C. = arc suppression coil.

Overvoltages			Body responsible for measurement	Graphical representation of overvoltage factor	Circuit
lean age factor	Maximum overvoltage factor			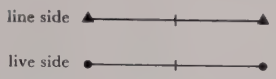	S = Test breaker K = Shunt reactor G = Generator T = Transformer
Line side	Live side	Line side			
all values less than 1·5			StGH	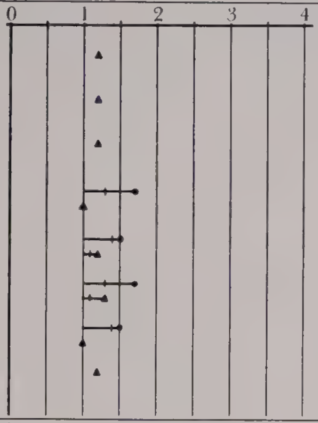	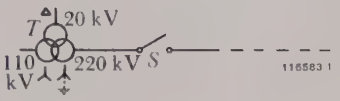
all values less than 1·5					
all values less than 1·5					
1·0	1·7	1·0			
1·1	1·5	1·2			
1·1	1·7	1·3			
1·0	1·5	1·0			
all values less than 1·5					
1·04	1·95	1·2	FKH	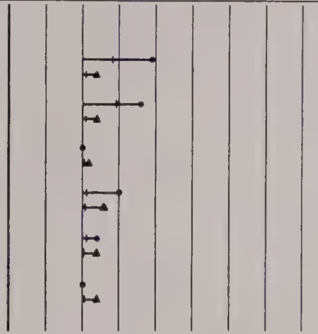	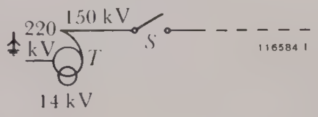
1·05	1·80	1·2			
1·01	1·0	1·1			
1·04	1·5	1·3			
1·02	1·2	1·2			
1·03	1·0	1·2			
1·0	1·0	1·0	StGH	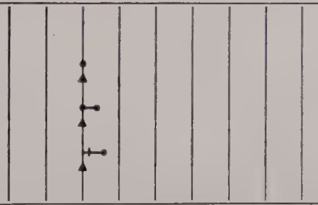	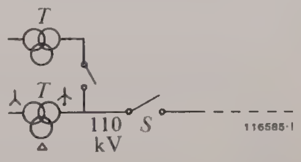
1·0	1·2	1·0			
1·0	1·3	1·0			
1·0	1·2	1·0	FKH	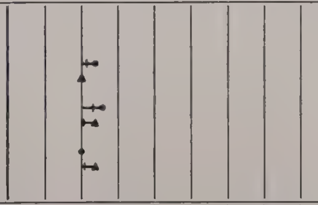	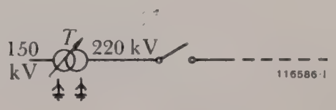
1·03	1·3	1·2			
1·04	1·0	1·2			
1·08	1·38	1·27	FKH	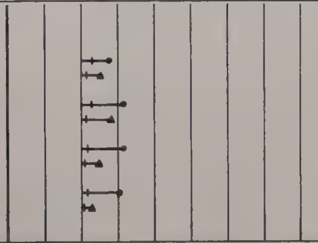	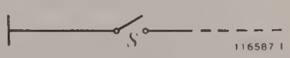
1·07	1·58	1·42			
1·05	1·58	1·24			
1·03	1·52	1·15			

TABLE II (cont.)

Overvoltages during line-dropping tests in h.v. systems

System data				Breaker				Feeding transformers	Line at no-load		
System Place (Country)	Neutral earthing [2]	Frequency c/s (Hz)	Short-circuit power MVA	Rated voltage kV	Type	Parallel resistor	Breaking capacity MVA		Service voltage kV	Length km	No-load current A
EdF [1] Fontenay (France)	single-pole test; one side solidly earthed	50		250	DCSF	non-linear	5000	23 MVA $10{\cdot}5\Big/\frac{66}{\sqrt{3}}\Big/\frac{231}{\sqrt{3}}$ kV	130	27	14
										223	84
										432	160
BEWAG Reuter (Germany)	solid unearthed	50		110	DCVF	non-linear	2500	40 MVA 10/110 kV	120	14 cable 0·257 µF/km	70
IV Petäjävesi (Finland)	unearthed	50		220	DCVF	non-linear	5000	64 MVA 10/110/220 kV	230	280	130
				110	DCVF	non-linear	2500		105		56
EdF Saint-Pierre Cognet (France)	solid	50		220	DCSF	non-linear	5000	55 MVA 10/230 kV	230	line with small purely ohmic load [3]	25
	unearthed										25
											50
EdF Fessenheim (France)	solid	50		250	DCSF	non-linear	5000	45 MVA 10·3/150/240 kV	245	line with purely ohmic load [3]	24
											47
											71
											94
	with impedance 100 Ω								247		23
											47
											70
											93
	with impedance 400 Ω								237		24
											49
	unearthed								237		24
											49
									158		18
											37
											55
											73
											155

---

[1] For full names see end of Table III on page 212. [2] A.S.C. = arc suppression coil.

[3] In this case an unloaded line was not interrupted, but a purely ohmic feeder to the system.

Overvoltages				Body responsible for measurement	Graphical representation of overvoltage factor	Circuit
Mean voltage factor		Maximum overvoltage factor			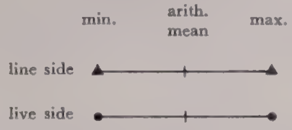	S = Test breaker K = Shunt reactor G = Generator T = Transformer P_R = Ohmic load
ve le	Line side	Live side	Line side			
	1·0	1·0	1·0	EdF	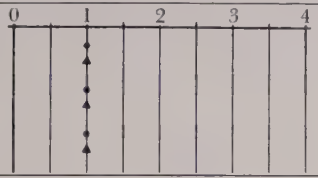	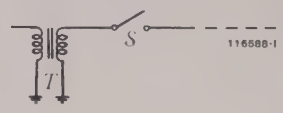
	1·0	1·0	1·0			
	1·0	1·0	1·0			
		2·0	1·1		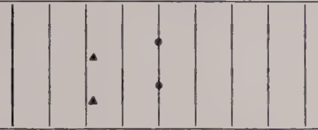	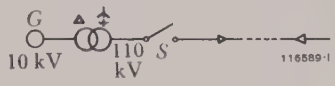
		2·0	1·1			
						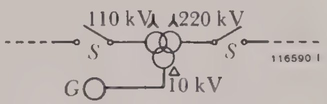
5	1·0	1·7	1·0	EdF	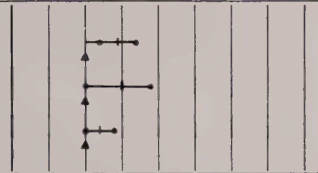	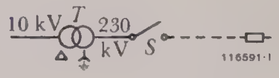
5	1·0	1·9	1·0			
2	1·0	1·4	1·0			
15		1·6		EdF	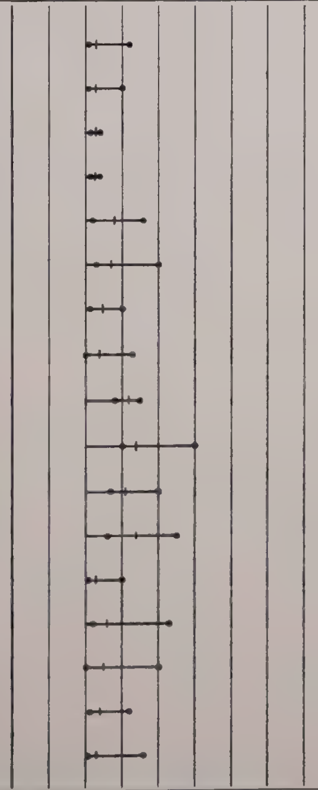	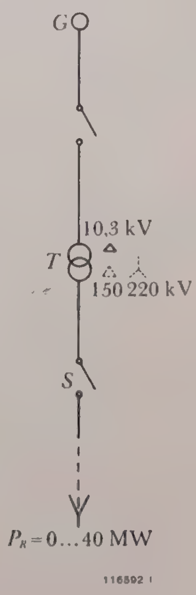 G 10,3 kV T 150 220 kV S P_R = 0…40 MW 116892 I
15		1·5				
15		1·2				
15		1·2				
4		1·8				
35		2				
25		1·5				
2		1·65				
5		1·75				
7		2·5				
55		2				
7		2·25				
15		1·5				
3		2·15				
25		2				
2		1·6				
15		1·8				

TABLE III

Voltages when disconnecting capacitor banks

System data			Breaker					Capacitor bank		
System Place (Country)	Neutral earthing	Service frequency c/s (Hz)	Rated voltage kV	Type	Parallel resistor	Breaking capacity MVA	Supply transformers or state of system	Service voltage kV	Rated power MVar	Rated current A
ATEL[1] Lachmatt (Switzerland)	a.s.c.	50	60	DCVF	non-linear	1500	Normal; capacitor bank Bottmingen not on	50	15·75	315
							Normal; capacitor bank Bottmingen switched on			
							Phase T earthed; capacitor bank Bottmingen not on			
							Phase T earthed; capacitor bank Bottmingen switched on			
ÖVG Bisamberg (Austria)	unearthed	50	110	DCVF	non-linear	2500	normal	110	10·0	91
BPA Port Angeles (USA) Grandview (USA)		60	110	DCFV	non-linear	3000		110	20·25	186

Note: In each series of tests 10 interruptions were carried out.

---

[1] Explanation of the abbreviated names in Tables I, II, III:

Switzerland: ATEL = Aare-Tessin Electricity Co.
BB = Brown Boveri, Baden
FKH = Swiss High-Voltage Research Commission
KZ = Kraftwerke Zervreila AG.
GBBM = Gesellschaft für den gemeinsamen Bau und Betrieb der Station Mettlen
MK = Maggia-Kraftwerke AG.

Germany: RWE = Rheinisch-Westfälisches Elektrizitätswerk AG.
EVS = Energieversorgung Schwaben GmbH.
PE = Preussische Elektrizitäts-AG.
StGH = Studiengesellschaft für Höchstspannungsanlagen
BW = Bayernwerk AG.
BEWAG = Berliner Elektrizitätswerke AG.

Finland: IV = Imatran Voima OY
France: EdF = Electricité de France, Direction des Etudes et Recherches
Austria: ÖVG = Österreichische Verbundgesellschaft
Sweden: KglV = Kungl. Vattenfallsstyrelsen
USA: BPA = Bonneville Power Administration

The measurements in Tables I, II and III are published with the consent of the following power companies and measuring authorities: Studiengesellschaft für Höchstspannungsanlagen (Prof. H. Baatz); Electricité de France, Direction des Etudes et Recherches (M. Y. Baron); Forschungskommission des Schweiz. Elektrotechn. Vereins (SEV) und des Verbandes Schweiz. Elektrizitätswerke (VSE) für Hochspannungsfragen (Prof. K. Berger); Brown Boveri, Baden (BB).

Overvoltages				Body responsible for measurement	Graphical representation of overvoltage factor arith. mean max. live side —+——● bank side —+——▲	Circuit B = Towards Bottmingen 8 km distant C = Capacitor bank 15·75 MVar K = Shunt reactors L = Arc suppression coil S = Test breaker T = Phase T earthed
Mean overvoltage factor		Maximum overvoltage factor				
Live side	Bank side	Live side	Bank side			
1·06	1·25	1·17	1·83	FKH	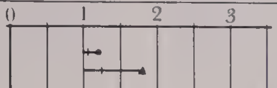	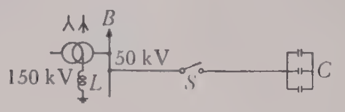
1·1	1·35	1·35	1·90			
1·6	1·85	2·18	2·33			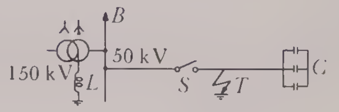
1·77	1·86	1·84	2·36			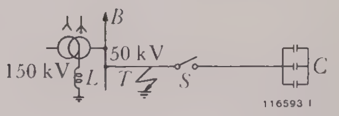
1·07	—	2·48				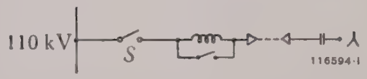

at the next or subsequent peak of the service-frequency driving voltage, whereas in the classical case, without current chopping, it reaches $2u_0$. In the above formula λ_1 is the damping coefficient of the oscillation. Comprehensive test results are also available regarding line dropping and the interruption of capacitive currents (see Tables II and III).

Less is known regarding the magnitude and rate of change of the voltage during restriking, and the resultant stresses imposed on the transformers and other parts of the system. The following section will therefore be devoted to restriking.

3. Restriking

Restriking may take place when low inductive or capacitive currents are interrupted. Up to now the fact that restriking exists had been taken more or less for granted and the occasional resultant increases in voltage studied. But less was known about the form and magnitude of the abrupt voltage change. Later this article will discuss the current and voltage waves when restriking occurs during the most important types of switching operation.

Essentially, restriking always represents a reclosure of the circuit in the breaker S (Fig. 1 and 5). A

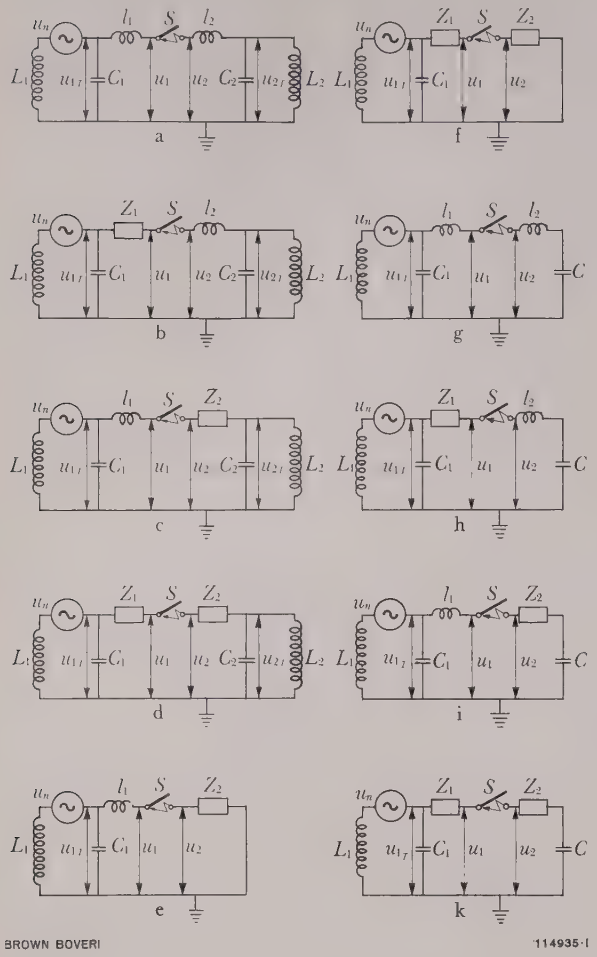

Fig. 7. – Diagrams of investigated closing actions (restrikes) in single-pole circuits

a–d = Transformers at no-load, i.e. low inductive currents
e, f = Lines and cables at no-load
g–k = Capacitor banks of capacitance C
L_1, C_1 = Inductance and capacitance of supply system
L_2, C_2 = Inductance and capacitance of unloaded or reactor-loaded system
l_1, l_2 = Inductance of the (short) lengths of line between source of power and breaker, and between breaker and disconnected element
Z_1, Z_2 = Impedances of (long) lengths of line between source of power and breaker, and between breaker and disconnected element
C = Capacitor bank
S = Circuit-breaker
u_n = System voltage
u_1 = Voltage to earth of live breaker terminal
u_{1T} = Voltage at terminals of supply transformer
u_2 = Voltage to earth of disconnected breaker terminal
u_{2T} = Voltage at terminal of transformer to be connected

number of the simplest single-pole arrangements occurring in practice have been investigated, assuming a single restrike in each. The various cases are depicted schematically in Fig. 7.

With transformers at no-load, or low inductive currents (a–d), it is assumed, for instance in ‘a’, that there is only a short length of line with the inductance l_1 between the feeding transformer L_1 and the breaker, and between the breaker and the transformer L_2 being switched there is also a short length of line with the inductance l_2. If these lines (or cables) are longer, e.g. several hundred metres or more, they are denoted by an impedance (Z_1, Z_2), as in cases ‘b’, ‘c’ and ‘d’. The cases ‘e’ and ‘f’ refer to the connection of lines or cables at no-load; cases ‘g’–‘k’ to the connection of capacitor banks.

The voltage curves of some of the forty cases of restriking calculated are tabulated in Fig. 8.

In each case the curves of the voltages u_{1T} and u_{2T} at the transformer terminals, and u_{2C} at the capacitor terminals are plotted for closure of the breaker. The initial voltage at the live terminal of the breaker immediately before closure is taken to be 1 in each case; that of the opposite terminal -1. The calculations were performed with the aid of a digital computer. All examples roughly conform to the conditions in a 150-kV system. The lines and cables were represented in some cases by a T network, in other by several T networks.

From these calculations and from theoretical considerations it is possible to make the following statements.

Amplitudes, natural frequency and rate of change of voltage during restriking

Discussion will be confined to two groups of circuits in Fig. 7, namely ‘a’ and ‘g’ on the one hand, and ‘d’, ‘f’, ‘k’ on the other.

As regards the phenomenon of restriking, *the circuits ‘a’ and ‘g’* are almost equivalent. Assuming that, before closure, the live terminal of the breaker is at a potential of $u_{1.0}$ to earth (momentary value of the supply voltage), while that of the terminal on the disconnected side is $u_{2,0}$, the effect of closing the breaker is to reverse the charge of the capacitances C_1 and C_2 through the small inductances l_1 and l_2. Hardly any current flows through the relatively large inductances L_1 and L_2. The charging process takes place in the form of a damped high-frequency oscillation having a natural frequency of

$$f_3 = \frac{1}{2\pi\sqrt{(l_1+l_2)\cdot\frac{C_1\cdot C_2}{C_1+C_2}}} \qquad (7)$$

in which C_1 and C_2, as already mentioned, are the input capacitances of the transformers in case 'a', while for case 'g' C_2 is the capacitance of the capacitor C. The changes of voltage at the transformer terminals also take place with the same natural frequency. This high-frequency oscillation of, say, 100 kc/s decays rapidly and usually has no effect on the medium-frequency breaker voltage, which commences to rise again immediately the restriking arc is extinguished (see Fig. 3). The "final potential" u_e of the two breaker terminals to earth at the end of the transient is as follows

$$u_e = \frac{C_1 u_{1,0} + C_2 u_{2,0}}{C_1 + C_2} \qquad (8)$$

which can easily be deduced from the balance of charges in the capacitances. The total amplitude of the undamped oscillation is equal to twice the initial potential difference, i.e. $2(u_{1,0}-u_{2,0})$, of which

$$2\cdot(u_{1,0}-u_e) = 2\cdot(u_{1,0}-u_{2,0})\cdot\frac{C_2}{C_1+C_2} \qquad (9)$$

is on the live side, while

$$2\cdot(u_e-u_{2,0}) = 2\cdot(u_{1,0}-u_{2,0})\cdot\frac{C_1}{C_1+C_2} \qquad (10)$$

is on the disconnected side. Hence it follows that both on the live side and on the connected or disconnected side the amplitude of the voltage change during restriking, assuming an undamped oscillation, are always less than twice the voltage required for the arc to strike across the breaker terminals. In reality the amplitudes are smaller, owing to damping. Supposing $C_1 = C_2$ and the overswing factor is 1·5, the total high-frequency change in voltage of

$$\frac{1}{2}\,1{\cdot}5\,(u_{1,0}-u_{2,0}) = 0{\cdot}75\,(u_{1,0}-u_{2,0})$$

is experienced by the terminals on both the live and disconnected side of the transformer, overswinging being included.

In the above discussion the existence of the supply voltage has been ignored. The final value u_e as given by (8) is in fact approximately attained at the end of the restriking transient. The service frequency driving voltage, however, had the momentary value $u_{1,0}$ when restriking commenced. The potential of the two breaker terminals temporarily bridged by the arc is now rapidly changed from u_e to $u_{1,0}$, the process taking effect with the relatively low natural frequency

$$f_4 = \frac{1}{2\pi\sqrt{L_1\cdot(C_1+C_2)}} \qquad (11)$$

also in the form of a damped oscillation. However, it is also possible for the arc to cease before the voltage $u_{1,0}$ is attained, in which case only the live side is charged up to $u_{1,0}$, while the disconnected side acts independently and decays according to its own rules. The service-frequency voltage changes so slowly during all the phenomena that it may be assumed to be constant and equal to $u_{1,0}$.

The circuits 'd', 'f' and 'k' in Fig. 7 can be treated in a slightly different manner, by considering the lines Z_1, Z_2 as split impedances. When the restrike takes place in the breaker S, the potential differences previously obtaining between the live and disconnected parts of the system divides in proportion to the surge impedances of the lines or cables on either side of the breaker. If the live terminal of the breaker is at the potential $u_{1,0}$, the disconnected terminal at $u_{2,0}$, and the surge impedances of the lines Z_1 and Z_2 are X_1 and X_2, the voltage on the live side jumps from $u_{1,0}$ to

$$u_{1,0} - (u_{1,0}-u_{2,0})\cdot\frac{X_1}{X_1+X_2} =$$

$$= \frac{u_{1,0}X_2 + u_{2,0}X_1}{X_1+X_2} \qquad (12)$$

Case in Fig. 7	Supply system			Line or cable				Transf. no-load				Natural frequency	
	Rated power	L_1	C_1	l_1		l_2		Rated power	L_2	C_2	C [1]	f_3	f_4
					equiv. length		equiv. length					$= \frac{1}{2\pi\sqrt{(l_1 + l_2)\,\frac{C_1 \cdot C_2}{C_1 + C_2}}}$ [2]	$= \frac{1}{2\pi\sqrt{L_1 \cdot C'}}$ [3]
	MVA	H	pF	µH	km	µH	km	MVA	H	pF	µF	appr. c/s	appr. c/s
a	100	0·0716	800	59·5	0·05 *F*	59·5	0·05 *F*	100	35·8	800	—	500 000	13 000
a	100	0·0716	800	59·5	0·05 *F*	59·5	0·05 *F*	20	119·37	800	—	500 000	13 000
a	20	0·3581	800	59·5	0·05 *F*	59·5	0·05 *F*	20	119·37	800	—	500 000	5 850
a	20	0·3581	800	18·2	0·05 *K*	1190	1 *F*	20	119	800	—	72 600	1 970
g	100	0·0716	800	59·5	0·05 *F*	59·5	0·05 *F*	—	—	—	1·42	335 000	500
g	20	0·3581	800	59·5	0·05 *F*	59·5	0·05 *F*	—	—	—	1·42	333 000	224
g	20	0·3581	800	1190	1 *F*	1190	1 *F*	—	—	—	1·42	34 000	220

[1] C = Capacitor bank, F = Line, K = Cable. [2] C_1 and C_2 include the input capacitances of the transformers, as well as the line capacitances. [3] C' is the resultant capacitance to be substituted for the medium-frequency oscillation.

Fig. 8. – Computed voltage curves during restriking (see also Table opposite)

L_1, C_1 = Inductance and capacitance of supply system
L_2, C_2 = Inductance and capacitance of unloaded or reactor-loaded transformer
l_1, l_2 = Inductance of (short) lengths of line between source of supply and breaker, and between breaker and disconnected element

Z_1, Z_2 = Impedances of (long) lengths of line between source of supply and breaker, and between breaker and disconnected element
C = Capacitor bank

u_{1T} = Voltage at terminals of supply transformer
u_{2T} = Voltage at terminals of transformer to be connected
u_{2C} = Voltage at terminals of capacitors to be connected

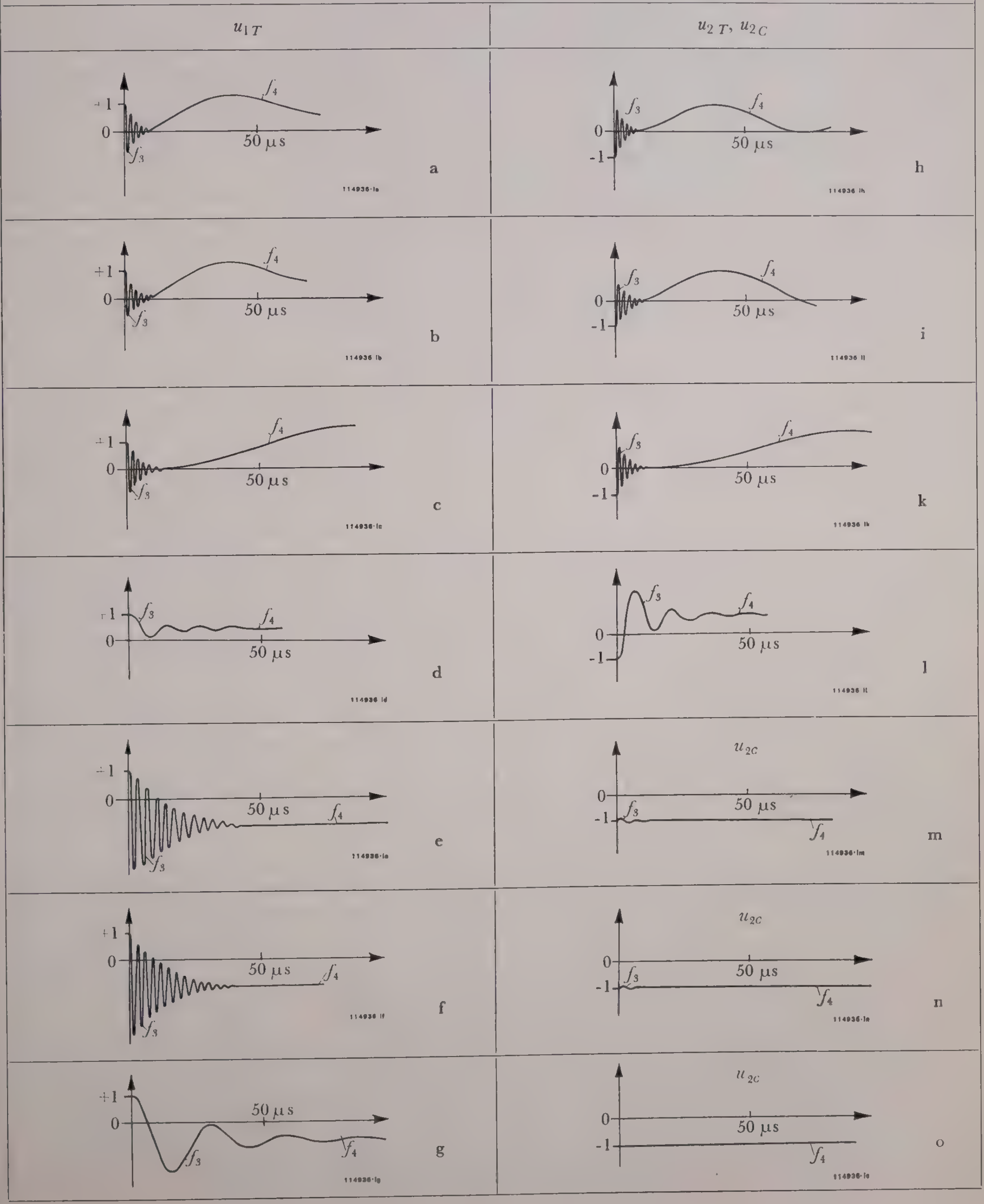

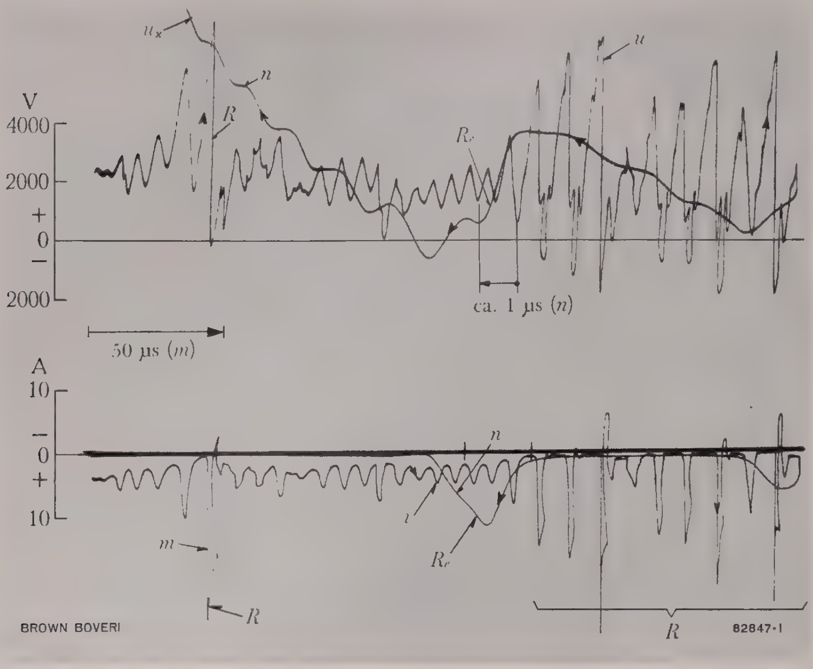

Fig. 9. – Oscillograms of breaker current i and breaker voltage u during the restriking stage when interrupting 41 A (sinusoidal, purely inductive, single-phase) at 24 kV with an airblast breaker

R = Restrikes
R_e = Last restrike
u_x = Rise of voltage after last restrike. Not all shown in the oscillogram, it rises to a peak of about 50 kV
m = Forward trace of cathode ray, linear time scale
n = Return trace of cathode ray, approx. 10–20 times faster than forwards; non-linear time scale.

The arrows on the current and voltage curves indicate the time direction.

that on the disconnected side from $u_{2,0}$ to the same value. Then, on the live side voltage surge for example, negative, with the amplitude

$$-\left(u_{1,0}-u_{2,0}\right)\cdot\frac{X_1}{X_1+X_2} \qquad (13)$$

travels along the line Z_1 to the source of supply and, say, a positive surge with the amplitude

$$\left(u_{1,0}-u_{2,0}\right)\cdot\frac{X_2}{X_1+X_2} \qquad (14)$$

along the line Z_2. When these waves arrive at the source (supply transformer) or the end of the energized line, it is possible for them to be fully or partly reflected, depending on the nature of the element encountered.

The *rate of change* of voltage at the breaker terminals is, theoretically, infinitely large. In practice, though, it is limited by the inertia of the arc when it has struck, because it can only change with a time constant of the order of 10^{-8} to 10^{-9} s. Furthermore the surges are flattened as they travel along Z_1 and Z_2, and the amplitude is damped.

A theoretical upper limit to the rate of change of the voltage surge at the transformer terminal can be estimated by considering the time constant between the input capacitance C of the transformer and the series surge impedance X of the line. Supposing $C = 8 \times 10^{-10}$ F and $X = 500\ \Omega$ (overhead line), the time constant $CX = 0{\cdot}4 \times 10^{-6}$ s which, to a rough approximation, is equivalent to the 1/50 impulse. The same consideration applied to underground cable does indeed yield a smaller time constant, but in practice there is usually a length of line between the cable end-box and the transformer terminal, and always between the cable end-box and the breaker, so that the conditions are less severe.

A large number of measurements have been taken in the Company's testing station and in power systems, in which the time taken by the voltage collapse was always a few μs at least. In no case was the voltage change more rapid than the 1/50 impulse. As a matter of fact the phenomena during restriking closely resemble atmospheric discharges.

All other cases (b, c, e, h, i) in Fig. 7 are combinations of the two extreme cases described and may be assessed accordingly.

The oscillograms in Fig. 9–11 illustrate cases in which there were a large number of restrikes. In Fig. 9 the restriking voltages only attained a relatively small amplitude (micro-restrikes). These curves apply to the disconnection of air-cored reactors carrying a sinusoidal current.

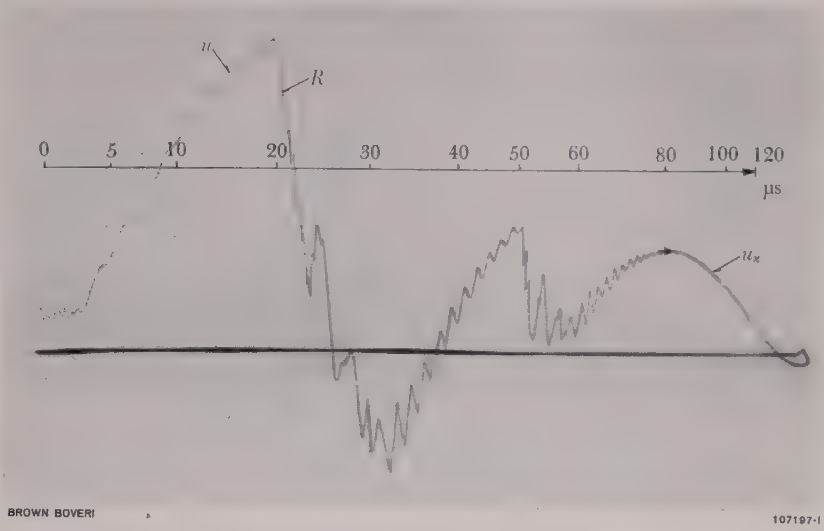

Fig. 10. – Oscillogram of the transformer voltage when an unloaded single-phase transformer, rated 5000 kVA, ratio 30/7 kV, is disconnected by an airblast breaker on the 7-kV side

Restriking and final decay of voltage (u_x) to zero. Other notation as in Fig. 9.

Fig. 10 shows the voltage when a single-phase transformer is disconnected. Each restrike lasts several µs.

Fig. 11 represents the disconnection of a three-phase transformer. In none of these oscillograms have the restrikes the idealized severe form described in the foregoing because the calculated curves in

a

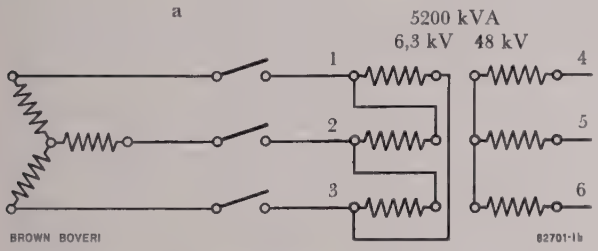

c

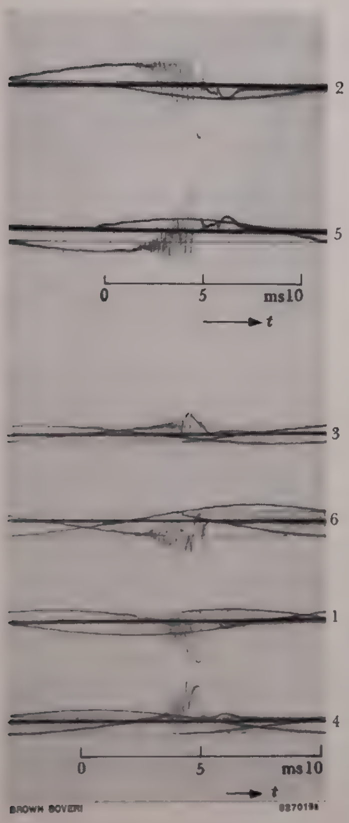

Fig. 11. – Disconnection of a three-phase transformer rated 5200 kVA, ratio 48/6·3 kV by an airblast breaker on the secondary side

a: Circuit

b: Oscillogram of the voltages to earth at the middle terminals (2·5) on the primary and secondary sides of the transformer
$t = 0$ refers to the commencement of restriking

c: As 'b', except that the voltages of all primary and secondary transformer terminals are measured
1, 2, 3 = Secondary (low-voltage) transformer terminals
4, 5, 6 = Primary (high-voltage) transformer terminals

b

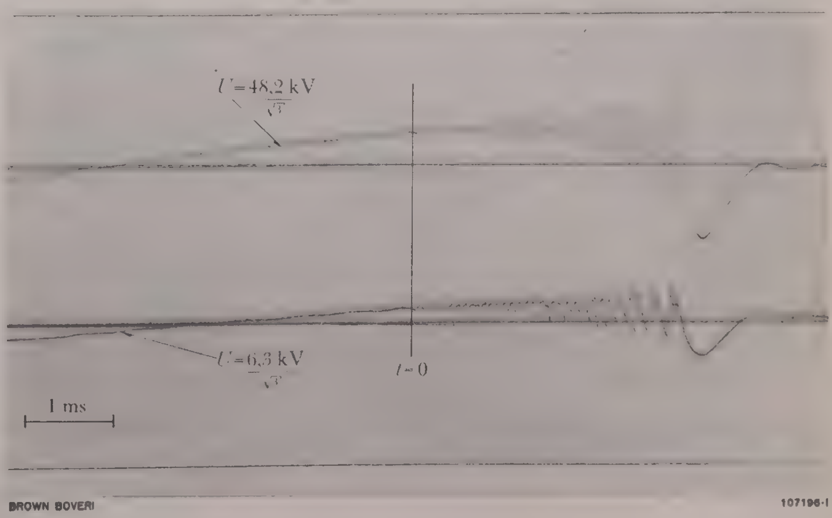

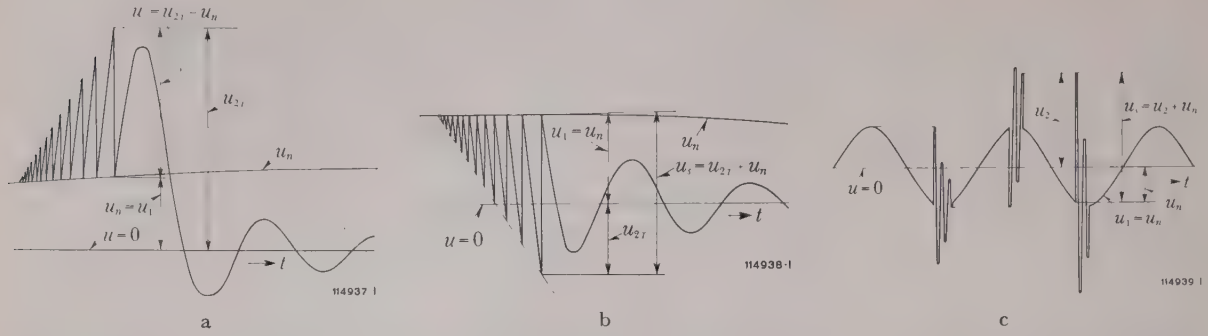

Fig. 12. – Wave-forms of overvoltages produced by the interruption of low inductive and capacitive currents. Particularly illustrating the abrupt voltage change due to restriking

u_1 = Voltage to earth of the live breaker terminal
u_{2T} = Voltage at the terminals of the transformer to be connected
u_n = System voltage
u_s = Voltage between breaker terminals
t = Time

a: *Low inductive current*

The restriking sequence takes place with increasing momentary value of the service-frequency voltage

b: *Low inductive current*

The restriking sequence takes place with decreasing momentary value of the service-frequency voltage

c: *Capacitive current*

The capacitance on the live side is assumed to be small compared with the disconnected capacitance.

Fig. 8 apply to the greatly simplified and idealized circuits in Fig. 7. The circuits actually occurring often contain additional elements, such as instrument transformers, capacitive voltage dividers, reactors, complex combinations of lines and cables, or they may have loaded or unloaded lines, etc., connected to the live side. Internal repercussions in the transformer are likewise possible. Nevertheless the present investigation (Fig. 8) may be deemed to have covered the principal features of restriking. The additional system elements referred to result in an interruption or dispersion of the restriking process, in other words they reduce its severity, both in amplitude and in the rate of change.

Magnitude of the abrupt voltage change during restriking

In Fig. 8 this magnitude was always considered on the basis of an initial unit voltage difference of $|u_2 - u_1| = 2$ between the breaker terminals. But the actual height is determined by the electrical strength of the break, or by the formulae (1) to (3), or both. In order to be able to make a more accurate statement, the problem may be considered as follows with the aid of Fig. 12a, b and c.

The starting point is the stipulation that the overvoltage must not lead to flashover between live parts and earth; therefore an upper voltage limit u_{max} to earth must be specified.

With low inductive currents we may distinguish between two different sets of conditions, as in Fig. 12a and b. In the former, restriking takes place with decreasing momentary value of the service-frequency current, i.e. with increasing momentary value of the service-frequency voltage. The voltage u_{2T} between the transformer terminal and earth is in this case equal to the sum of the absolute values of the system voltage and the breaker voltage,

$$|u_{2T}| = |u_s| + |u_n|$$

In contrast, the restriking stage in Fig. 12b occurs as the service-frequency current is increased, i.e. the momentary value of the service-frequency voltage is decreasing. In this case, owing to the reversed polarity, the voltage u_{2T} between the transformer terminal and earth is equal to the difference between the absolute values of the breaker voltage and system voltage

$$|u_{2T}| = |u_s| - |u_n|$$

Owing to the fact that, under otherwise equal conditions, a breaker may in principal have the same chopping current, regardless of whether the momentary current is increasing or decreasing, it may be assumed that the breaker voltage u_s is fundamentally equal in Fig. 12a and b. However, this implies that the overvoltage u_{2T} to earth is greater in Fig. 12a than in 12b. Now the live terminal before a restrike is always at the potential of the driving (system) voltage, even though as a result of the preceding restrike there may have been a temporary, rapidly damped high-frequency oscillation. Hence the simple change in voltage (without the high-frequency overswing) totals

$$|u_s| = |u_{2T}| - |u_n| \leqslant |u_{max}| - |u_n|$$

When interrupting a capacitive current the behaviour is quite different, as may be seen in Fig. 12c. Assuming once more that the maximum admissible voltage u_{max} to earth is specified, it follows from the simplified representation in Fig. 12c that the simple voltage change in the case of a restrike is

$$|u_2| + |u_n| \leqslant |u_{max}| + |u_n|$$

Thus, with a capacitive current, and with the same permissible overvoltage to earth, the simple voltage change caused by restriking is roughly $2u_n$ higher than with an inductive current. The breakdown voltage u_s across the breaker contacts may then be assumed to be less with an inductive current than with a capacitive. This also agrees with actual conditions because, during the process of restriking when interrupting an inductive current, the contacts are normally still opening whereas, at the second or third restrike when interrupting a capacitive current, the contacts are already fully open. The abrupt voltage increases calculated in this manner, including the high-frequency overswing are propagated in separate fractions, as already mentioned, on the live and disconnected sides in accordance with (9) and (10), or (13) and (14). When interrupting a large capacitance fed from a less powerful system, it is possible for the whole voltage change to be transferred to the feeding transformer. Since this abrupt change can be $2u_n$ higher than when an inductive current is interrupted, the capacitive interruption must be treated as the more severe. Conversely it may be inferred that, with inductive currents, higher overvoltages to earth are admissible than with capacitive, assuming an equally large voltage change on restriking is permissible in both cases.

Inductive and capacitive transformation ratio of the transformer

Fig. 11b shows the voltage curve for the high and low-voltage sides of the same transformer phase. It is noticeable that the secondary voltage does not conform exactly to the primary. This is partly due to the capacitive transformation of the restriking voltage. Whereas the transformer inductively transforms the medium-frequency voltage changes and oscillations, more rapid phenomena, such as restrikes, are at least partly transformed at the capacitive ratio. The outcome of this may be that larger (or smaller) overvoltages are experienced on the secondary side than on the primary side, i.e. the side which is disconnected. Supposing a transformer stepping down from 30 to 1 kV—i.e. with an inductive transformation ratio of 30—is fed and disconnected on the 30-kV side, restrikes are transferred with the, in most cases smaller, capacitive ratio to the 1-kV side so that the overvoltage factor on the secondary side is larger in proportion than on the primary side. In such cases a sure remedy is to use lightning arresters on the secondary side, if increasing the capacitive ratio by modifying the design of the transformer is to be avoided.

Current surges caused by restriking are usually harmless, with the exception of those produced by the interruption of capacitor banks (see also C, page 223 and [18]). The current decays with the same natural frequency f_3 as in formula (5) or (7) and its amplitudes are usually insignificant.

4. *Breakers with Parallel Resistors*

When correctly dimensioned, ohmic resistors in parallel with the breaker are able to damp the overvoltages. With *small inductive currents*, e.g. case 'a' in Fig. 7, a parallel resistor r damps effectively when

$$r < \sqrt{\frac{L_2}{C_2}} \qquad (15)$$

and, when the supply system is weak, when

$$r < \sqrt{\frac{L_1}{C_1}} \qquad (16)$$

If $\sqrt{L/C}$ in itself is small and, according to formulae (1), (2) and (3), does not permit high overvoltages, a resistance is of course superfluous. It has a balancing effect between the live side and disconnected side. If conditions (15) and (16) are fulfilled, the voltage across the breaker terminals is at the most

$$u_{max} < i_a r \tag{17}$$

where i_a is the chopping current. In this manner it is possible in principle to reduce the overvoltages indefinitely although, for economic reasons, there is a practical limit. Moreover, it has been established that restriking occurs less frequently, or not at all, when parallel resistors are used.

When *interrupting capacitive currents* the parallel resistor can ease the task of the breaker if it can discharge the capacitance sufficiently rapidly, i.e. within half a cycle of the service frequency, or thereabouts. Thus for a frequency of 50 c/s, rC must be less than 10^{-2} s.

B. Interruption of Three-Phase Circuits

1. Small Inductive Currents

When the *neutral* of the supply system and of the transformer to be disconnected are *solidly earthed*, the phenomena in individual phases during interruption are largely independent of one another. Each phase with the earth-wire forms a separate circuit which is hardly affected by the neighbouring phases. This case of solid earthing, which is being practised to an increasing extent in e.h.v. systems, can be dealt with relatively easily by the theories put forward under A, and overvoltages can be calculated approximately. But one arrangement frequently encountered in solidly earthed systems should be mentioned at this point because it does not conform to the above theory. This is when several transformers are in parallel in one power station, and the neutral of only one is solidly earthed, as is often the case. If one of the unearthed transformers is disconnected, conditions become more complicated, as will now be explained.

In systems with the neutral unearthed or resistance earthed lively changes in its potential may be anticipated in the restriking stage. Each restrike in one phase causes a sudden change in the voltage of the neutral or neutrals. But it is quite impossible to formulate any law, particularly when all three phases are in the restriking stage at once, as in Fig. 11c. Moreover it is pointed out that when interrupting low inductive currents it is clearly impossible to speak of the first, second or third phase to clear, although it often happens that the restriking stages and the definite interruption of the three phases are clearly successive. The fact that the neutral potential suddenly changes also influences subsequent restriking in the three phases. If, due to a displacement of the neutral voltage, the voltage difference in one pole increases or decreases, the next restrike in that pole may occur earlier or later, or perhaps not at all. Thus the three phases can influence one another during the restriking stages.

Only a few measurements have been made of the magnitude of the neutral voltages during such phenomena. The readings are nevertheless in every case lower than the overvoltages at the transformer terminals and may rarely be expected to exceed the service-frequency peak value of the phase voltage.

In view of the complexity of the voltage curves and the impossibility of calculating them accurately, the following points are most important:

(a) The electric strength of the gap between the opening breaker contacts restricts the overvoltages occurring there. This effects a balance between the three phases so that neither the terminals nor the neutrals of the transformer can attain infinitely high potentials.

(b) The many measurements carried out by Brown Boveri (see Table I) and the results published by numerous other authors prove that the overvoltages are harmless in most cases [4–6, 19, 20].

In the rare cases of higher overvoltages lightning arresters are a safe and reliable means of limiting the rise, if necessary; alternatively the breaker may be equipped with suitable resistors.

(c) The abrupt voltage changes caused by restriking are roughly of the same order of magnitude as the overvoltages between transformer terminals and earth, though of course the overswing must be added. But the parts of the system on either side of the breaker only experience part of the total surge, in proportion to their surge impedances, or other characteristic impedances (see A. 3).

2. *Capacitive Currents*

The voltage stresses experienced during the disconnection of capacitor banks without restriking was dealt with in an earlier publication [18]. When the system neutral is solidly connected to the neutral of the capacitor bank, the maximum breaker voltage is equal to twice the phase voltage; otherwise it is 2·5 times the phase voltage. The voltages to earth are insignificant. When disconnecting lines or cables at no-load the conditions are rather different, nevertheless when interruption is free from restriking, the overvoltages are likewise small (see also Tables II and III).

If repeated restrikes occur the voltage may possibly resonate upwards. The actual restriking process is as described in A. 3. When restriking occurs in one breaker pole and the neutrals are not solidly earthed, their potential is displaced, with the result that the two other poles are often subjected to an unduly high voltage difference and are themselves "forced" to restrike. Here too it is hardly possible to take into account all imaginable forms of three-phase interruption with restriking. If there is only *one* restrike per phase, the overvoltages are generally not very high.

Lightning arresters cannot be used for protection in this case, if on sparkover they are incapable of absorbing the high capacitive power. It is better to use non-restriking breakers or to equip the breakers with suitable parallel resistors (see formula 18).

Restrikes when switching capacitor banks may possibly cause appreciable *current surges*, especially when the amplitude of the restriking voltage is large. Extreme values, i.e. of the order of magnitude of short-circuit currents can be attained, for instance, when one of two adjacent capacitor banks is connected, or its disconnection is accompanied by restriking [18].

C. *Making Small Inductive and Capacitive Currents*

As mentioned before, the phenomena during making are fundamentally the same as during restriking, and the laws formulated in A. 3 are likewise applicable. The abrupt voltage change is however limited and is seldom higher than the phase voltage, to which increases due to overswinging must be added. Neither on making inductive nor capacitive currents are the overvoltages severe. When switching on transformers at no-load the well-known elevated and distorted service-frequency inrush surge follows the initial high-frequency transient. This is not the case with restriking because usually the breaker arc ceases at one of the few zeros of the high-frequency current wave.

D. *Conclusions Regarding Shape and Size of Overvoltages*

When low inductive currents are interrupted, voltages are produced which either rise at a medium frequency or decay with a damped oscillation and these may be discontinuously interrupted by restrikes. From experience, the medium-frequency voltages are harmless in by far the majority of cases. Instances where these voltages attain or exceed the insulation level of the installation are extremely rare. The height of the abrupt voltage change caused by restriking is of the same order as that of the medium-frequency overvoltages, but a damped high-frequency overswing must be added to it. This abrupt voltage change, however, divides itself between the live and disconnected sides in proportion to certain characteristic impedances of the system elements, or the surge impedances of the lines connected to the breaker terminals, so that the parts of the installation never experience the full voltage change of restriking. Besides, part of this voltage change is taken up by the arc voltage between the breaker contacts. The rate of change of the collapsing voltage during restriking is always less than that of a 1/50 standard impulse.

During line-dropping and generally when interrupting capacitive currents, it is possible for the voltage to increase stepwise to inadmissibly high values if several restrikes take place. In principle the restrikes themselves obey the same laws as apply to the interruption of small inductive currents.

Unduly high overvoltages resulting from inductive interruptions can be limited by lightning arresters or by resistors in parallel with the breaker. For capacitive interruptions the best remedy is to use non-restriking breakers or suitable resistors parallel to the breaker.

(KME) P. BALTENSPERGER

Bibliography

[1] K. Berger and R. Pichard: Die Berechnung der beim Abschalten leerlaufender Transformatoren, insbesondere mit Schnellschaltern, entstehenden Überspannungen. Bull. schweiz. elektrotech. Ver. 1944, Vol. 35, p. 560–70.

[2] H. Meyer: The Fundamental Problems of High-Voltage Circuit-Breakers. Brown Boveri Rev. 1950, Vol. 37, No. 4/5, p. 108–22.

[3] P. Baltensperger: Overvoltages due to the interruption of small inductive currents. CIGRE Report No. 116/1950.

[4] P. Baltensperger: Line-Dropping and Reactor-Load Interruption Tests with a Brown Boveri 220-kV Airblast Circuit-Breaker in the Stadsforsen Power Station (Sweden). Brown Boveri Rev. 1951, Vol. 38, No. 12, p. 391–410.

[5] K. Berger: Überspannungen beim Schalten leerlaufender Transformatoren und Leitungen. Bull. schweiz. elektrotech. Ver. 1953, Vol. 44, No. 9, p. 397-409.

[6] A. F. B. Young: Some researches on current chopping in high-voltage circuit-breakers. I.I.E.E. Vol. 100, Part II, No. 76, August 1953, p. 337–53.

[7] M.H. Prigent: Mécanisme de l'enclenchement et de la coupure des batteries de condensateurs raccordées en dérivation dans les réseaux à moyenne tension. Bull. Soc. franç. Elect., Vol. IV/7, 1954, No. 45, p. 513–26.

[8] P. Baltensperger and P. Schmid: Lichtbogenstrom und Überspannungen beim Abschalten kleiner induktiver Ströme in Hochspannungsnetzen. Bull. schweiz. elektrotech. Ver. 1955, Vol. 46, No. 1, p. 1–13.

[9] K. G. Darrow, V. E. Phillips, A. J. Schultz and R. B. Shores: Test circuits for capacitance switching devices. Pwr Appar. and Syst. August 1955, p. 624–35.

[10] I. B. Johnson, A. J. Schultz, N. R. Schultz and R. B. Shores: Some fundamentals of capacitance switching. Pwr Appar. and Syst. 1955, p. 727–36.

[11] AIEE Committee Report: Report on the operation of switched capacitors. Pwr Appar. and Syst. 1955, p. 1255–61.

[12] O. Loh: Strom-Spannungsspitzen und thermische Belastung der Schaltstücke beim Ein- und Zuschalten von Kondensatoren. Arch. Elektrotech. 1956, Vol. 42, No. 3, p. 164–83.

[13] W. H. Cuttino and Miles Maxwell: The natural frequency of parallel capacitor banks. Pwr Appar. & Syst. 1956, p. 662–5.

[14] J. Buter: Schalten von Blindlastkondensatoren. Elektrotech. Z. Edn A, Vol. 78, 1957, No. 1, p. 12–19.

[15] P. Fourmarier: Essais relatives aux surtensions de déclenchement des moteurs à haute tension. Bull. Soc. franç. Elect. 1957, 7e série, Vol. VII, No. 75, p. 166–80.

[16] H. Kindler: Beitrag zur Untersuchung der Vorgänge beim Abschalten leerlaufender Leitungen in Hochspannungsnetzen. Elektrotech. Z. Edn A, 1957, Vol. 78, No. 13, p. 449–57.

[17] H. Flöth: Ausgleichsvorgänge beim Parallelschalten von Kondensatoren. Elektrotech. Z. Edn A, 1957, Vol. 78, No. 16, p. 577–83.

[18] F. Schär and P. Baltensperger: Capacitor switching in the Lachmatt substation (Switzerland) of the Aare-Tessin Electricity Co. (ATEL). CIGRE Report No. 138/1958.

[19] R. Gert et al.: Contribution to the study of overvoltages. Results obtained in Czechoslovak systems. CIGRE Report No. 336/1958.

[20] E. L. White and M. P. Reece: Statistical data on switching surges in the British 132-kV Grid. CIGRE Report No. 337/1958.

[21] J. Ehlert Knudsen: Measurements of capacity-current switching-over-voltages and resulting transformer failure. Ingeniøren, International Edition, 1958, Vol. 2, No. 4, p. 112–20.

[22] G. von Geijer, G. Jancke and B. Holmgren: Choice of insulation level in networks containing long high-voltage power lines. CIGRE Report No. 414/1958.

[23] S. B. Griscom, J. W. Skooglund, A. R. Hileman: Analytical of overvoltages caused by disconnecting-switch operation. Pwr Appar. & Syst. 1958, No. 38, p. 833–7.

[24] H. L. Rorden, J. M. Dils, S. B. Griscom, J. W. Skooglund, Edward Beck: Investigations of switching surges caused by 345-kV disconnecting-switch operation. Pwr Appar. & Syst. 1958, No. 38, p. 838–44.

THE EFFECT OF SWITCHING SURGES ON TRANSFORMERS, REACTORS AND INSTRUMENT TRANSFORMERS

621.316.5.015.3

Voltage surges produced by the interruption of h.v. switchgear may possibly give rise to severe dielectric stresses in the associated elements of the system, especially those having windings (transformers, reactors, instrument transformers). This article proves that circuit-breakers conforming to contemporary standard practice cannot harm correctly dimensioned elements. Moreover, in many cases it is impossible to use lightning arresters to protect these elements against the effects of inadmissibly high switching surges because, frequently, the charges which have to be dissipated when long cables or capacitor banks are disconnected are so heavy that there is a risk of the arresters being thermally over-stressed. Operational breakdowns in transformers due to switching surges have not been experienced by this Company, but in the recent literature there was an account of a transformer failing due to excessively high overvoltage in a circuit-breaker in which restriking occurred.

System Elements and Switching Surges

AS EXPLAINED in the foregoing article,[1] overvoltages of many different forms can be produced when transformers, lines, cables and capacitor banks are disconnected at no-load. The question which immediately arises is whether these elements are endangered by the voltage surge. This point will now be investigated in detail, the remarks being confined to elements with windings, i.e. power transformers, instrument transformers and reactors. Only in such elements can internal transients be produced by external surges. For lines, cables and capacitor banks the question of their being endangered by switching overvoltages is easy to answer; it is merely necessary to ensure that the voltage surges do not exceed the permitted insulation level. Although surges of many different forms can be produced by switchgear operation, it is possible to crystallize out three distinct basic forms, as described in the foregoing article; these are medium-frequency voltage rises, high-frequency restrikes and heavily damped medium-frequency oscillations. These basic forms and their effect on windings will now be closely analysed. The stresses imposed on the system elements are computed by suitably superposing these basic forms.

Restriking

Restrikes are high-frequency phenomena. However it is known that the rate at which the voltage varies at the affected element (e.g. transformer) is never extremely high. It is feasible for the rate of rise of a full-wave impulse with a rise time of 1 μs to be attained in isolated cases. But in general the inductance of the line connecting the system element and circuit-breaker is so high that the voltage takes longer to collapse. A duration of only a few tenths of a microsecond is attained during type tests with chopped-wave impulses in the manufacturer's workshops. This is only possible as a result of the extremely short connection between the chopping spark-gap and the test object. In practice such an arrangement never exists.

In order to assess the effect of rapid changes of voltage on windings, it must first be borne in mind that, for the internal stresses on a part of a winding, the main factor is the size of the abrupt change in voltage and not how high the potential of the input terminal was before and after the change.

Fig. 1a shows a simplified equivalent circuit diagram of a winding with the capacitances C_1 and C_2 and with N_1 and N_2 the respective numbers of turns. Before the fault the incident potential to earth of the winding is assumed to be U_{2a}. This voltage is

---

[1] See page 195.

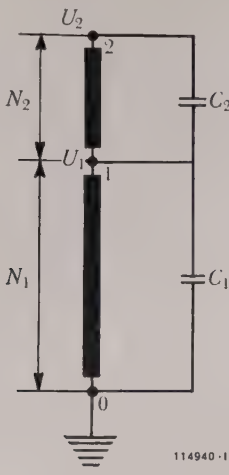

Fig. 1a. – Simplified equivalent diagram of a winding for determination of the voltage at point 1

U_1, U_2 = Potentials to earth at points 1 and 2
C_1, C_2 = Capacitances
N_1, N_2 = Numbers of turns 0–1 and 1–2

distributed linearly along the winding, as shown by curve 1 in Fig. 1b. Now if we suppose the incident potential changes momentarily to U_{2e}, the potential of the point 1 of the winding becomes

$$U_{1e} = U_{1a} + \frac{C_2}{C_1 + C_2}\,(U_{2e} - U_{2a})$$

and the voltage between points 1 and 2 works out to

$$U_{2e} - U_{1e} = (U_{2a} - U_{1a}) + \frac{C_1}{C_1 + C_2}\,(U_{2e} - U_{2a})$$

Particularly if N_2 is small compared with the total number of turns, which is quite possible if we consider the coil at the input end of a disc-coil winding, it will be immediately recognized that this voltage is determined almost entirely by the capacitances and the amplitude of the voltage change $(U_{2e} - U_{2a})$. This is clearly visible in Fig. 1b. Strictly speaking, this argument applies to infinitely rapid rates of change of voltage. But it is known that this kind of voltage variation represents the severest possible stress on elements of windings. With reduced rate of rise of the voltage surge, the amplitudes of the resultant stresses also diminish.

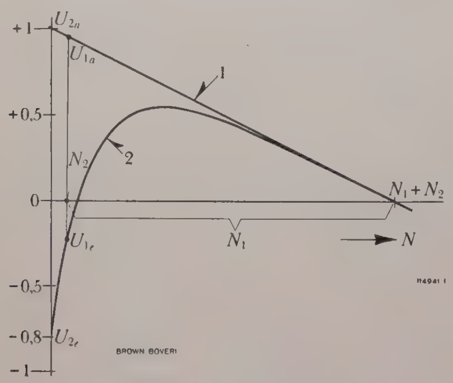

Fig. 1b. – Potential in the winding in Fig. 1a

1 = Steady-state voltage distribution with a terminal potential U_{2a}
2 = Voltage distribution after the change $(U_{2e} - U_{2a})$

A representative example of this is shown in Fig. 2. It shows the impulse voltages measured across the initial coil of a large transformer with voltage impulses having different rise times. It can be seen that the effect on the amplitude of extending the rise time can be quite pronounced. Therefore it may be concluded that, for a voltage change of given amplitude, the stress on the winding elements decreases in the following order: Impulses chopped in the tail, full-wave impulses, restrikes during switching. The amplitude of the chopped impulse amounts to 115% of the full-wave test voltage. Since, from experience, overswing by as much as 50% can occur during such tests, the amplitude of the voltage change during this test actually amounts to

$$1{\cdot}15 \times 1{\cdot}5 \times 100 = 173\%$$

In the succeeding article[2] it will be proved that it is reasonable to stipulate that a circuit-breaker must not produce an overvoltage to earth more than 72% of the full-wave impulse test voltage. Under the most unfavourable conditions, assuming restriking occurs at a voltage symmetrical to the earth potential, the maximum amplitude of the voltage change may be expected to be

$$2 \times 72 = 144\%$$

This amplitude is approximately $\left(\frac{173 - 144}{173} = 0{\cdot}17\right)$, i.e. 17% below that experienced with the chopped-wave impulse, and since the rate of rise is also much less steep, it will be seen that, under the conditions laid down for the circuit-breaker, an isolated restrike cannot possibly harm a correctly dimensioned winding.

---

[2] See page 231.

Another question which might be raised is whether a rapid succession of restrikes could not perhaps prove dangerous. All investigations carried out by Brown Boveri in this direction have contradicted this. The main reason is that it is more or less a rule that the amplitudes of restrikes occurring in rapid succession are relatively small, while restrikes of appreciable amplitude can only take place at fairly long intervals.

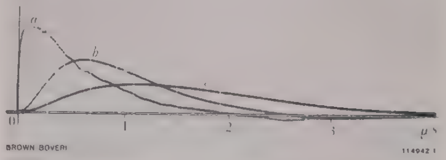

Fig. 2. – Voltage across the initial coil of a large transformer with surges having different rise times

a: Rise time 0·1 μs
b: Rise time 1 μs
c: Rise time 3 μs

Medium-Frequency Voltage Rises and Damped Oscillations

As demonstrated in the foregoing article, the frequencies experienced are within the range 200 c/s to 5 kc/s. At these modest frequencies the distribution of the voltage along the windings is linear and a severe voltage stress is only experienced between the beginning of the winding and earth. The question of danger to the insulation is covered by the succeeding article.

Now the following problem could arise: Since every winding is an element capable of resonance with numerous natural frequencies, it is feasible for the decaying medium-frequency oscillation of a switching overvoltage to cause an unexpected increase in the interior of the winding, due to resonance. But for various reasons it is not permissible to speak of a real danger.

In power transformers the minimum natural frequencies which occur are normally well above 10 kc/s. This can be illustrated by two typical examples. On disc-coil windings, which exhibit a greater inclination to oscillate than the layer windings also used in large transformers, the periodicity of the slowest oscillation equals twice the transit time through the winding. With high-voltage windings this transit time is normally of the order of magnitude of 15 to 40 μs, corresponding to frequencies of 33 to 12·5 kc/s. Fig. 3 shows the variation of the voltage with time between the mid-point of a disc-coil winding and earth on application of a voltage impulse. In this case the transit time is about 17·5 μs and the lowest natural frequency 28·5 kc/s. If there is a regulating winding in series with the main winding, it may oscillate separately. From experience, the natural frequencies in this case are from 10 to 50 kc/s. An example is given in Fig. 4. The voltage was measured across the regulating winding of a 14-MVA three-phase transformer with a ratio of 13·5/150 kV + 21% when an impulse was applied to the input terminal and the neutral was earthed. From the time scale it can be determined that the natural frequency is 17 kc/s approximately.

For reactors conditions closely resemble those with power transformers, whereas with voltage transformers lower natural frequencies are possible. But here assistance is gained from the fact that, firstly, the exciting oscillation (the switching surge) is always heavily damped and, secondly, the internal damping by the ohmic resistance of voltage transformer windings is greater than in power transformers.

Summarizing, it may be stated that the medium-frequency phenomena associated with switching surges do not give any reason to fear dangerous voltage rises in the windings. It is merely necessary

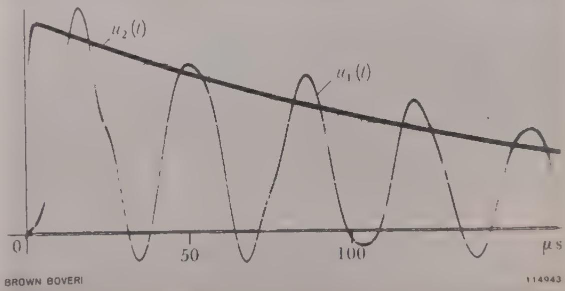

Fig. 3. – Variation of voltage with respect to time $u_1(t)$ between the mid-point and the earthed end of a disc-coil winding on application of an impulse $u_2(t)$

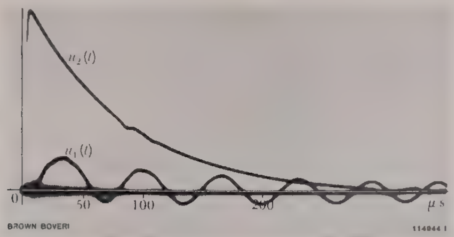

Fig. 4. – Variation of voltage with respect to time $u_1(t)$ across the regulating winding of a three-phase transformer rated 14 MVA, 13·5/150 kV + 21%, on application of an impulse $u_2(t)$

to ensure that the amplitudes of the voltages experienced between the input terminal and earth are limited to reasonable levels (see the succeeding article).

Transmission of Surges to the Secondary Side of Transformers

A transformer continues to act as a transformer during transient phenomena. Surges are therefore inductively transmitted to the secondary winding in proportion to the turns ratio. Added to this there is a capacitive component resulting from the geometry of the winding. Fig. 5 depicts the transmission of a voltage surge to the secondary of a 14-MVA three-phase transformer for 13·5/150 kV, connected delta/star. The capacitive component is insignificant. Since the change to the inductive voltage distribution takes place through a transient oscillation having the natural frequency of the secondary winding, it is quite feasible for the insulation level to be exceeded at the unloaded secondary terminals, even though this does not happen on the primary side. Owing to the admittances of the connected lines, cables, machines, etc., the surges are usually limited to harmless values in the well-known manner (see curve 3 in Fig. 5). On the other hand it is essential for the secondary side of an *unloaded transformer* to be protected by lightning arresters. These remarks apply in the first place to the transmission of impulse voltages, but it is clear at a glance that if a secondary winding is adequately protected against the effects of the transmission of such voltages, there should be little to fear from switching surges. For the high-frequency part (restrikes) the same remarks apply as for impulse voltages, whereas the medium-frequency parts are only transformed in proportion to the turns ratio. Nevertheless it is advisable to point out that, according to the definition, the secondary of the transformer is unloaded; therefore overvoltage protection directly at the secondary terminals is essential.

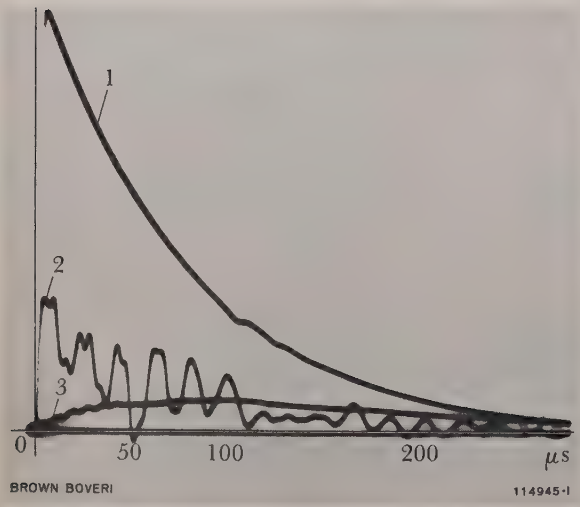

Fig. 5. – The voltage $u_2(t)$ transmitted to the secondary of a three-phase transformer rated 14 MVA, 13·5/150 kV, connected delta-star, on application of an impulse $u_1(t)$ to the 150-kV winding

Curves 1: Impulse voltage $u_1(t)$
2: $u_2(t)$ with secondary unloaded
3: $u_3(t)$ when secondary loaded with $R = 100\ \Omega$

Overvoltage Protection

For a long time it was customary, when designing the overvoltage protection in electric transmission systems, only to entrust lightning arresters with the protection against atmospheric overvoltages, stipulating that they should not respond to service-frequency voltage increases or even medium-frequency switching overvoltages. For this reason the majority of regulations covering arresters only specify minimum values of the 50-c/s sparkover voltage. Recently though, in connection with the efforts being made to lower the insulation level, there is a certain tendency to reverse this policy, in that arresters are being increasingly used to protect against overvoltages of non-atmospheric origin. Thus, VDE specifications, for instance, are now stipulating the maximum 50-c/s sparkover voltage [1].[3]

There is not the least reason why lightning arresters should not be employed to afford protection against inductive surges, such as are produced when unloaded transformers or reactors are disconnected. The explanation for this is that the energy stored in a transformer at no-load is so small that there is no risk whatsoever of the arrester connected to it being overloaded.

Capacitive surges, however, are quite a different matter. The regulations, of IEC [2] for instance, stipulate that the arresters normally used in h.v. systems and having a rated discharge current of 10 kA with an 8/20 waveshape, must be able to withstand a rectangular current wave with a peak value of 150 A, lasting 2000 µs. This corresponds to a charge dissipation of $150 \times 2000 \times 10^{-6} = 0{\cdot}3$ As. Now there is not the slightest doubt that in h.v. systems, especially those containing cable sections, much higher charges can be expected. For example, a 10 km length of 220-kV cable with a capacitance of 2 µF and charged to a peak voltage of 650 kV, corresponding to 72% of the reduced impulse voltage of 900 kV, carries a charge of $2 \times 0{\cdot}65 = 1{\cdot}3$ As.

The basic phenomenon of discharging a capacitive voltage surge may be considered with reference to Fig. 6a. The cable or line is represented by its surge impedance Z and transit time T, the arrester by a spark-gap S, and the non-linear resistor $R(i)$, and the supply side by the inductance L, the e.m.f. of the latter being of minor importance for the present considerations. A concrete example was calculated, assuming a 10 km length of 220-kV cable with a surge impedance of $Z = 45\ \Omega$, a transit time of $T = 90$ µs, and charged to 600 kV, was discharged through an arrester type HDF 175 s, with a sparkover voltage of 600 kV.

When the potential of the cable reaches the sparkover voltage of the arrester, the current begins to flow in the non-linear resistor of the arrester. Immediately following sparkover, the voltage of the arrester drops to a value determined by the voltage distribution of Z and $R(i)$. This is illustrated in Fig. 6b.

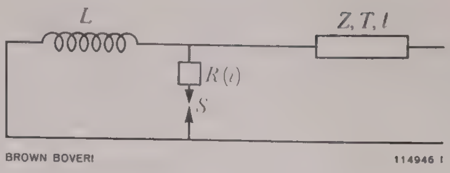

Fig. 6a. – Equivalent diagram for calculating the current in an arrester when a cable discharges

Z = Surge impedance of the cable
l = Length of cable
T = Transit time of cable (one-way)
$R(i)$ = Non-linear resistor
S = Spark-gap
L = Inductance of supply system

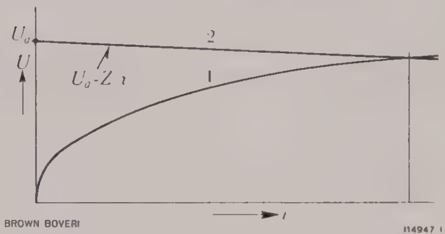

Fig. 6b. – Current-voltage characteristic of the arrester (1) and the cable (2)

U_a = Sparkover voltage of the arrester
U = Voltage
i = Current

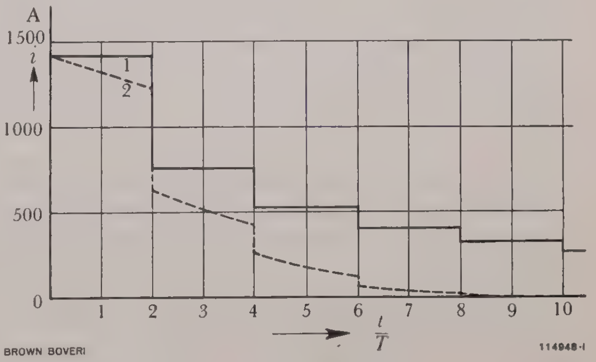

Fig. 6c. – Calculated discharge current from a 10-km length of 220-kV cable charged to 600 kV peak, discharging through an arrester type HDF 175 s

Transit time (one-way) $T = 90$ µs

1: $L = \infty$ (infinitely weak system)
2: $L = 0{\cdot}155$ H, corresponding to a three-phase short-circuit capacity of 1000 MVA at the location of the arrester

Suppose L is ∞ to begin with, which corresponds to a system with a very small short-circuit power. The discharge wave emitted by the arrester is reflected at the open end of the cable and, after twice the transit time, causes a change in the current at the arrester, as shown by Fig. 6c. A stepped current characteristic is produced, and the entire charge of 1·2 As has to be discharged by the arrester. If, however, L is not ∞, a portion of the charge flows back to the source of supply, the current unloading the arrester being greater, the smaller the value of L, because $\mathrm{d}i/\mathrm{d}t$, the rate of rise of the current, is given by e/L, where e is the supply voltage and L the inductance. Curve 2 in Fig. 6c depicts the computed current curve assuming a three-phase short-circuit capacity of 1000 MVA at the location of the arrester. It will be observed that the relief to the arrester is quite pronounced; the charge to be dissipated drops from 1·2 As to 0·36 As which, although 20% above the figure stipulated by IEC, can still be handled by the arrester.

---

[3] The figures in square brackets refer to the bibliography at the end of the article.

From this example it can be seen that arresters are in many cases also capable of limiting capacitive overvoltages. Now it must be remembered that, in the event of restriking in a breaker, several such stresses are experienced in rapid succession at intervals of 1 ms or less. Under such circumstances and with unfavourable system conditions it is no longer possible to guarantee that the arrester will not be damaged. Hence it is advisable to employ non-restriking circuit-breakers at such points.

Operational Experience

Voltage surges caused by switchgear operation are the object of considerable interest at present. The reason is simply the desire to make sure that internal surges will not lead to breakdown of the equipment, resulting in interruption of the service and necessitating repairs. This article has endeavoured to show that the system elements, particularly transformers, are not exposed to harm from switching surges. Of course, an essential prerequisite is that they are correctly dimensioned, as regards both impulse and power-frequency test voltages. These arguments are fully corroborated by practical results (see the bibliography on page 224). This Company has not had a single operational fault due to switching overvoltages. The same is true—with an isolated exception, mentioned below—for the numerous switching tests performed in power systems. The only known case of failure due to switching tests is described in the article [3], which deals with the disconnection of different lengths of cable. Provided the voltage surges produced by the breaker were below the values at present held to be reasonable, everything was in order. Only when a very long cable was interrupted and the above value considerably exceeded, did the transformer break down.

Conclusions

Power equipment whose insulation strength has been confirmed by testing with impulses and at the power frequency, need not fear switching surges, provided these do not exceed the maximum values commonly stipulated nowadays. Lightning arresters are suitable for protection against inductive voltage surges; with capacitive overvoltages the conditions should be carefully studied first. At exposed points it is preferable to employ non-restriking circuit-breakers.

(KME) M. CHRISTOFFEL

Bibliography

[1] Leitsätze für den Schutz elektrischer Anlagen gegen Überspannungen. VDE 0675/9.57.

[2] Recommendations for Lightning Arresters. IEC publication No. 99-1; 1958.

[3] J. EHLERT KNUDSEN: Measurement of Capacity-Current Switching-Overvoltages and a Resulting Transformer Failure. Ingeniøren, International Edition, 1958, Vol. 2, No. 4, p. 112–20.

PERMISSIBLE SWITCHING OVERVOLTAGES AND DIELECTRIC TESTS

621.316.5.015.3:621.317.333.6

From measurements taken inside and outside the Company the author deduces that, for all high-voltage equipment, including power and instrument transformers, the minimum insulation strength with respect to overvoltages caused by switchgear operation in service can be obtained by twice deducting 15% from the full-wave impulse test voltage, thereby taking into account the longer duration of the stress and the possibility of ageing. Provided suitable precautions are taken to keep the switching overvoltages below the limit thus given, there should be no fear of damage to properly dimensioned equipment.

THE *wave-forms of switching overvoltages* were described in the first article in this issue (page 195). Fig. 1 reproduces the main variants once more and indicates the idealized half-wave having the same peak value. Thus it will be seen that the surge when interrupting low inductive currents, for instance, can be represented by a half-wave of $^1/_{500}$ s duration. This kind of half-wave, with the same peak value, would impose an almost equally severe stress on the equipment. Analogously the surges when interrupting capacitive currents can be represented by a half-wave lasting $^1/_{100}$ s (Fig. 1 d).

Stresses Imposed on Electrical Equipment by Switching Overvoltages

The question to be studied here is the extent to which switching surges represent a severe stress or even danger to the electrical equipment, the latter covering not only transformers and switchgear, but also the insulation of the parts connected to them, i.e. busbars, feeders, instrument transformers, and so on. All these are subjected to the transient and raised by oscillation to a high potential. Even with switching surges, provided restriking does not take place, the voltage distribution in transformer windings is almost linear. The potential difference between two points on the winding is then proportional to the number of turns between them, as in steady-state operation, and the stresses imposed on the coil or layer insulation are negligible. Under these circumstances it is indeed only possible for the line end of the transformer winding (bushing, end clearance and adjacent main insulation) and such other elements as are between the transformer and the breaker to be exposed to any risk of flashover or breakdown.

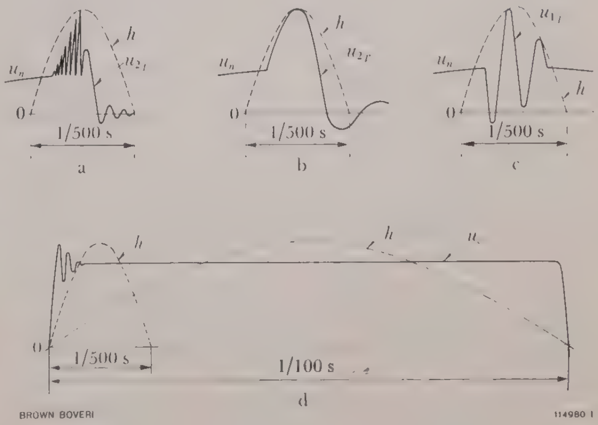

Fig. 1. – Various forms of overvoltages

Comparison with representative voltage half-waves lasting 0·002 and 0·01 s

a: Transformer voltage u_{2T}, disconnected at no-load with restriking

b: Transformer voltage u_{2T}, disconnected at no-load without restriking

c: Overvoltage u_{1T} in feeding system when an inductive or capacitive current is interrupted without restriking

d: Overvoltage u_C during and after restriking on the disconnected side of a capacitive element

h = Representing voltage half-wave
u_n = Driving (system) voltage

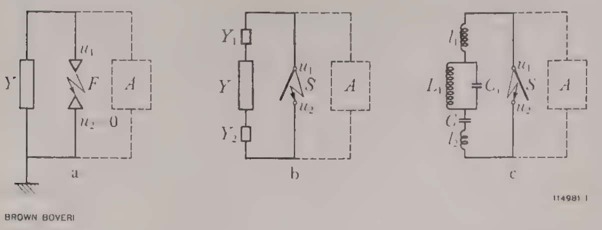

Fig. 2. – Diagrammatic comparison of circuit for testing with chopped-wave impulse and with restriking in the breaker

a: Chopped-wave test
b: General circuit diagram for restriking in the breaker
c: Diagram corresponding to case 'g' in Fig. 7, page 214

A = Source of supply
Y = Impedance being tested, or stressed
F = Spark-gap
S = Circuit-breaker
Y_1, Y_2 = Impedances between breaker terminal and Y
l_1, l_2 = Inductances of short line sections between breaker and disconnected part of system
L_1, C_1 = Inductance and capacitance of feeding system
C = Capacitor bank
u_1 = Voltage to earth of live breaker terminal
u_2 = Voltage to earth of disconnected breaker terminal

When *restriking* takes place in the breaker, however, conditions become altogether different. The phenomenon has a similar effect to chopped-wave impulses on the transformer, when the voltage, having attained a high value, is made to collapse by a special chopping spark-gap (under test conditions this usually takes place after the peak, a few microseconds after the start of the impulse). At the gap the voltage drops to zero in a period of the order of 10^{-8} s (see Fig. 2a). At the test object an oscillating transient is produced, with a frequency largely determined by the capacitance of the transformer and the inductance of the connecting line. It is usually around 1–2 Mc/s and is therefore so high that the whole of the voltage change, from the peak value of the test voltage to the opposite peak of the overswing can almost be considered as a rectangular surge as far as the phenomena in the transformer are concerned. The brief surge, of the magnitude of a total change equal to the sum of the two amplitudes, causes severe transient oscillations in the winding concerned, their shape varying with the constructional features of the transformer. Thus the potential differences between adjacent points on *layer* windings, which have a good behaviour on impulse, are quite modest. In contrast, with a homogeneous *coil* winding, the well-known distribution is obtained, with concentration of the greater part of the total voltage across the initial part of the winding. Unless special precautions are taken, the resultant stresses on the turns and coils can be very severe under such circumstances.

In the worst case a restriking breaker, according to equations (1) and (2) on page 196, produces an abrupt change of voltage at the input end of the winding, approximately equal to twice the voltage across the breaker. Compared with the chopped-wave test, the effect on the winding is somewhat less severe because, unlike the test impulse, the voltage change is not effected directly at the transformer itself, but a certain distance away—at least 10 m—and therefore the phenomenon does not strike the winding quite so suddenly (see Fig. 2 b and c). The frequency of the decay oscillation, however, is less, so consequently the duration of the overswing and the voltage stress is prolonged, and this may help to increase the stress on the winding insulation.

Test Voltages

The deciding factor is the magnitude of the overvoltage experienced. If it remains far enough below a voltage of comparable nature, at which the object was tested on completion of manufacture, to ensure that it fulfilled certain specifications, the stresses resulting from breaker interruption may be deemed harmless. On the other hand, if the overvoltage nearly attains the test figure, the question of whether the object is adequately safeguarded

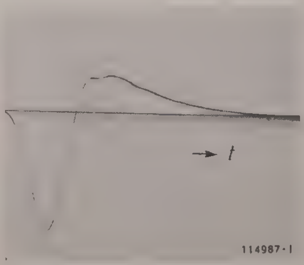

Fig. 3. – Oscillogram of the half-wave test voltage

t = Time

TABLE I

IEC test voltages for systems with reduced insulation (effectively earthed neutral)

Maximum system voltage U_{max} kV	IEC test voltages[1]		Chopped-wave impulse $1{\cdot}15\,U_{p\,1/50}$ kV	$k_1 = \frac{\sqrt{3}\,U_{p}\sim}{U_{max}}$	$k_2 = \frac{\sqrt{3}\,U_{p\,1/50}}{\sqrt{2}\,U_{max}}$
	Power-frequency $U_{p}\sim$ kV	With 1/50 impulse $U_{p\,1/50}$ kV			
123	185	450	520	2·60	4·47
145	230	550	630	2·75	4·65
170	275	650	750	2·80	4·68
245	395	900	1050	2·79	4·50
300	460	1050	1210	2·66	4·29
420	630	1425	1640	2·60	4·16

[1] For power-frequency voltage, r.m.s. values; for impulse, peak values.

against flashover or breakdown in service must be carefully investigated. As readers will know, every item of h.v. equipment has to withstand a voltage roughly equal to three times its maximum admissible sustained phase-to-neutral voltage for a period of 1 minute. In many cases a further test with a full-wave 1/50 impulse, or even with a chopped-wave impulse, is stipulated. The details of these tests are laid down by national regulations, and in many cases by IEC recommendations. The latter, for example, visualize uniform values for the one-minute power-frequency voltage and the 1/50 impulse voltage for all equipment, i.e. transformers, switchgear, insulators, bushings, cables, etc., for use at the higher service voltages (see Table I).

Another column of the same table shows the figure of 1·15 times the full-wave peak, which roughly corresponds to the increase in the flashover voltage of external insulation under the influence of surges chopped after a few microseconds. If a chopped-wave impulse test is visualized at all, this figure is often specified for the amplitude of the test shot. The last two columns of the table show the ratio of the test voltage to the maximum service voltage (phase-to-neutral). For impulse tests the factor is between 4·68 and 4·16, slightly tailing off at the higher voltages.

Voltage tests after completion of an object, before delivery to the customer, are intended to subject it to stresses of a severity not likely to be experienced again in service. It is the task of the power company to keep the maximum possible overvoltages in their system down to a certain level by taking such precautions as may be necessary, thus ensuring that, under no circumstances, are the various items of equipment likely to experience voltages whose possible frequent recurrence might lead to a breakdown. In doing so they must also make allowance for a slight reduction in the insulation capacity as time goes by, due to ageing, contamination, absorption of moisture, and other effects which are not so well known.

The task of the manufacturer is to investigate whether the conventional tests—at service frequency and with impulse—can be considered adequate simulation of all stresses likely to be encountered in service in power systems, especially those resulting from switchgear interruption.

Tests with Simulated Switching Overvoltages

A number of articles have been published on the subject of the strengths which high-voltage equipment may be expected to exhibit in the face of switching overvoltages, giving a comprehensive picture of this field. Twenty years ago Brown Boveri

TABLE II

Impulse factors referred to the 1-minute power-frequency test voltage for oil-insulated arrangements on impulse and subjected to switching overvoltages (according to [4])

Arrangement	Impulse factors with			
	Standard impulse		Switching surge (1-ms range)	
	positive	negative	positive	negative
Rod gap, 76 mm wide	1·33	1·72	≈ 1·5	1·5
Two leads 14/18 mm dia. tied together	1·44	1·45	—	1·45
Lead to parallel plate, clearance 12·5 mm	1·93	2·16	1·89	2·18
The same, but with creepage path across insulating surface instead of oil gap	1·95	1·75	1·89	1·75
Two parallel leads, spaced 50 mm apart with wooden blocks	—	1·37	—	1·5
Lead to parallel plate, clearance 300 mm	—	1·44	—	1·37
The same, but with creepage path in oil	—	1·69	—	1·53
Two parallel plates with bent edges, clearance 50 mm	2·53	2·4	1·9	1·86

had already rendered an important contribution, and have recently published an up-to-date report on such measurements. One of the very first publications in this sphere is that of Wanger and Huber [1],[1] which contains measurements of flashover voltages on different kinds of supporting insulators, suspended strings of insulators, also spark-gaps, in particular in the region between the standardized impulse test and normal power-frequency voltages. The wave-shape of the impulses were varied; in some cases a half-value time of 1000 μs was chosen, and in others a rise time of 250 μs. Still longer times were obtained by cutting out one or more half-cycles from a basic 50-c/s voltage by means of a special switching device. Depending on the nature of the insulating path either no difference was observed, or at the most a very slight reduction when the stresss was applied for 1–10 ms, compared with the standard impulse on clean insulators. Measurements taken by Bellaschi and Rademacher [2] at voltages up to a peak value of 900 kV employing a damped oscillation (free oscillation by a transformer, on the primary side of which a capacitor was discharged) applied to a suspended insulator string, a rod gap, a bushing, a 25-mm gap immersed in oil, and point-to-plane in oil, led to the result that, in the majority of cases, the electric strength with respect to simulated switching overvoltages amounted to 90–95% of the value obtained with the standard impulse. In subsequent American publications the main stress is laid on the capacity of the materials and layouts employed in the construction of transformers to withstand stresses. Tests carried out on models of the end clearance of power transformers and oil-immersed instrument transformers indicated the probability of their being able to withstand switching overvoltages at least 25% higher than the power-frequency test voltage [3]. Particularly convincing were the results of investigations carried out in the High-Voltage Laboratory of the General Electric Co. [4], due to their broad scope and the meticulous care taken. Test voltages with peak values up to 1100 kV were employed; standard impulses, surges with a slow rise (100 μs), impulses chopped before reaching the maximum due to flashover on the test object or on a special spark gap, impulses with a long tail (rectangular), 1/1·7 ms impulses, and 60-c/s voltages lasting 1 min. For a series of model arrangements which are frequently employed, Table II above summarizes the most important results. The amplitude factors given therein represent the ratio of the peak breakdown or flashover voltage on impulse, or due to switching overvoltage, and the 1-min power-frequency voltage.

---

[1] The figures in square brackets refer to the bibliography at the end of the article.

As can be seen, the breakdown voltage in the 1-ms region is roughly 1·4 times the 1-minute voltage; but in most cases the switching overvoltages which can be withstood are appreciably higher. Compared with standard impulses, the values are mostly lower.

In a joint investigation carried out by a number of high-voltage laboratories in Western Germany, switching overvoltages were simulated by a long impulse with a damped 5-kc/s oscillation superposed. At test voltages up to a peak value of 400 kV the strength values determined in this way were compared with those obtained at the power frequency and by impulse tests on simple spark-gaps, insulators and bushings, as well as with bare and covered conductors immersed in oil [5]. A recent article [6] gave an account of Brown Boveri's own investigations, using the same electrode arrangement but, instead of a 5-kc/s test voltage, a half-wave lasting 2 ms was employed; the latter was cut out of the sinusoidal wave of a 250-c/s generator and stepped up in a transformer. An oscillogram of this test voltage is reproduced in Fig. 3. The results prove that the half-wave voltage is a very good means of simulating the medium-frequency stresses caused by switching overvoltages, that even the generation of higher test voltages does not present any difficulty; also that air as an insulating medium exhibits quite a different behaviour to oil, in that the electric strength with respect to switching overvoltages when breakdown or flashover occurs in air only differ slightly from the power-frequency values. Hence for external insulation it is not permissible to allow any higher figure than that obtained with the one-minute 50-c/s test. In contrast, the strength of arrangements insulated with oil is notably higher for medium-frequency voltages; indeed, in some cases a slightly higher figure was obtained than on impulse. As a rough average, the impulse breakdown voltages obtained during the joint investigation performed on behalf of VDE are about 10% higher than those with simulated switching overvoltages.

From previously unpublished figures obtained with three typical arrangements in oil, the results may be summarized, supplementing the foregoing remarks. For these tests the following objects were used:

a. Wire sample: two lengths of flat paper-insulated wire, held parallel in the middle part and splayed at the ends, insulation 1·3 mm thick, clearance in the parallel part 5 mm (Fig. 4a).

b. Longitudinal sample: loops of the same wire as in "a", standing edgewise and 30 mm apart on a slab of transformer board (Fig. 4b).

c. Circular sample: a metal cylinder surrounded by a wrapping of paper 2·5 mm thick, acting as one electrode, and an insulated ring of flat wire opposite one rounded end of the cylinder, as the other electrode, an oil-gap of 15 mm being provided between the two.

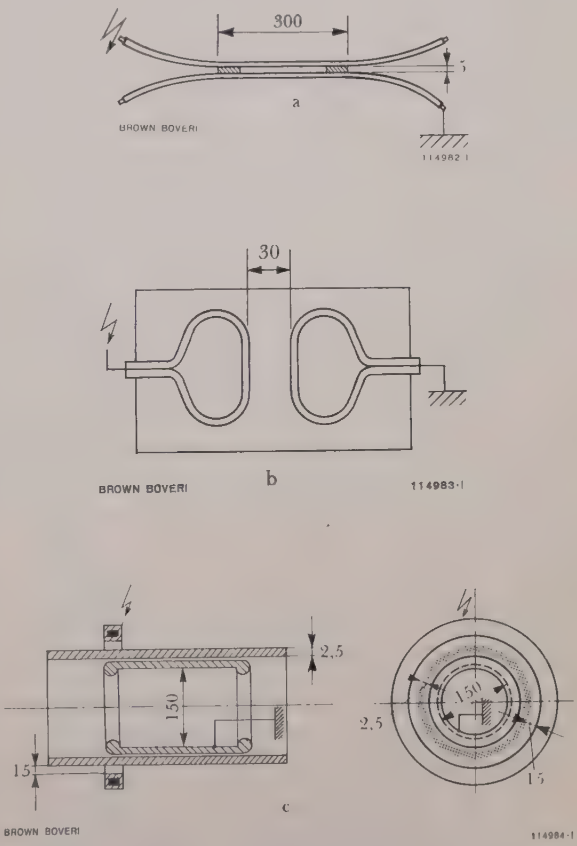

Fig. 4. – Arrangements tested

a: Wire sample
b: Longitudinal sample
c: Circular sample

TABLE III

Breakdown voltage U_B of oil-insulated arrangements on impulse and with half-wave stresses

Type of sample	Number	Test voltage	U_B kV	Average deviation σ kV	Reduction compared with 1/50 impulse %
Wire, 5 mm oil gap	30	Impulse 1/50	280	6·9	—
	47	Half-wave 250 c/s	245	9·8	12·5
Longitudinal, 30 mm	14	Impulse 1/50	628	16·7	—
	15	Half-wave 250 c/s	550	14·4	12·4
Circular	21	Impulse 1/50	470	11	—
	25	Half-wave 250 c/s	347	10	15·4

All these test objects were dried and impregnated in good-quality insulating oil, using the same procedure as for high-voltage transformers; they were not removed from the oil bath until breakdown had occurred. During the test the voltage was raised in steps of 4%, starting at half the anticipated value.

The breakdown voltages measured are listed in Table III above. The deviation of individual measurements from the mean was small all round, as may be gathered from the figures shown for σ. The results may therefore be considered very reliable.

Another fact which may be deduced from these measurements is the good agreement with those of the previously mentioned investigations, namely that when oil-insulated arrangements are stressed by voltages such as might be produced by the disconnection of a transformer, the insulation strength is of the order of 85 to 90% of the figure obtained with standard impulse tests.

Even though the majority of the test voltages in these investigations only reached quite moderate amplitudes, so that the results are at present only applicable to equipment for not unduly high rated voltages, besides which the arrangements in practice are often more complicated than those tested, it ought to be justifiable for the minimum withstand voltage of finished transformers to be estimated from the results of measurements on models. Here the one-minute test voltage could be taken as a starting point, utilizing the knowledge that the resistance to switching overvoltages is at least about 40% higher. Alternatively the full-wave 1/50 impulse test voltage U_p can be taken as the basis, allowance being made for the somewhat longer duration of the stress in the case of a freely oscillating voltage by deducting 15%. When restriking occurs, however, the conditions as regards to the rapid change when the voltage collapses are quite comparable, without any correction, to those when testing with a chopped wave of the same magnitude.

Insulation Strength of the Material and Maximum Permissible Switching Overvoltage

Before the maximum peak voltage permissible in service can be stated, it is necessary to specify the safety margin from a minimum withstand voltage, which must be proved by a particular test. In the upward direction this depends on the extent of a possible weakening of the insulation due to ageing or the repetition of severe electrical stresses; in the downward direction on the mode of operation of the overvoltage protection, i.e. the reliability with which voltages higher than foreseen are avoided. As regards the latter point, the conditions for switching surges are far more favourable than for overvoltages of atmospheric origin. Both with the simple rod or horn type of spark-gap and with the efficient lightning arresters which have been developed to such perfection in recent years, the sparkover value for non-atmospheric overvoltages is very close to the rated value under all conditions. With lightning

TABLE IV

Maximum value for switching overvoltages

Maximum service voltage U_{max} kV	Maximum admissible switching overvoltages (peak)		
	Based on impulse test $U_s = 0{\cdot}85 \times 0{\cdot}85 \times U_{p\,1/50}$ kV	Based on chopped-wave impulse $U_s' = 0{\cdot}85 \times 1{\cdot}15 \times U_{p\,1/50}$ kV	$k = \frac{\sqrt{3}\,U_s}{\sqrt{2}\,U_{max}}$
123	325	440	3·23
145	397	538	3·34
170	470	635	3·38
245	650	880	3·24
300	760	1030	3·10
420	1030	1395	3·00

discharges having a high rate of rise, simple spark-gaps permit still higher voltages at the protected object. Neither is there any reason to fear reduction of the insulation strength during service. Experience has shown that the short-time strength of insulating material in general is not reduced appreciably by repeated high stresses, nor possibly by ageing or deterioration with power-frequency overvoltages. In some cases such an effect is lacking altogether, for example in gaseous or liquid media, or when breakdown occurs without any preliminary discharge. In others a logarithmic relationship can be determined between the remaining strength and the number of stresses. For instance, in laboratory tests on paper-insulated wire test objects immersed in oil, a drop of 12% in insulation strength was observed after a total of 50 shots. But in service it is hardly likely that such severe stresses would be imposed so frequently within such a short time, therefore their cumulative effect is not experienced. Thus, after each severe stress by a high voltage the full insulation strength should be almost regained in the majority of cases.

Hence for practical requirements it ought to be perfectly adequate to restrict the maximum admissible service switching overvoltage to 85% of the minimum withstand voltage of the equipment when new. Table IV shows the resultant values following the twofold deduction of 15% (once for ageing, etc., and once for the longer duration), which work out at practically 72% of the impulse test voltages for the material. The last column gives the overvoltage factor k as the ratio of the maximum switching overvoltage to the maximum phase voltage. As a rough average k proves to be around 3·25, although a slightly lower figure should be allowed for e.h.v. systems.[2] Higher overvoltages exceed the permissible level and approach the minimum withstand voltage in the new state. They should be avoided by taking special precautions, primarily by limiting the overvoltages at their origin.

The insulation strengths for restriking overvoltages calculated on the basis of the test values with chopped waves (third column in Table IV) are a good deal higher than would be permissible if allowance were only made for the preceding medium-frequency rise. Consequently restrikes in the breaker are incapable of causing faults in properly designed transformers. For all other high-voltage equipment—having no windings—they represent no hazard whatsoever.

It may therefore be claimed that sufficient evidence has been brought to prove that, provided the maximum switching overvoltages which can occur in a power system are limited to a reasonable figure, there is little risk of their harming transformers—which demand particular care—and certainly no real risk to other electrical equipment, provided it is correctly designed. Consequently this Company takes the view that there is no need to test the equipment with a stress resembling the switching overvoltage. The information given in the present article permits the minimum withstand voltage to be estimated with sufficient accuracy. If, despite this, it is not possible to gain a clear picture of the behaviour of a particular arrangement when developing a new design, the true strength of this element could always be determined by itself in a model test with any desired approximation.

---

[2] Here k is referred to the maximum admissible service (phase) voltage and not, as is often found, to the rated voltage of the insulation (*Reihenspannung* as per VDE, insulation class as per ASA). Owing to the 15% difference between the two, the numerical value of the hereby defined overvoltage factor is about 15% lower than the figure obtained with the other definition.

Conclusion and Proposal for Limiting Switching Overvoltages

The stresses to which electrical equipment is subjected and its behaviour in the face of switching overvoltages have to a large extent been physically explained and can often be predicted reasonably accurately. Restrikes ought not to harm properly designed transformers.

When choosing the circuit-breaker care must be taken to ensure that the highest values attainable by switching surges do not exceed 72% of the impulse test voltage. Then all system elements are adequately protected, both to earth and with respect to stresses inside the winding.

Special tests to prove the ability to withstand switching overvoltages do not appear to be necessary; the conventional tests with the power-frequency voltage and with a full-wave impulse should be quite enough for type tests.

(KME) B. GÄNGER

Bibliography

[1] W. WANGER and W. HUBER: Flashover Voltage of Insulators and Spark Gaps in the Intermediate Range between Impulse-Voltage Testing and Voltage Testing at Operating Frequency. Brown Boveri Rev. 1940, Vol. 27, No. 12, p. 231 to 243.

Also W. WANGER: The flashover voltage of dirty and wet insulators when subjected to impulses of varying duration. CIGRE Report No. 209, 1939.

[2] P. L. BELLASCHI, L. P. RADEMACHER: Dielectric strength of station and line insulation to switching surges. AIEE Trans. 1946, Vol. 65, p. 1047–53.

[3] E. J. ADOLPHSON, F. J. VOGEL: A study of the co-ordination of modern arresters and transformer insulation. Pwr App. & Syst. 1956, p. 1108–13.

W. C. FARNETH, F. J. VOGEL: Switching surges and long-duration voltage tests on transformer insulation. Pwr App. & Syst. 1956, p. 1198–1201.

[4] H. E. FIEGEL, J. S. KRESGE: Effects on transformer insulation structures of long-duration waves representative of switching surges. Pwr App. & Syst. 1957, No. 28, p. 1312–20.

[5] P. JACOTTET: Durchschlagverhalten von Anordnungen in Luft und unter Öl bei Schaltüberspannungen. Elektrotech. Z. Edn A, 1958, Vol. 79, No. 10, p. 337–45.

[6] B. GÄNGER, G. HOSEMANN: Switching Surges and Insulation Strength. Brown Boveri Rev. 1959, Vol. 46, No. 5, p. 279–87.

PROGRESS IN THE MEASUREMENT OF VERY HIGH, RAPIDLY CHANGING IMPULSE VOLTAGES

621.317.32.015.3

The author reviews the comprehensive development work which has been carried out in the sphere of measuring impulse voltages, with particular reference to with steep-front waves and to a series of very accurate arrangements for measuring impulses up to 2·3 MV. The determination of the error and calibration of systems for measuring impulse voltages were investigated theoretically and experimentally, revolutionary calibration methods and test equipment being devised as a result.

Fundamentals of the Measurement of Impulse Voltages

THE CONTINUALLY increasing voltages at which e.h.v. power lines are being operated are repeatedly imposing new requirements on measuring methods and equipment. In many countries 380-kV systems are already in service; in others the problems of transmission at still higher voltages, e.g. 500 or 650 kV, are being seriously discussed. At the same time as the rated transmission voltage, the test voltages, including the impulse voltages, are also increased. The ability to measure the latter as accurately as possible is most important because overstressing the h.v. equipment on test due to the indicated voltage being too low, or due to simulation of higher test voltages than really exist, should be avoided.

Attention was particularly devoted to the measurement of very high, rapidly changing impulse voltages, subsequently referred to as steep-front waves. Whereas the peak values of full-wave and tail-chopped impulses can be measured very accurately (error ±1%) by careful design of the circuit, the measurement of steep-front impulses can be accompanied by appreciable errors if the behaviour of the measuring systems under such circumstances is not taken fully into account. The extent and the significance of the problem can be estimated from the results of experiments suggested by the High-Voltage Committee of CIGRE (International Congress on Large Electrical Networks) in 1953, and carried out in a number of laboratories [1].[1] The 50%-flashover voltage for the standard 1/50 impulse, as well as for impulses chopped in the front at chopping times up to $T = 0{\cdot}5$ μs, were measured with a 250-mm sphere gap. Whereas the individual flashover voltages agreed very well—the amount of scatter of the measurements was less than 1%—measurement of impulses chopped in the front after 0·5 μs yielded inadmissibly high deviations of 20–30%, most of which could not be traced back to the usual scatter factors. The obvious step was to seek the reason for the widely differing measurements in the measuring system itself. It was necessary to account for the error because the impulse voltages in question were quite modest—200 to 300 kV—so that at higher figures, unless a remedy could be discovered, the deviation could be expected to be still greater due to the area over which the measuring equipment was unavoidably spread.

The importance and extent of the problem was also recognized at an early stage by Brown Boveri, and exhaustive theoretical and experimental investigations were undertaken in two principal directions. On the one hand, methods were developed for the precise mathematical derivation of the error in the system when measuring steep-front waves, with corresponding calibration equipment to determine them experimentally. On the other hand, by studying the effect of the individual elements of a impulse test circuit, new, very accurate systems were evolved which were particularly suited to the measurement

---

[1] The figures in square brackets refer to the bibliography at the end of the article.

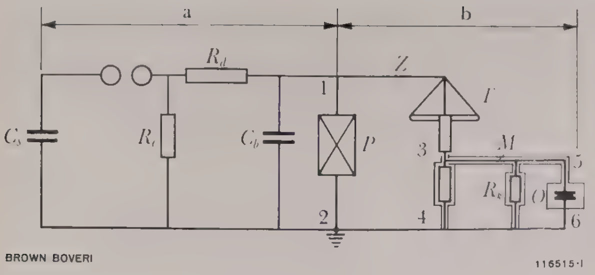

Fig. 1. – General arrangement of an impulse circuit

a: Impulse generating equipment b: Measuring system

C_s = Impulse capacitance
R_e = Discharge resistance
R_d = Damping resistance of impulse generator
C_b = Load capacitance
P = Test object
T = Voltage divider
M = Measuring cable
R_k = Terminating resistance of cable
Z = High-voltage lead
O = Oscillograph

Between 1 and 2: Voltage input to measuring system
Between 3 and 4, or 5 and 6: Output voltage

of steep-front impulses. This development led to arrangements with screened ohmic dividers or, for certain special measurements, with low purely ohmic dividers which, in conjunction with the proved system employing capacitive voltage dividers used for measuring full-wave and tail-chopped impulses, offers a complete guarantee for the accuracy of measurements of impulses up to very high voltages indeed.

Theory

An impulse measuring system normally consists of a voltage divider with a h.v. lead to the test object, leads to the recording instrument—in most cases an oscillograph—and the latter itself. Since only the shape of the voltage wave at the test object has to be measured, and not the voltage drop in the lead between the impulse generator and the test object, the measuring system is located after the object, seen from the generator (Fig. 1). Whereas, in previous investigations, the main source of error was considered to be the voltage divider, another approach is necessary for the measurement of steep-front impulses:

The entire measuring system should be treated as a quadripole, whose input voltage is between lead and earth (points 1 and 2 in Fig. 1) while the output voltages at the low-voltage tapping of the divider (points 3 and 4), or the deflector plates of the oscillograph (points 5 and 6).

Modern trends in the construction of voltage dividers run parallel to this development. As long as only the divider was considered a possible source of error, the purely capacitive divider held the reputation of being ideal for the measurement of impulse voltages, because its ratio is independent of frequency. In this respect it is not difficult to comprehend the efforts to compensate for the effect of the capacitance to earth of ohmic dividers by connecting capacitors in parallel with the resistance, thus producing a divider which, though nominally mixed, functions in practice as a capacitive divider [2]. Furthermore an attempt was made to eliminate, as far as possible, the influence of the capacitance to earth of ohmic dividers by equipping them with screening electrodes [3, 4]. These measures were only successful with systems for measuring moderately high impulse voltages up to about 100 kV peak. Goossens and Provost [5] adopted a different approach by adapting the resistance distribution of ohmic dividers as accurately as possible to the capacitive distribution between electrode arrangements, thus endeavouring to eliminate the influence of the capacitance to earth of the resistor column. Investigations into the influence of the voltage divider on the output voltage likewise follow a logical course, from the division of steady-state alternating voltages [6], via the reproduction of the standard 1/50 and rectangular impulses [2, 7], to the determination of error with steep-front waves [8, 9].

When determining the error of the quadripole shown in Fig. 1, the task is somewhat simplified by the fact that the error is mainly caused by the high-voltage part—comprising the divider and the lead to it—and to a much smaller extent by the low-voltage part. When the output cables are properly terminated and not too long (less than 20 m) and, with the excellent quality of modern cold-cathode oscillographs—or even hot-cathode oscillographs—it is possible to ignore the share of the low-voltage side even when dealing with such rapid phenomena as the impulse chopped after 0·5 μs [10, 11].

Errors of the Measuring System

To determine the error of the arrangement in Fig. 1, a suitable equivalent circuit diagram for the h.v. side must first be derived. To begin with, an equivalent circuit must be determined for the divider itself which, as is well known, can be represented by a chain consisting of a large number of identical elements. A voltage divider may be treated as a chain of N identical longitudinal impedances z_l and transverse impedances z_q (Fig. 2). If a unit step-function $U_n = U(1)_t$ is applied to the h.v. input of the divider, the voltage $U_n(t)$ at the output is given by

$$u_n(t) = U \frac{\sinh \frac{n}{N} \sqrt{\frac{Z_l}{Z_q}}}{\sinh \sqrt{\frac{Z_l}{Z_q}}} \tag{1}$$

where $Z_l = N z_l$ and $Z_q = z_q/N$.

The transverse impedance of a chain element is given by the capacitance to earth c_e; the longitudinal impedance z_l generally comprises a resistance r, an inductance l and a series capacitance c, in parallel with which is the inherent capacitance c_0 of the element.

In operational form equation (1) may be written as

$$U_n(p) = U \frac{\sinh \frac{n}{N} \sqrt{\frac{\left(R + L \cdot p + \frac{1}{C \cdot p}\right) \cdot C_e \cdot p}{1 + \left(R + L \cdot p + \frac{1}{C \cdot p}\right) \cdot C_0 \cdot p}}}{\sinh \sqrt{\frac{\left(R + L \cdot p + \frac{1}{C \cdot p}\right) \cdot C_e \cdot p}{1 + \left(R + L \cdot p + \frac{1}{C \cdot p}\right) \cdot C_0 \cdot p}}} \tag{2}$$

with $R = N \cdot r, \quad L = N \cdot l,$

$$C = \frac{1}{N} c, \quad C_0 = \frac{1}{N} c_0, \quad C_e = N \cdot c_e$$

The general diagram as in Fig. 2 can be simplified further because for all voltage dividers the inductance L can be ignored owing to the non-inductive design of the capacitors and the resistance winding. Moreover, for the ohmic part $C \approx \infty$ and $1/Cp \approx 0$; for the capacitive divider $R = 0$. Assuming a correctly compensated mixed divider, whose capacitive and ohmic potential distributions are equal, and a capacitance to earth which is very small compared with the parallel capacitance ($C_e \ll C_{01}$); also assuming the screened ohmic divider has a resistance winding matching the capacitive potential distribution of the screening electrodes, we obtain the equivalent diagrams shown in Fig. 3a–d for the ohmic, the capacitive, the mixed and the screened ohmic dividers, respectively. These equivalent circuit composed of concentrated elements, on the application of a unit step-function $u_N(t) = U(1)_t$ at the h.v. input, yield the same resultant voltage $u_n(t)$ at the output as the chain diagram of the corresponding dividers. In order to arrive at the complete equivalent diagram for the high-voltage divider of a measuring system like that in Fig. 1, we must also take into account the input lead and, if provided, the damping resistor R_d.

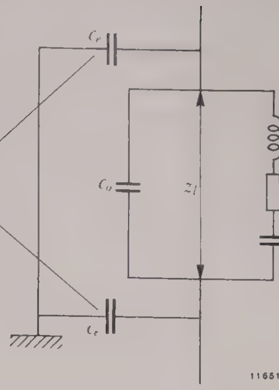

Fig. 2. – Element of the voltage divider, which may be represented as a chain system

l = Inductance
r = Resistance
c = Longitudinal capacitance
c_0 = Parallel capacitance
c_e = Capacitance to earth of one element
z_1 = Longitudinal impedance
z_q = Transverse impedance

Up to now it has been usual in the literature to represent the h.v. lead in the equivalent circuit diagram by concentrated inductance L, the magnitude of which can be reasonably accurately determined from the inductance of an overhead line with $l_z = 1{\cdot}25$ μH/m. But in reality this lead is a complex electrical arrangement of split longitudinal inductance l_z and capacitance to earth c_z, of negligible resistance r_z, to which must be added the mutual capacitances c_z' to adjacent objects, i.e. mainly the test object and the divider (Fig. 4).

Fig. 3. – Equivalent circuit diagrams for voltage dividers

$u_N(t)$ = Input voltage
$u_n(t)$ = Output voltage

a: *Ohmic divider*
R_r = Resistance of h.v. part
R_n = Resistance of l.v. part
C_e = Capacitance to earth of resistance column

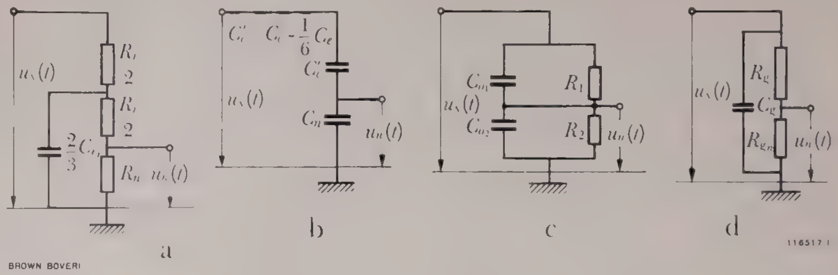

b: *Capacitive divider*
C_c = Capacitance of h.v. part
C_e = Capacitance to earth of divider
C_n = Capacitance of l.v. part
C_c' = Reduced h.v. capacitance

c: *Mixed divider*
C_{01} = Capacitance of h.v. part
R_1 = Resistance of h.v. part
C_{0_2} = Capacitance of l.v. part
R_2 = Resistance of l.v. part

d: *Screened ohmic divider*
C_g = Capacitance of the screening
R_g = Resistance of the h.v. part
R_{g_n} = Resistance of l.v. part

Exhaustive investigations into the effect on prediction of the error of an impulse measuring system of neglecting the capacitance to earth of the h.v. lead, from which only the final result shown in Fig. 5 is reproduced [12], indicate that, even when measuring very rapid surges, it is permissible to employ the simplified representation of the h.v. lead as a concentrated inductance L. Fig. 5 shows the limiting chopping time T_g for a linear steep-front impulse in terms of the divider capacitance C, and the ratio C/C_z of the equivalent capacitance of the divider to that lead, for which the simplified representation has already been permitted. Hence, according to Fig. 5, this is justified for steep-front waves chopped after 0·5 μs, even for measuring systems in which the equivalent capacitance of the divider is small and practically equal to the capacitance of the h.v. lead. When the divider capacitance C is large compared with that of the lead C_z, the simplified representation of the lead is permissible for still shorter chopping times than $T = 0{\cdot}5$ μs.

At this point it is perhaps advisable to stress that the above simplification and neglecting the individual parameters both of the divider and the h.v. lead, as discussed so far, only refer to the theoretical de-

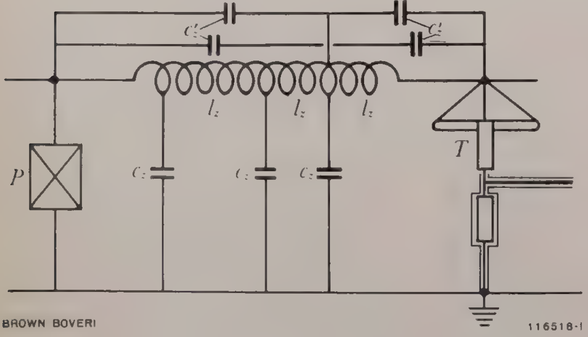

Fig. 4. – General equivalent circuit diagram of the h.v. lead

P = Test object
T = Voltage divider
l_z = Inductance per unit length
c_z = Capacitance per unit length
c_z' = Mutual capacitances of the lead to test object and divider

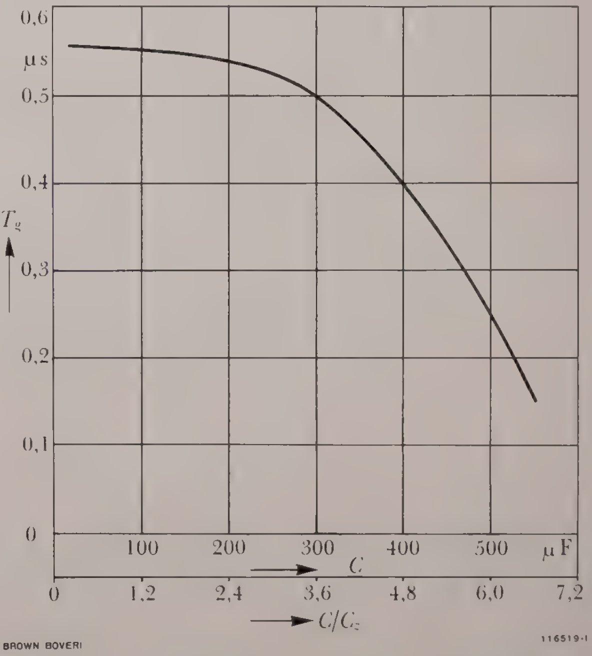

Fig. 5. – Limiting chopping time of linear steep-front waves permitting the simplified representation of the h.v. lead as a concentrated inductance

T_g = Limiting chopping time
C = Equivalent capacitance of voltage divider
C_z = Total capacitance to earth of h.v. lead

termination of the error from calculated or measured quantities for an impulse measuring system. When the latter is calibrated in the laboratory, all the small factors which have so far been neglected are naturally taken into account in their entirety.

Fig. 6 is the general equivalent diagram for the measuring systems employing the voltage dividers shown in Fig. 3a–d. $u_1(t)$ is the voltage applied to the measuring system, $u_2(t)$ that tapped off the l.v. output. In order to simplify and standardize the present considerations still further, instead of $u_2(t)$ we introduce the standardized voltage $u_{2_0}(t)$, reduced to the h.v. side of the divider, given by the divider ratio at a d.c. voltage of u_0 as follows.

$$u_{2_0}(t) = u_2(t) \cdot u_0 \tag{3}$$

thus making it possible to omit the l.v. part of the dividers shown in Fig. 3a–d.

The general equivalent diagram in Fig. 6 thus represents the quadripole of an impulse measuring system, as mentioned earlier. To determine the error of this arrangement with different kinds of applied impulses $u_1(t)$, there are two basic methods which may be adopted.

With the *step-function method* the error Δu can be determined for any input function $u_1(t)$ with the aid of the Laplace transformation or the Duhamel integral from the well-known reproduction of the arrangement with an applied step function.

With the *frequency-response method* the input impulse $u_1(t)$ is resolved into harmonic components according to Fourier, and with known characteristics for the amplitude $A(f)$ and phase angle $\Phi(f)$ of the frequency response, the error is determined for each harmonic. Since the measuring system is linear, the total error can be obtained by summation of the errors caused by the individual harmonics.

Whereas the step-function method is already commonly used for the measurement of impulse voltage, there is no record of any method being used for direct determination of the error from the frequency response of the measuring system. This is partly due to the difficulty of determining the phase angle of the measuring system with sufficient accuracy in a given frequency range.

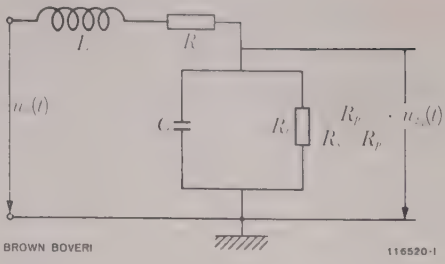

Fig. 6. – General equivalent circuit diagram of a system for measuring impulse voltages

L = Inductance of the input (h.v.) lead
R_s = Series resistance
C = Capacitance to earth of divider
R_p = Parallel resistance
$u_1(t)$ = Input voltage
$u_{2_0}(t)$ = Standardized output voltage

First we have to derive the theoretical fundamentals of the step-function method and the newly developed frequency-response calibration method for determining the error of an impulse-measuring system and then, from the results of practical measurements, confirm the correctness of the two methods, which lead to identical results.

Step-Function Method

It is a well-known fact that the output voltage $u_{2_0}(t)$ of a quadripole composed of linear elements, and with the voltage $u_1(t)$ applied, can be determined from the step-function response $\psi(t)$ of the quadripole. The output voltage can thus be found with the aid of the Laplace transformation or the Duhamel integral. According to the Laplace transformation the output voltage in the illustrated range may be expressed by

$$U_{2_0}(p) = U_1(p) \cdot \psi(p) \cdot p \tag{4}$$

and

$$u_{2_0}(t) = \mathrm{L}^{-1}\,[U_{2_0}(p)] \tag{5}$$

According to the Duhamel integral

$$u_{2_0}(t) = \int_{v=0}^{v=t} u_1(v)\,\frac{\mathrm{d}}{\mathrm{d}(t-v)}\,[\psi(t-v)]\,\mathrm{d}v \tag{6}$$

or

$$u_{2_0}(t) = \int_{v=0}^{v=t} \psi(t-v)\,\frac{\mathrm{d}}{\mathrm{d}v}\,[u_1(v)]\,\mathrm{d}v \tag{7}$$

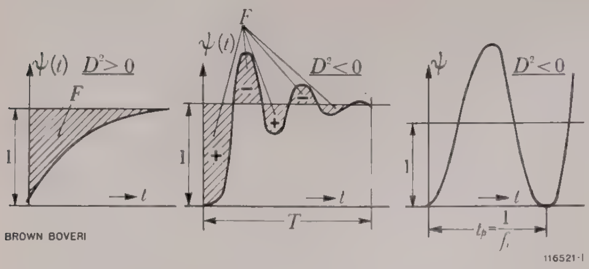

Fig. 7. – Step-function responses of the general measuring system

a: *Response function $\psi(t)$ with overcritical damping for $D^2 > 0$*

F = Area between step-function impulse and response, representing time constant τ

b: *Damped response oscillation for $D^2 < 0$*

F = Resultant area between step-function impulse and response

T = Chopping time of a linear steep-front wave for which the step-function response has already attained its steady-state final value

c: *Undamped response oscillation for $D^2 < 0$*

t_p = Duration of one cycle of the resonance frequency f_r

When determining the step-function response $\psi(t)$ of the equivalent circuit in Fig. 7, we must distinguish between the following cases.

a. With an over-critically damped measuring system with positive discriminant $D^2 > 0$

$$\psi(t) = 1 - \frac{k}{k-l}\,e^{-lt} - \frac{l}{k-l}\,e^{-kt} \tag{8}$$

where

$$k, l = \frac{1}{2}\left[\frac{R_s}{L} + \frac{1}{R_p C}\right] \pm$$

$$\pm \sqrt{\frac{1}{4}\left(\frac{R_s}{L} + \frac{1}{R_p C}\right)^2 - \frac{R_s + R_p}{R_p} \cdot \frac{1}{LC}} \tag{9}$$

in which, for systems actually used, k is always $\gg l$ and $\frac{l}{k-l}\,e^{-kt} \approx 0$. Likewise equation (8) can be simplified to

$$\psi(t) = 1 - e^{-lt} = 1 - e^{-\frac{t}{\tau}} \tag{10}$$

in which $\tau = 1/l$ is the time constant of the step-function response.

b. For a lightly damped measuring system with $D^2 < 0$

$$\psi(t) = 1 - \frac{\omega_0}{\omega}\,e^{-\frac{a_0}{2}} \cos(\omega t - \varphi) \tag{11}$$

with

$$\frac{a_0}{2} = \frac{1}{2}\left[\frac{R_s}{L} + \frac{1}{R_p C}\right] \tag{12}$$

$$\omega_0^2 = \frac{R_s + R_p}{R_p} \cdot \frac{1}{LC} \tag{13}$$

$$\omega = \sqrt{\omega_0^2 - \frac{a_0^2}{4}} \tag{14}$$

$$\varphi = \arctan \frac{a_0}{2\omega} \tag{14a}$$

For systems without any damping whatsoever ($R_s = 0$, $R_p = \infty$)

$$\psi(t) = 1 - \cos \omega_0 t \tag{15}$$

with

$$\omega_0 = \frac{1}{\sqrt{LC}} \tag{16}$$

c. For a critically damped system

$$\psi(t) = 1 - \left(1 + \frac{a_0}{2}\,t\right) \cdot e^{-\frac{a_0}{2}t} \tag{17}$$

In the measurement of impulse voltages this case seldom arises and will therefore not be considered further.

Fig. 7a, b and c show the response $\psi(t)$ to unit step functions applied to the general equivalent circuit of an impulse-measuring system, according to (10), (11) and (15).

Now that the step-function response $\psi(t)$ is known, we can determine the error with a standard 1/50 impulse, and with the particularly interesting steep-front waves chopped after the time T in accordance with (4) to (7). The standard 1/50 impulse can be represented by the function

$$u_1(t) = U \cdot K\,(e^{-\alpha t} - e^{-\beta t}) \tag{18}$$

in which

$K = 1{\cdot}0167$

$\alpha = 0{\cdot}0142 \times 10^6\ [\mathrm{s}^{-1}]$

$\beta = 6{\cdot}073 \times 10^6\ [\mathrm{s}^{-1}]$

The standardized output 1/50 impulse is obtained by employing the Laplace transformation or Duhamel's integral, as follows:

$$u_{20}(t) = U \cdot K \left(\frac{e^{-\alpha t} - e^{-\frac{t}{\tau}}}{1 - \alpha\tau} - \frac{e^{-\beta t} - e^{-\frac{t}{\tau}}}{1 - \beta\tau}\right) \tag{19}$$

for a step-function response of the system as in equation (10) with a positive discriminant.

For the case of a damped step-function response according to equation (1) we obtain

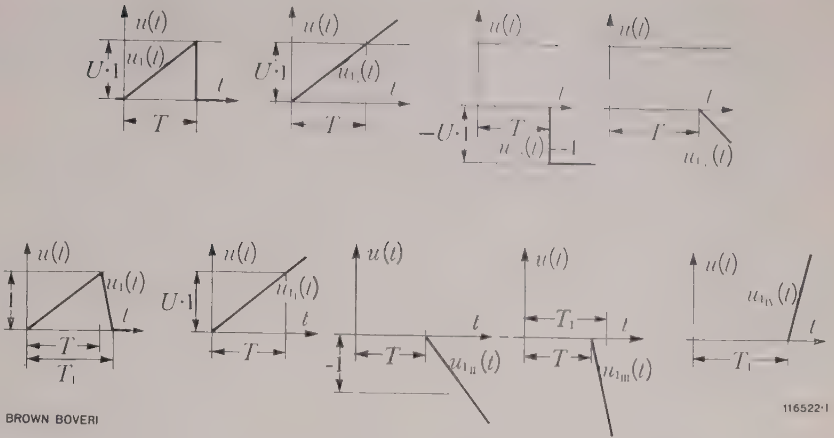

Fig. 8. – Components of a chopped linear steep-front wave

a: *With infinitely short collapse time*
$u_1(t)$ = Chopped linear steep-front wave
$u_{1_1}(t) \dots u_{1_3}(t)$ = Components of the steep-front wave
T = Chopping time
t = Time axis

b: *With finite collapse time*
$u_1(t)$ = Chopped steep-front wave
$u_{1_I}(t) \dots u_{1_{IV}}(t)$ = Components of the steep-front wave
T = Chopping time
$(T_1 - T)$ = Collapse time

In both 'a' and 'b' the curve of the impulse voltage on the left is composed of the components on the right.

$$u_{2_0}(t) = U \cdot K\left(e^{-\alpha t} - e^{-\beta t} - \frac{\beta - \alpha}{\omega} \cdot e^{-\frac{a_0}{2}t} \cdot \sin \omega t\right) \tag{20}$$

and for an undamped, oscillating step-function response according to equation (15)

$$u_{2_0}(t) = U \cdot K\left(e^{-\alpha t} - e^{-\beta t} - \frac{\beta - \alpha}{\omega_0} \sin \omega_0 t\right) \tag{21}$$

The error in a system with a 1/50 standard impulse is characterized by reduction of the peak value according to (19), or by a damped or undamped oscillation according to (20) or (21) superposed on the input impulse. When the measuring circuit is carefully designed, it is nowadays possible for standard impulses up to very high values to be measured very accurately, the error amounting up to $\pm 1\%$, so that in this respect there are no difficulties to be expected.

System Error for Steep-Front Impulses

When measuring front-chopped or steep-front impulses the shape of the impulses is assumed to be as shown in either Fig. 8a or b. Fig. 8a shows a linear steep-front impulse with an infinitely short collapse time, which can be resolved into the three components, as follows:

$$u_{1_1}(t) = U \cdot \frac{t}{T} \quad \text{for } 0 < t < T \tag{22}$$

$$u_{1_2}(t) = -U \cdot 1 \quad \text{for } T < t < \infty \tag{23}$$

$$u_{1_3}(t) = -U \cdot \frac{t - T}{T} \quad \text{for } T < t < \infty \tag{24}$$

The collapse of the voltage in an infinitely short time, as assumed therein, is physically impossible. Fig. 8b depicts the shape of a steep-front wave with a finite collapse $(T_1 - T)$, which more nearly corresponds to practical conditions. Since the steep-front impulse is usually chopped by means of electrode arrangements under normal atmospheric conditions, it is permissible to substitute the duration of a spark discharge in air (approx. 25–30 μs) as a reasonably close approximation to $T_1 - T$.

The components of the chopped steep-front impulse as in Fig. 8a are:

$$u_{1_I}(t) = U \cdot \frac{t}{T} \quad \text{for } 0 < t < T \tag{25}$$

$$u_{1_{II}}(t) = -U \cdot \frac{t - T}{T} \quad \text{for } T < t < \infty \tag{26}$$

$$u_{1_{III}}(t) = -U \cdot \frac{t - T}{T_1 - T} \quad \text{for } T < t < \infty \tag{27}$$

$$u_{1_{IV}}(t) = U \cdot \frac{t - T_1}{T_1 - T} \quad \text{for } T_1 < t < \infty \tag{28}$$

As regards the output steep-front impulse in Fig. 8a or b we are primarily interested in the peak value, whereas the indicated collapse of the voltage, which is reproduced with considerable distortion by the measuring system, owing to its great steepness, assumes only secondary importance. As will be demonstrated subsequently, the system error is nearly always given by the initial rising part of the steep-front impulse and occurs at the moment of chopping, i.e. when $t = T$. Only with measuring systems having an oscillating step-function response as in equation (15)—see Fig. 7c—and an assumed steep-front wave with an infinitely short collapse time, and chopping times of $T < 0{\cdot}5$ μs, will the second component $u_{12}(t)$ in Fig. 8a contribute a small share to the total error.

In detail, the system error with steep-front impulses is obtained as follows, using either the Laplace transformation or Duhamel's integral:

$$u_{2_{01}}(t) = U\left[\frac{t}{T} - \frac{\tau}{T}\left(1 - e^{-\frac{t}{\tau}}\right)\right] \qquad (29)$$

and the error at the moment of chopping $t = T$:

$$\Delta u(T) = u_{1_1}(T) - u_{2_{01}}(T) = $$
$$= U\frac{\tau}{T}\left(1 - e^{-\frac{T}{\tau}}\right) \approx U\frac{\tau}{T} \qquad (30)$$

because in systems for measuring impulse voltages the time constant τ is roughly one order of magnitude smaller than chopping time T which has to be measured. In this case the system error is only caused by the rising part of the linear steep-front impulse.

For a step-function response according to equation (11) (Fig. 7b), the output steep-front impulse as in Fig. 8a with infinitely short collapse time is given by

$$u_{2_{01}}(t) = U\left(\mp e^{-\frac{a_0}{2}t} \cdot \frac{\sin \omega t}{\omega t} - \frac{1}{2\,\omega^2 t^2}\right) \qquad (31)$$

in which the second term derives from the collapse of the steep-front wave. On account of the different phase angle of the two parts from equation (31), it is customary to express the maximum possible error for $t \approx T$.

$$\Delta u(T) = u_1(T) - u_{2_0}(T) = $$
$$= U\left(\mp e^{-\frac{a_0}{2}T} - \frac{1}{2\,\omega^2 T^2}\right) \qquad (32)$$

The fraction $1/2\,\omega^2 T^2$ is due to the continued charging of the capacitance of the divider by the voltage induced in the h.v. lead by the assumed infinitely short collapse, and only assumes any significance when chopping times are very short and ω very small—i.e. in systems with a low resonance frequency. For the measurement of steep-front waves chopped after $T \geqslant 0{\cdot}5$ μs, and allowing for finite duration of collapse, as in Fig. 8b, the system error becomes almost

$$\Delta u(T) = U \cdot e^{-\frac{a_0}{2}T} \cdot \frac{\sin \omega T}{\omega T} \qquad (33)$$

For measuring systems with an undamped oscillating step-function response, as in Fig. 7c, the corresponding error is

$$\Delta u(T) = U \cdot \frac{\sin \omega_0 T}{\omega_0 T} \qquad (34)$$

A particularly interesting case, and one which should be aimed at when measuring impulse voltages, occurs when the damped oscillating step-function response as in Fig. 7b has almost decayed at the instant of chopping $t = T$. The system error at that moment is then simply

Fig. 9. – Transformation of linear steep-front impulses

$u_1(t)$ = Input impulse
$u_{2_0}(t)$ = Standardized output impulse
Δu = System error
T = Chopping time
t = Time axis

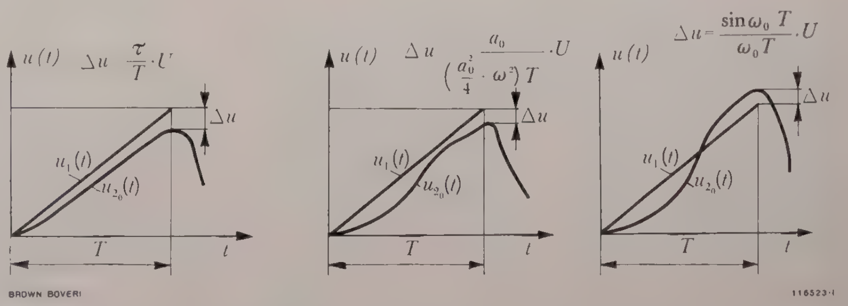

a: *For a system with overcritical damping* $D^2 > 0$
τ = Time constant of the step-function response

b: *For a system with damped response oscillation which has practically decayed at the moment chopping occurs*
a_0 = Damping factor
ω = Angular frequency

c: *For an undamped response oscillation*
ω_0 = Resonance frequency of response oscillation

$$\Delta u(T) = U \cdot \frac{a_0}{\left(\frac{a_0^2}{4} + \omega^2\right) \cdot T} \qquad (35)$$

Fig. 9a, b and c show how the linear steep-front impulse appears at the output, and indicate the system error according to equations (29), (30), (34) and (35), Fig. 10 shows the relationship between the error Δu and the chopping time T for different values of the time constant τ of the step-response, or of $a_0/(a_0^2/4 + \omega^2)$.

Now, for a measuring system with an overcritically damped and an oscillating step response, which has almost decayed at the moment of chopping (see Fig. 7a and b), the area F enclosed by the step-function impulse and its response will be determined, and its corresponding time t_f.

For a step-function response according to equation (10) (Fig. 7a)

$$F = t_f = \int_0^\infty \left[1 - \left(1 - e^{-\frac{t}{\tau}}\right)\right] \mathrm{d}t = \tau \qquad (36)$$

and for a response according to equation (11) (Fig. 9b).

$$F = t_f = \int_0^\infty \frac{\omega_0}{\omega} e^{-\frac{a_0}{2}t} \cdot \cos(\omega t - \varphi)\, \mathrm{d}t = \frac{a_0}{\omega_0^2} \qquad (37)$$

Hence, taking equations (30) and (35) into account, the areas F represent the error of a measuring system with a steep-front impulse, for which we are looking.

The two equations (36) and (37) provide a means of carrying out the step-function calibration of a measuring system with steep-front impulses. A voltage rising rapidly relative to the expected step-function response of the system has to be applied to the high-voltage input to the system—in fact it can almost be treated as a rectangular impulse—and the output voltage recorded on the oscillograph. From the area F corresponding to time t_f so determined we can work out the error for a linear steep-front impulse. For measuring systems with highly damped oscillating response according to equation (11) or (15), quantities a_0 and ω or ω_0 needed for determination of the error can also be obtained from the step-function response. Obviously, the error for a 1/50 impulse can also be deduced from the parameters of the step-function response.

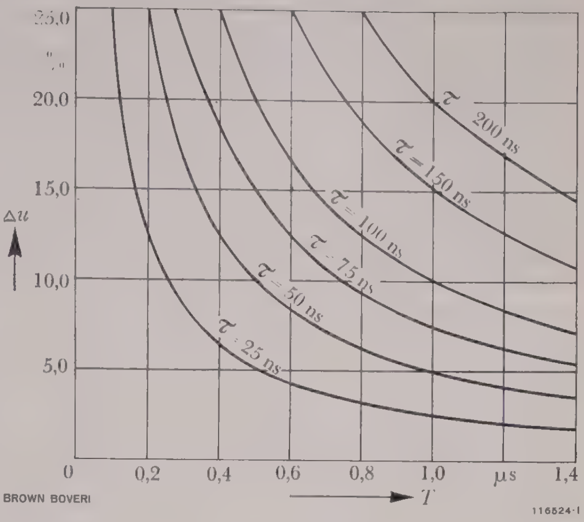

Fig. 10. – System error when measuring linear steep-front impulses

Δu = Percentage system error
T = Chopping time
τ = Time constant of the step-function response of an overcritically damped measuring system

Determining the System Error for Steep-Front Impulses from the Frequency Response of the Measuring System

By applying the Fourier integral

A non-repetitive function $u_1(t)$ defined over a period $0-T$ can be expressed in the well-known manner by the Fourier integral

$$u_1(t) = \int_0^\infty [a(\omega) \cos \omega t + b(\omega) \sin \omega t]\, \mathrm{d}\omega \qquad (38)$$

with the coefficients

$$a(\omega) = \frac{1}{\pi} \int_0^T u_1(\xi) \cos \omega\xi\, \mathrm{d}\xi \qquad (39)$$

and

$$b(\omega) = \frac{1}{\pi} \int_0^T u_1(\xi) \sin \omega\xi\, \mathrm{d}\xi \qquad (40)$$

Substituting (39) and (40) in (38), we obtain

$$u_1(t)_{t=T} = \frac{1}{\pi} \int_0^\infty \mathrm{d}\omega \int_0^T u_1(\xi) \cos[\omega(t-\xi)]\, \mathrm{d}\xi \qquad (41)$$

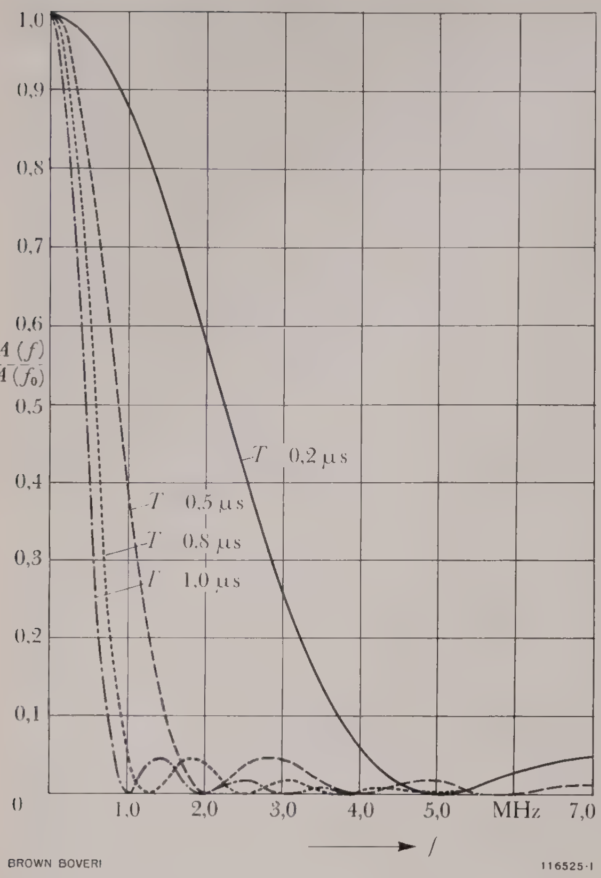

Fig. 11. – Frequency spectra of linear steep-front waves

Ratio of the amplitude $A(f)$ at frequency f to the d.c. component $A(f_0)$ for different chopping times T.

For a linear steep-front impulse of the form

$$u_1(t) = U \cdot \frac{T}{t}$$

$$u_1(T) = \frac{1}{\pi} U \int_0^\infty \mathrm{d}\omega \int_0^T \frac{\xi}{T} \cos[\omega(t-\xi)]\,\mathrm{d}\xi =$$

$$= \int_0^\infty U \cdot \frac{1-\cos\omega T}{T\pi\omega^2}\,\mathrm{d}\omega \qquad (42)$$

Equation (42) represents the continuous frequency spectrum of a linear steep-front impulse having the form $u_1(t) = Ut/T$ at the instant of chopping $t = T$. Frequency spectra for a steep-front wave chopped after $T = 0{\cdot}2$, $0{\cdot}5$, $0{\cdot}8$ and $1{\cdot}0$ µs are reproduced in Fig. 11.

Now if the amplitude ratio $A(\omega)$ and phase angle $\Phi(\omega)$ between the applied and standardized output voltage are known at the steady-state alternating voltage, we obtain for the output steep-front impulse at $t = T$

$$u_{2_0}(T) = \int_0^\infty U \cdot A(\omega) \cdot \frac{1-\cos[\omega T - \Phi(\omega)]}{T\pi\omega^2}\,\mathrm{d}\omega \quad (43)$$

It is most convenient to solve equations (42) and (43) graphically by representing $u_1(T)$ and $u_{2_0}(T)$ by corresponding areas F_1 and F_2. The system error at the moment of chopping for $t = T$ is then given by

$$\Delta u(T) = \frac{F_1 - F_2}{F_1} = 1 - \frac{F_2}{F_1} \qquad (44)$$

This method is hardly suitable for practical applications as it relies on involved graphical evaluation. Its value lies in the frequency spectra obtained for linear steep-front waves, as shown in Fig. 11, which give a good picture of the frequency range covered by such impulses.

A completely new method will now be derived, for which only a few harmonic frequencies and an easily determined correction factor are needed to establish the system error of a measuring system with a steep-front wave.

Determining the system error by harmonic analysis according to Fourier of a periodic time function $f(t)$ containing a linear steep-front impulse in the interval $0-T$

The newly developed method for determining the system error from the frequency response—amplitude $A(\omega)$ and phase angle $\Phi(\omega)$ characteristics—of the measuring system at only a few harmonic frequencies is based on the following facts.

Firstly it will be proved that the sum of the harmonic sine or cosine impulse in the interval $0-T$ obtained by the harmonic analysis of a periodic function of time $f_1(t)$ and $f_2(t)$, as in Fig. 12a and b, which contains the linear steep-front impulse between 0 and T, is identical with the linear steep-front impulse.

Also derived is that for measuring systems with an overcritically damped step-function response according to equation (10), or with a response whose oscillation has just decayed at the moment of chopping T, according to (11), i.e. for systems in which the error at the moment of chopping is governed by the initial, rising part of the steep-front impulse, it will be possible to change from harmonic sine or cosine impulses to corresponding periodic harmonic oscillations for the determination of the system error.

The periodic functions $f_1(t)$ and $f_2(t)$ depicted in Fig. 12a and b are given by

$$f_1(t) = U \sum_{n=0}^{n=\infty} \frac{8}{(2n+1)^2\pi^2}(-1)^n \sin\left[(2n+1)\cdot\pi\cdot\frac{t}{2T}\right] \tag{45}$$

$$f_2(t) = U\left\{0{\cdot}5 - \sum_{n=0}^{n=\infty} \frac{4}{(2n+1)^2\pi^2}\cos\left[(2n+1)\cdot\pi\cdot\frac{t}{T}\right]\right\} \tag{46}$$

The identity of the sum of harmonic sinusoidal impulses with the linear steep-front impulse in the same interval $0-T$ is effected by the identity of the Fourier coefficients $a(\omega)$ and $b(\omega)$ as in (39) and (40) for the steep-front impulse on the one hand, and the sum $a^*(\omega)$ and $b^*(\omega)$ of all harmonic sine impulses on the other. The proof given below is carried out for the analysis according to equation (45).

An analogous proof can also be provided for the analysis according to equation (46).

For the linear steep-front impulse

$$a(\omega) = \frac{1}{\pi}\int_0^T U\cdot\frac{t}{T}\cos\omega t\,\mathrm{d}t =$$

$$= \frac{U}{\pi}\left[\frac{1}{\omega}\sin\omega T + \frac{1}{\omega^2 T}(\cos\omega T - 1)\right] \tag{47}$$

$$b(\omega) = \frac{1}{\pi}\int_0^T U\cdot\frac{t}{T}\sin\omega t\,\mathrm{d}t =$$

$$= \frac{1}{\pi}U\left[\frac{1}{\omega^2 T}\sin\omega T - \frac{1}{\omega}\cos\omega T\right] \tag{48}$$

whereas after a certain amount of intermediate calculation for the sum of all sinusoidal impulses in the interval $0-T$ we obtain

$$a^*(\omega) =$$

$$= U\cdot\frac{1}{\pi}\cdot\frac{8}{\pi^2}\sum_{n=0}^{n=\infty}\frac{1}{(2n+1)^2}\cdot\frac{\omega\sin\omega T - (-1)^n(2n+1)\dfrac{\pi}{2T}}{\omega^2 - (2n+1)^2\cdot\dfrac{\pi^2}{4T^2}} \tag{49}$$

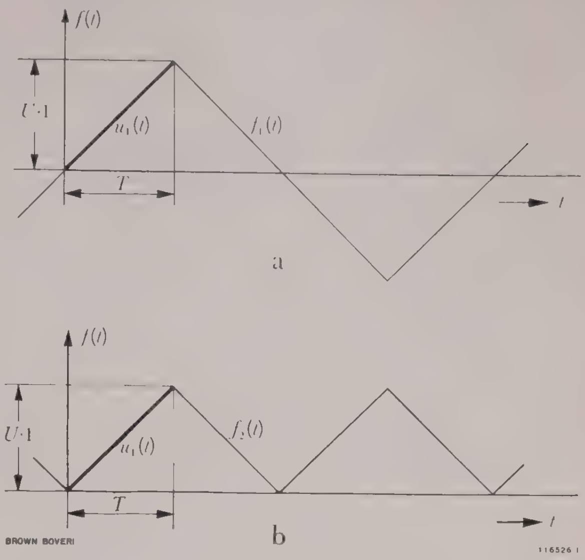

Fig. 12. – Periodic functions of time, according to Fourier, containing the steep-front wave

a: $f_1(t)$ = Function of time according to Fourier
T = Chopping time
$u_1(t)$ = Linear steep-front wave

b: $f_2(t)$ = Function of time according to Fourier

$$b^*(\omega) =$$

$$= -U\cdot\frac{1}{\pi}\sum_{n=0}^{n=\infty}\frac{8}{(2n+1)^2\pi^2}\cdot\frac{\omega\cos\omega T}{\omega^2 - \dfrac{(2n+1)^2\pi^2}{4T^2}} \tag{50}$$

With the aid of the function

$$\mathrm{f}(x) = \frac{\sin u\pi}{\pi}\left(\frac{1}{u} - \frac{2u}{u^2-1^2}\cos x + \frac{2u}{u^2-2^2}\cos 2x - \ldots\right) \tag{51}$$

in which

$$\mathrm{f}(x) = \cos ux \qquad 0 < x < \pi \tag{52}$$

and the Leffler-Mittag development of the function $\frac{1}{\cos Z}$, i.e.

$$\frac{1}{\cos Z} = 4\pi\sum_{n=0}^{n=\infty}\frac{(-1)^n(2n+1)}{(2n+1)^2\pi^2 - 4Z^2} \tag{53}$$

we obtain, with the conversion performed in Appendix I, the identity of the corresponding coefficients

$$a(\omega) \equiv a^*(\omega) \text{ and } b(\omega) \equiv b^*(\omega)$$

Thus the linear steep-front impulse can be replaced by the sum of harmonic sine or cosine impulses according to equations (45) and the output

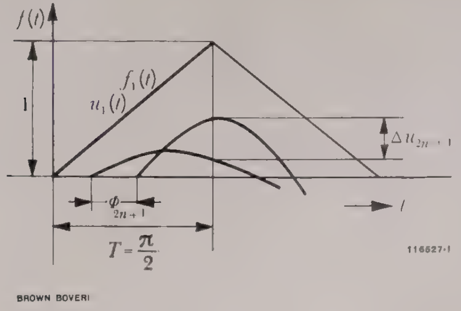

Fig. 13. – Determination of the system error at chopping caused by the $(2n+1)$th harmonic

$f_1(t)$ = Function of time according to Fourier
$u_1(t)$ = Linear steep-front wave
T = Chopping time
$A(f_{2n+1})$ = Amplitude ratio of the $(2n+1)$th harmonic
Φ_{2n+1} = Phase displacement of the $(2n+1)$th harmonic
Δu_{2n+1} = System error for the $(2n+1)$th harmonic at the moment chopping occurs

voltage of the system resulting from applying the sum of these harmonic impulses can be determined with the aid of the Laplace transformation or Duhamel's integral. If this calculation is carried out, as will be shown later, for measuring systems with overcritically damped step-function response or with the oscillating response almost decayed at the moment of chopping $t = T$, the output voltage will consist of two summands.

The first of these is identical with the output voltage $u_{2_{0\mathrm{I}}}(t)$ at steady-state alternating voltage, while the second is a transient voltage $u_{2_{0\mathrm{II}}}(t)$ which, according to the assumptions made regarding the system investigated, is negligible compared with $u_{2_{0\mathrm{I}}}(t)$. Hence the system error is determined by $u_{2_{0\mathrm{I}}}(t)$ and can be derived from the frequency response of the system at the steady-state alternating voltage.

To provide evidence of this change to steady-state alternating voltages, the measuring system is assumed to have a step-function response according to (10), e.g. with damping resistor, capacitive divider and short h.v. lead of negligible inductance. The equivalent circuit diagram of the system then reduces itself to a $R\,C$ network with the time constant

$$\tau = R_s C \tag{54}$$

At the moment of chopping, the output steep-front impulse is given by

$$u_{2_0}(T) = u_{2_{0\mathrm{I}}}(T) + u_{2_{0\mathrm{II}}}(T) = \sum_{n=0}^{n=\infty} U \cdot$$

$$\cdot \frac{8}{(2n+1)^2\pi^2}\left\{\left[(-1)^n - \frac{M^2\tau^2}{M^2\tau^2+1}\right] + (-1)^n \cdot \frac{M\tau}{M^2\tau^2+1} \cdot e^{-\frac{T}{\tau}}\right\} \tag{55}$$

and the system error by

$$\Delta u(T) = \sum_{n=0}^{n=\infty} U \cdot$$

$$\cdot \frac{8}{(2n+1)^2\pi^2}\left[\frac{M^2\tau^2}{M^2\tau^2+1} + (-1)^n \frac{M\tau}{M^2\tau^2+1} \cdot e^{-\frac{T}{\tau}}\right] \tag{56}$$

Since it was assumed that $\tau \ll T$ and $e^{-\frac{T}{\tau}} \approx 0$, the latter equation is reduced to:

$$\Delta u(T) \approx \sum_{n=0}^{n=\infty} U \cdot \frac{8}{(2n+1)^2\pi^2} \cdot \frac{M^2\tau^2}{M^2\tau^2+1} \tag{57}$$

in which M denotes the angular frequency

$$M = \frac{(2n+1)\pi}{2T} \tag{58}$$

For a Fourier series as in (46), in similar manner:

$$\Delta u(T) \approx \sum_{n=0}^{n=\infty} U \cdot \frac{4}{(2n+1)^2\pi^2} \cdot \frac{M'^2\tau^2}{M'^2\tau^2+1} \tag{59}$$

with

$$M' = \frac{(2n+1)\pi}{T} \tag{60}$$

It will now be proved that the system error given by equation (57) is equal to the error from the sum of corresponding alternating voltages. Fig. 13 shows the system error at the moment of chopping, caused by the $(2n+1)$th harmonic. Since the measuring system effects a phase displacement $\Phi(f_{2n+1})$ and a change of amplitude of $A(f_{2n+1})$, it can easily be seen that the system error is

$$\Delta u_{2n+1}(T) = U \cdot \frac{8}{(2n+1)^2\pi^2}\{1 - A(f_{2n+1}) \cos[\Phi(f_{2n+1})]\} \tag{61}$$

and the total system error

$$\Delta u(T) = \sum_{n=0}^{n=\infty} U \cdot \frac{8}{(2n+1)^2\pi^2}\{1 - A(f_{2n+1}) \cos[\Phi(f_{2n+1})]\} \tag{62}$$

Likewise for a Fourier analysis using equation (46)

$$\Delta u(T) = \sum_{n=0}^{n=\infty} U \cdot \frac{4}{(2n+1)^2\pi^2}\{1 - A(f_{2n+1}) \cos[\Phi(f_{2n+1})]\} \tag{63}$$

in which the harmonic frequencies are determined by the chosen series and the chopping time T.

For the analysis according to equation (45)

$$f_1 = \frac{1}{4T}, \quad f_3 = \frac{3}{4T}, \quad f_{2n+1} = \frac{2n+1}{4T} \qquad (64)$$

and according to (46)

$$f_1 = \frac{1}{2T}, \quad f_3 = \frac{3}{2T}, \quad f_{2n+1} = \frac{2n+1}{2T} \qquad (65)$$

The amplitude ratio $A(f_{2n+1})$ and the phase displacement $\Phi(f_{2n+1})$ for the $(2n+1)$th frequency of the $R_s C$ system, are as follows:

$$A(f_{2n+1}) = \frac{\frac{1}{MC}}{\sqrt{R_s^2 + \frac{1}{M^2 C^2}}} = \frac{1}{\sqrt{1 + M^2 \tau^2}} \qquad (66)$$

$$\cos[\Phi(f_{2n+1})] = \frac{\frac{1}{MC}}{\sqrt{R_s^2 + \frac{1}{M^2 C^2}}} = \frac{1}{\sqrt{1 + M^2 \tau^2}} \qquad (67)$$

Substituting (66) and (67) in equation (62) we obtain

$$\Delta u(T) = \sum_{n=0}^{n=\infty} U \cdot \frac{8}{(2n+1)^2 \pi^2} \cdot \frac{M^2 \tau^2}{M^2 \tau^2 + 1} \qquad (68)$$

Equation (68) is identical with (57), thereby proving it is permissible to change from harmonic impulses to harmonic oscillations. Similarly this changeover can be derived for the general equivalent circuit for impulses as in Fig. 7 [12].

According to equations (57) and (59), the system error at the moment of chopping is given by an infinite series of harmonic frequencies and is thus of little practical use. However, this is where the property of an impulse voltage measuring system, only to transmit a.c. voltages up to a certain limiting frequency f_g, affords welcome relief.

Fig. 14 shows the amplitude ratio $A(f)$ of an impulse measuring system. For f_g the limiting frequency, $A(f_g) = 0$ and the system error for all higher frequencies in the range $f_g < f < \infty$, according to (62) is given by

$$\Delta u_{corr} = K = \sum_{n=n_g}^{n=\infty} U \cdot \frac{8}{(2n+1)^2 \pi^2} \qquad (69)$$

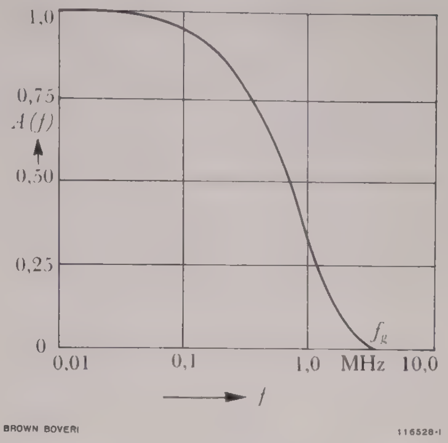

Fig. 14. – Amplitude curve of an impulse measuring system

f = Frequency
f_g = Limiting frequency
$A(f)$ = Amplitude ratio

Those harmonics which are no longer transmitted by the measuring system give rise to an output error equal to the sum of their amplitudes. However, this sum can be determined from the difference between the sums of all harmonics which, at the moment of chopping, produce the steep-front input impulse with the reduced value 1, and all harmonics up to the limiting frequency f_g. Then

$$K = U \cdot 1 - \sum_{n=0}^{n=n_g} U \cdot \frac{8}{(2n+1)^2 \pi^2} \qquad (70)$$

For practical measurements it will be possible to break off the calculation at a frequency $f'_g < f_g$. For instance, f'_g can be taken as the frequency at which $A(f) = 0{\cdot}1–0{\cdot}2$. Utilizing

$$A(f'_g) \cdot \cos \Phi(f'_g) = x \qquad (71)$$

the correction which has to be inserted is

$$K' = (1 + x) \cdot K \qquad (72)$$

the sign depending on the phase shift $\cos \Phi(f'_g)$. The difference between K and K' in practice will be very small and the system error will be somewhere between the two nearly equal errors obtained by inserting K and K'.

For the Fourier analysis according to (46) the correction is

$$K = 0{\cdot}5 - \sum_{n=0}^{n=n_g} \frac{4}{(2n+1)^2 \pi^2} \qquad (73)$$

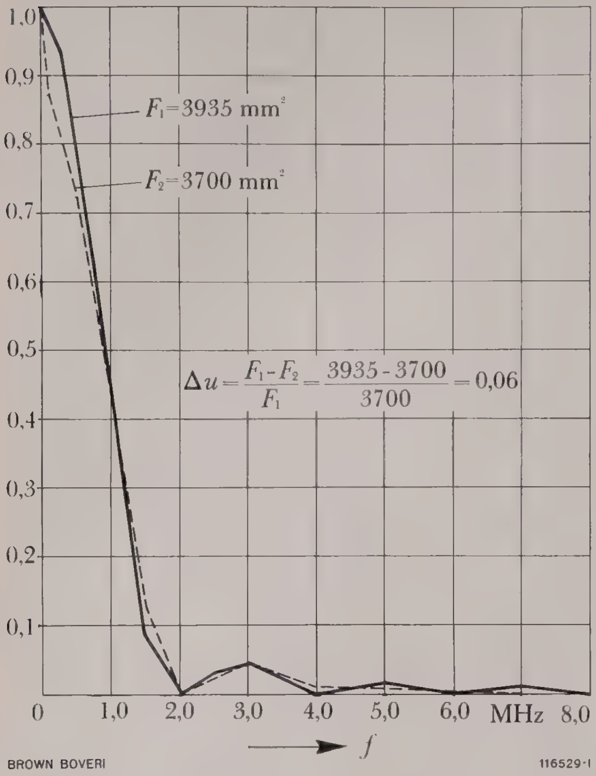

Fig. 15. – Determination of the system error for a steep-front impulse chopped after $T=0{\cdot}5\,\mu s$, according to Fourier's integral

F_1 = Area representing input impulse
F_2 = Area representing output impulse
Δu = System error
f = Frequency

To confirm the relationship derived for the system error with rectangular and steep-front impulses, the error of a system like the one in Fig. 6 will now be calculated for an impulse chopped after $T = 0{\cdot}5$ µs. The system is assumed to have a screened ohmic voltage divider with the following parameters.

Inductance of 10-m h.v. lead	$L = 12{\cdot}5\ \mu\text{H}$
Damping resistor	$R_s = 300\ \Omega$
Resistance of the voltage divider	$R_p = 30\ \text{M}\Omega$
Screen capacitance of the divider	$C = 100\ \text{pF}$

From these we obtain the following:

$$\frac{a_0}{2} = \frac{1}{2}\left(\frac{R_s}{L} + \frac{1}{R_p C}\right) =$$

$$= \frac{1}{2}\left(\frac{300}{12{\cdot}5}\cdot 10^6 + \frac{10^{12}}{3\,.\,10^4\,.\,100}\right) = 12\,.\,10^6\left(\frac{1}{s}\right)$$

$$\omega_0 = \sqrt{\frac{R_p + R_s}{R_p}\cdot\frac{1}{LC}} =$$

$$= \sqrt{\frac{30000+300}{30000}\cdot\frac{10^{18}}{12{\cdot}5\,.\,100}} = 28{\cdot}25\,.\,10^6\left(\frac{1}{s}\right)$$

$$\omega = \sqrt{\omega_0^2 - \frac{a_0^2}{4}} = 25{\cdot}6\,.\,10^6\left(\frac{1}{s}\right)$$

Hence the influence of R_p can be ignored. For damping at the moment of chopping

$$e^{-\frac{a_0}{2}T} = e^{-6} = 0{\cdot}0025$$

i.e. the oscillation of the step-function response according to (11) has almost completely decayed at $t = T$. According to equation (35), the system error

$$\Delta u(T) =$$

$$= \frac{a_0}{\omega_0^2\, T} = \frac{24\,.\,10^6}{798\,.\,10^{12}\,.\,0{\cdot}5\,.\,10^{-6}} = 0{\cdot}06 \text{ or } 6\%.$$

The calculation of the system error for the application of the Fourier analysis as in equation (46) is given in the table opposite for the same numerical example. As will be seen, the agreement with the result obtained by the step-function method is very close.

For the same measuring system let us now calculate the error for steep-front impulse chopped after 0·5 µs, using the Fourier integral. The numerical evaluation of the two integrals is carried out for the input impulse according to (42) and for the reduced output impulse according to (43).

The frequency spectra of the two impulses are illustrated in Fig. 15. The input impulse $u_1(T)$ is represented by the area $F_1 = 3935$ mm² while area $F_2 = 3700$ mm² corresponds to the output impulse $u_{2_0}(T)$. Hence the system error is

$$\Delta u(T) = \frac{F_1 - F_2}{F_2} = \frac{3935 - 3700}{3935} = 0{\cdot}06 \text{ or } 6\%$$

Here too the error agrees closely with the figure obtained with the other two methods.

The theoretical part of this article will conclude with a demonstration of the internal relationship between the step-function and the frequency-response methods of calibration, as given by the Bromwich-Wagner integral, which permits the derivation of the step-function response from the frequency response of the measuring system.

Error of a measuring system with a screened ohmic divider for a linear steep-front wave chopped after $T = 0{\cdot}5\ \mu s$; Fourier analysis according to equation (46)

Harmonic	Frequency f Mc/s	$A(f)$	$\cos[\Phi(f)]$	Δu_{2n+1}
1st	1·0	1·03	0·979	—0·0034
3rd	3·0	1·262	0·701	0·00518
5th	5·0	1·029	—0·241	0·0203
7th	7·0	0·515	—0·731	0·01136
9th	9·0	0·219	—0·868	0·00626
11th	11·0	0·196	—0·914	0·00395
13th	13·0	0·129	—0·95	0·0027
Correction	$K = 0{\cdot}0148$ $K' = 0{\cdot}0165$			
Total system error			$0{\cdot}061 < \Delta u < 0{\cdot}0628$	

The Bromwich-Wagner Integral as Common Starting Point of the Step-Function Response and Frequency-Response Methods of Determining the Error of an Impulse Measuring System

The relationship between the frequency, as amplitude ratio $A(2\pi f)$ and phase angle $\Phi(2\pi f)$, and the step-function response of an impulse measuring system is given by the Bromwich-Wagner integral:

$$\psi(t) = \frac{1}{2\pi j}\int_{-j\infty}^{+j\infty} \frac{S(p)\cdot e^{pt}}{p}\,dp \qquad (74)$$

Moreover,

$$1 = \frac{1}{2\pi j}\int_{-j\infty}^{+j\infty} \frac{S(0)\, e^{pt}}{p}\,dp \qquad (75)$$

the connection with the frequency response being given by the function

$$S(p) = S(j\,2\pi f) = \mathrm{Re}\,(2\pi f) + j\cdot \mathrm{Im}\,(2\pi f) \qquad (76)$$

$\mathrm{Re}\,(2\pi f)$ and $\mathrm{Im}\,(2\pi f)$ are the real and imaginary parts of $S(p)$, which work out to

$$\mathrm{Re}\,(2\pi f) = A\,(2\pi f)\cos\Phi\,(2\pi f) \qquad (77)$$

$$\mathrm{Im}\,(2\pi f) = -A\,(2\pi f)\sin\Phi\,(2\pi f) \qquad (78)$$

from the amplitude and phase angle characteristics of the system. The calculation of equations (74) and (75) performed in (13) yields the following three expressions for the step-function response $\psi(t.)$

$$\psi(t) = \mathrm{Re}(0) + \frac{1}{\pi}\int_0^\infty \left[\frac{\mathrm{Re}(2\pi f) - \mathrm{Re}(0)}{2\pi f}\sin 2\pi f t + \frac{\mathrm{Im}(2\pi f)}{2\pi f}\cos 2\pi f t\right] d(2\pi f) \qquad (79)$$

$$\psi(t) = \frac{2}{\pi}\int_0^\infty \frac{\mathrm{Re}\,(2\pi f)}{2\pi f}\sin 2\pi f t\, d(2\pi f) \qquad (80)$$

$$\psi(t) = \mathrm{Re}(0) + \frac{2}{\pi}\int_0^\infty \frac{\mathrm{Im}\,(2\pi f)}{2\pi f}\cos 2\pi f t\, d(2\pi f) \qquad (81)$$

Thus the step-function response $\psi(t)$ can be determined from the completely real part of $S(p)$ as in equation (80), from the imaginary part for a known value of $\mathrm{Re}(0)$—with d.c. voltage $f = 0$—or from both parts of $S(p)$.

If $\mathrm{Re}\,(2\pi f)$ and $\mathrm{Im}\,(2\pi f)$ of an impulse-measuring system are given, it is possible to effect an approximation by straight lines, bounded respectively by the frequencies f_1 and f_2, as in Fig. 16. For each straight-line section, with a height of h_1, $h_2 \ldots h_n$, we can determine the corresponding part of the step-function response $\psi_1(t)$, $\psi_2(t), \ldots \psi_n(t)$ with the aid of the functions $\eta\,(f_2 t)$ and $\zeta\,(f_2 t)$, as

$$\psi_n(t) = 2\,\eta\,(f_2 t) \qquad (82)$$

$$\psi_n(t) = 0{\cdot}5 + \eta\,(f_2 t) + \zeta\,(f_2 t) \qquad (83)$$

$$\psi_n(t) = 1 + 2\,\zeta\,(f_2 t) \qquad (84)$$

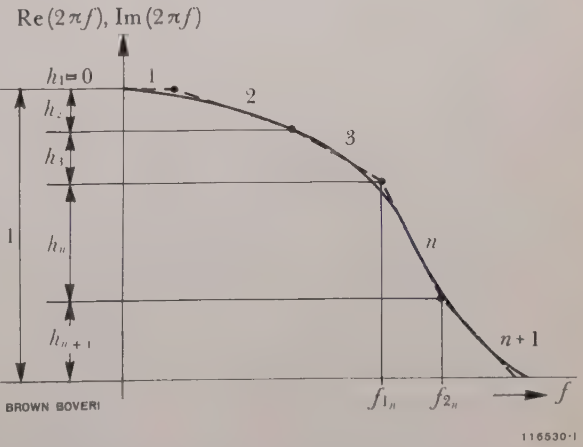

Fig. 16. – Derivation of the step-function response from the frequency response of an impulse measuring system

Approximation to the curve of $\mathrm{Re}\,(2\pi f)$ or $\mathrm{Im}\,(2\pi f)$ by straight lines 1, 2, ...n, $n+1$, having the heights h_1, h_2, ...h_n, h_{n+1}

f_{1n}, f_{2n} = Limiting frequencies of the n-th straight line

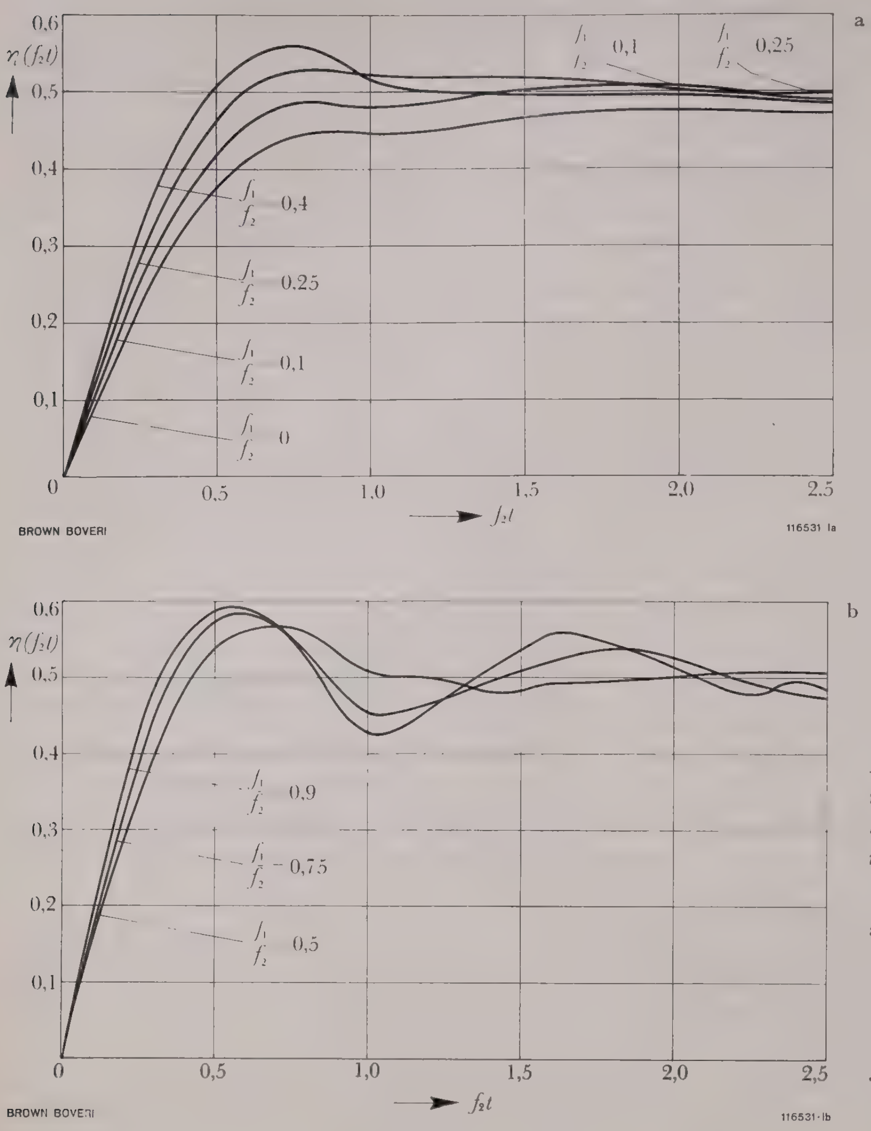

Fig. 17. – Inverse function for deriving the step-function response from the frequency response of an impulse measuring system, for different ratios f_1/f_2

a, b: Inverse function $\eta(f_2 t)$ for determining the step-function response from $\mathrm{Re}(2\pi f)$

f_1, f_2 = Limiting frequencies
t = Time

The curve for $f_1/f_2 = 0{\cdot}75$ is also applicable for $f_1/f_2 = 0{\cdot}8$

The inverse functions $\eta(f_2t)$ for the real part $\mathrm{Re}(2\pi f)$ and $\zeta(f_2t)$ for the imaginary part $\mathrm{Im}(2\pi f)$ are derived in Appendix II. The shape of $\eta(f_2t)$ is shown in Fig. 17a for the parameters $f_1/f_2 = 0$, 0·1, 0·25 and 0·4 and in Fig. 17b for $f_1/f_2 = 0{\cdot}5$, 0·75, 0·8 and 0·9. Curves of $\zeta(f_2t)$ are shown in Fig. 18a for $f_1/f_2 = 0$, 0·1 and 0·2, and in Fig. 18b for $f_1/f_2 = 0{\cdot}5$, 0·75 and 0·9.

For practical determination of the step-function response it is most convenient to use equation (82).

The total step-function response $\psi(t)$ is obtained by adding all partial responses:

$$\psi(t) = \sum_{0}^{n} \psi_n(t) \cdot h_n \qquad (85)$$

Experimental Investigations

From the theoretical investigations into the error of measuring systems, especially with steep-front impulses, valuable hints and pointers were gained for the continued development of the measuring equipment, particularly the voltage dividers, as the following summary indicates.

Systems for measuring steep-front waves should have as small a time constant τ as possible, or the highest possible angular frequency ω of the step-function oscillation; effective damping being especially desirable in the latter case. These requirements can be fulfilled, firstly by constructing a measuring system with a voltage divider having a low capaci-

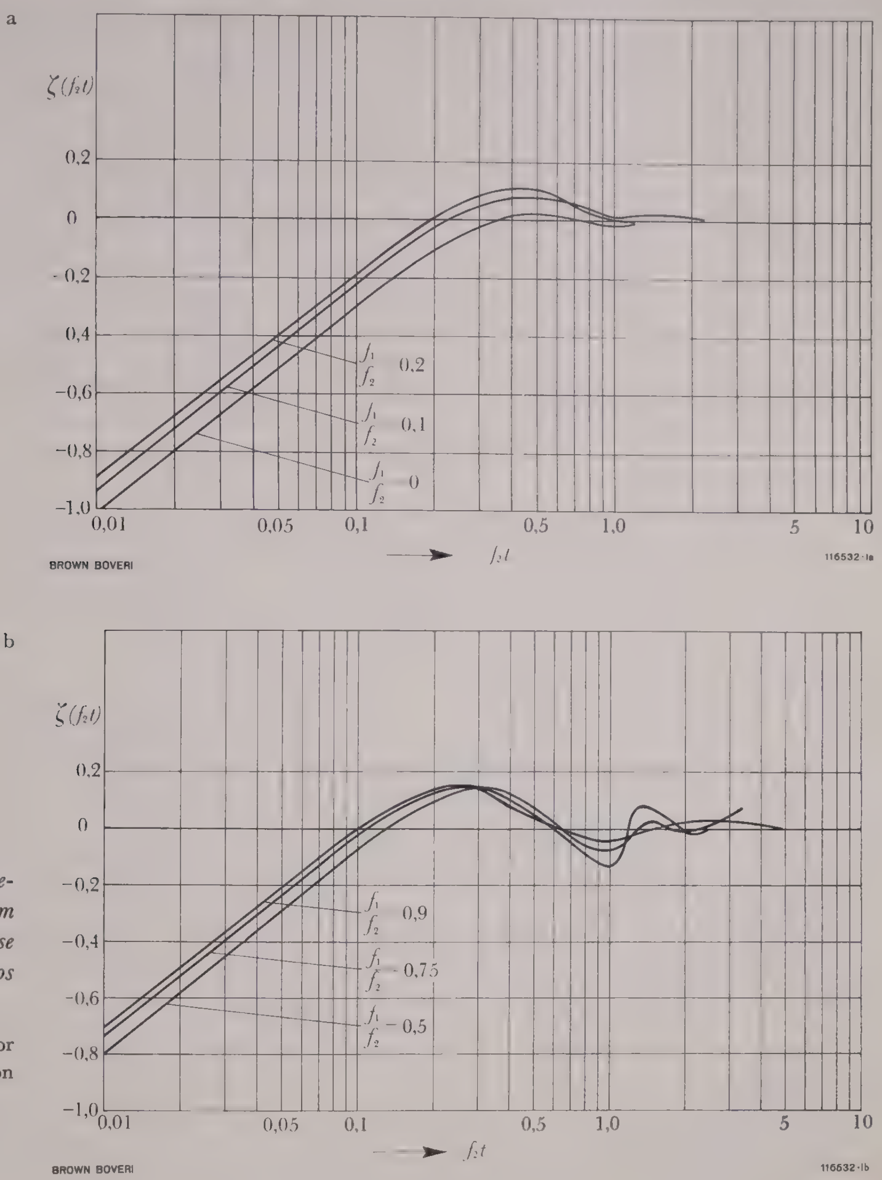

Fig. 18. – Inverse function for deriving the step-function response from the frequency response of an impulse measuring system, for different ratios f_1/f_2

a, b: Inverse function $\zeta(f_2 t)$ for determining the step-function response from $\mathrm{Im}(2\pi f)$

f_1, f_2 = Limiting frequencies

t = Time

tance to earth C. Although the inductance L of the system can be reduced to a certain extent by using the shortest possible connections, e.g. of copper strip, and by efficient earthing, its magnitude is largely determined by the distance between the voltage divider and the test object, which in turn depends on the amplitude of the impulse voltage, and the possibility of the two parts being of different height. A purely ohmic divider with a low resistance of, say, 1000 to 2000 Ω would indeed provide a small time constant τ, but from the practical aspect is attended with disadvantages which prevent it being used for the measurement of full-wave impulses without considerably reducing the half-value time, or necessitating an increase in the capacity of the impulse generator. Thus to perform a series of tests with full-wave and chopped impulses, the use of two voltage dividers would be inevitable, a solution which, apart from being uneconomical, would hamper the speedy execution of the tests.

Neither can the use of the *capacitive voltage divider* with small equivalent capacitance C be recommended if it has to be calibrated alone. The lower the capacitance C of the h.v. part of the divider, the more it influences the rated transformation ratio u_0. This means that a divider of this kind

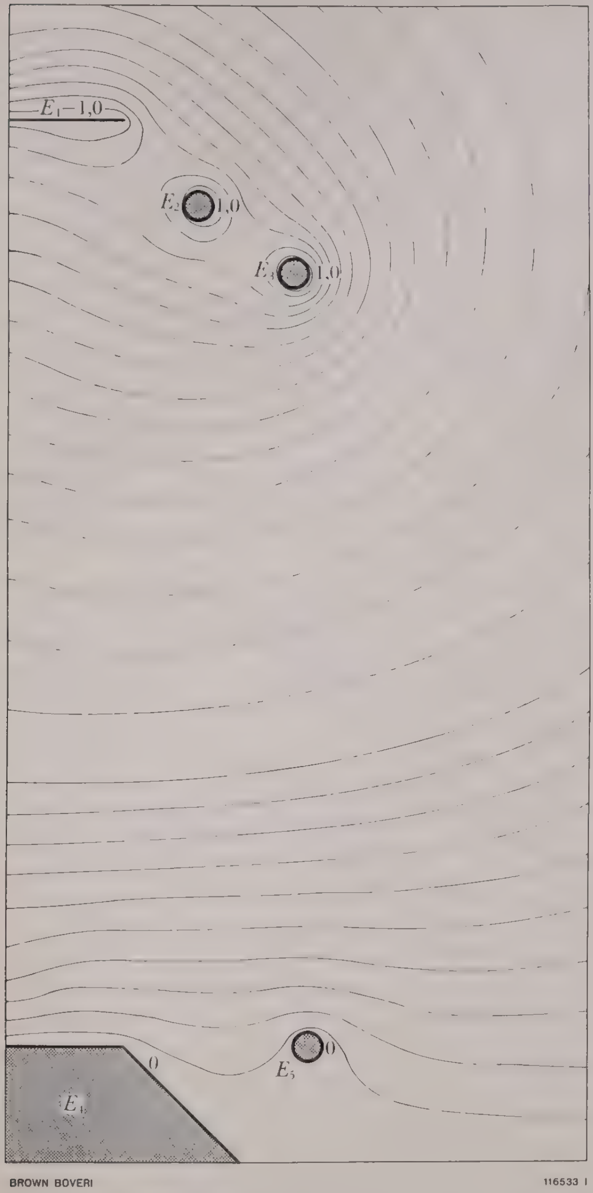

Fig. 19. – Potential distribution of one variant for the screening electrodes of a voltage divider, as measured in the electrolytic tank

E_1, E_2, E_3 = Screening electrodes at high voltage (potential 1·0)
E_4, E_5 = Screening electrodes at earth potential (0)

would be particularly dependent on the spatial layout, because the leakage capacitance between the divider and adjacent objects would affect the rated ratio each time, and this is irksome owing to the small h.v. capacitances involved, because they have to be measured in a bridge circuit, e.g. Schering bridge, which in turn represents an intervention in the leakage and earth capacitance conditions of the divider, existing during the test.

Brown Boveri therefore decided to develop a series of screened ohmic voltage dividers. With a suitable electrode arrangement these can be made with a low capacitance C, while the resistance of the divider R_p, at 6000–10 000 Ω, can be matched to the requirements of the half-value time of the full-wave tail. The rated ratio u_0 of a measuring system having a screened ohmic divider is only determined by the resistance R_{rg} of the h.v. part of the divider, the damping resistance R_d which may possibly be provided, the resistance R_{gn} of the low-voltage part of the divider, and the terminating resistance of the measuring leads and, regardless of the layout of the system, can be determined once and for all by a simple Wheatstone bridge circuit.

A prerequisite for a *screened divider* of high quality is the ability to match the resistance winding as far as possible to the potential distribution in the axis of the screening electrodes. Having carried out exhaustive investigations of various arrangements in the electrolytic tank, the potential distribution obtained in one such case being reproduced in Fig. 19, an electrode system was chosen consisting of a circular plate with a pair of concentric rings at the high-voltage end and a truncated cone with one ring at the earthed end. This arrangement was adopted for all sizes of divider examined, so that they are all proportional to one another geometrically. Dividers have been constructed for 0·2, 0·9 and 2·3 MV full-wave, the basic dimensions being indicated in Fig. 20 (see also the front cover). The ring at the earthed end was omitted from the 0·2-MV divider. The wound resistance columns, which have a particularly low inductance, are almost completely matched to the potential distribution of the screening electrodes by multi-stage graduation of the winding. The 2·3-MV divider, which consists of a number of columns mounted vertically above one another, can be extended for still higher voltages by the addition of more such elements. The control capacitance C can be calculated from the equipotential lines of the diagram (see Fig. 19). For the 2·3-MV divider it is about 110 pF, for the 0·9-MV divider about 50 pF, and for the 0·2-MV divider 20 pF. For the measuring system with the 2·3-MV divider a h.v. lead up to 7 m long and a 320-Ω damping resistance is provided; with the smaller dividers the figures are 4·5 m and 500 Ω for 0·9 MV, and 1 m and 700 Ω for 0·2 MV. The total resistance of each voltage divider is adapted to the parameters of the corresponding impulse generating equipment.

Before the individual systems were calibrated, they were tested for their electric strength, with conspicuous success. For example the 2·3-MV system was tested with several full-wave shots of different polarity up to 2·4 MV. Fig. 21 a shows the peak value of 2·3 MV, which was held several times, while Fig. 21 b depicts the external flashover from the upper ring to the connecting flange between two resistance elements, without the divider itself suffering any ill-effects. The high impulse withstand voltage of 2·3 MV with a height of only 5·0 m is proof of the perfect match between the resistance column and the capacitive voltage distribution of the divider.

Parallel to the development of new voltage dividers, equipment was also constructed for calibrating and determining the error of systems for measuring impulse voltages.

Fig. 22 shows the circuit diagram of a low-voltage step-function generator for 400-V impulses. The impulse is produced by short-circuiting a d.c. voltage applied to a high resistance R_h, using the normally-open contact of a special mercury switch in the relay Q. The symbol r_s denotes a smoothing and protective resistance; C the smoothing capacitor, G the rectifier and S_Q the coil of the mercury switch Q, which is energizing with a.c. at 50 c/s. By synchronizing the step function impulses in time with the mains frequency and the time base of the oscillograph it is possible to simulate an apparently static step-function impulse on the screen.

If the step-function response has to be determined for an impulse measuring system with a rated ratio of 1000–2000 when the applied impulse has an amplitude of several hundred volts, it must be measured with the aid of high-grade amplifiers because, at the l.v. tapping off the divider, voltages of the order of a few hundred millivolts are obtained. The amplifier distorts the curve of the step-function response, and the larger the amplifier's front time T_{av} is compared with the front time T_a of the step-function response, the more pronounced the distortion be-

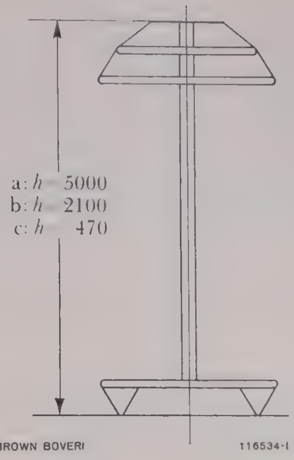

Fig. 20. – Relative size of the newly developed screened ohmic voltage dividers

a: Divider for 2·3 MV
b: Divider for 0·9 MV
c: Divider for 0·2 MV

h = Height in mm

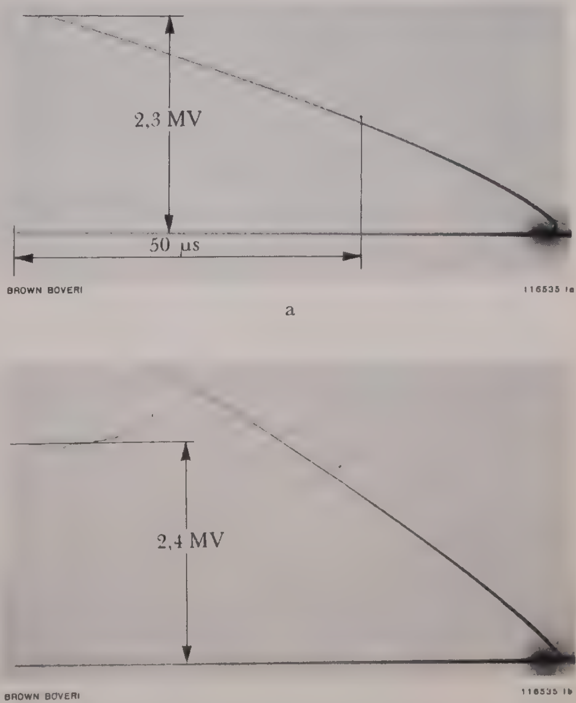

Fig. 21. – Impulse withstand voltage of the new divider for 2·3 MV

a: Full-wave 1/50 impulse held at 2·3 MV

b: Flashover between outer ring and a connecting flange at 2·4 MV. The simulated rise in voltage is the result of the reduction in the ratio of the divider by the flashover.

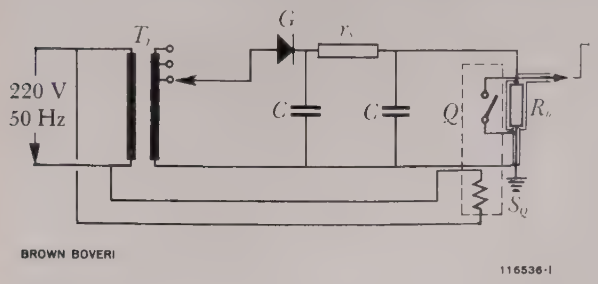

Fig. 22. – Circuit diagram of the low-voltage step-function generator

T_r = Transformer
G = Rectifier
r_s = Protective resistor
R_h = High resistance
C = Smoothing capacitor
Q = Mercury relay
S_Q = Relay coil

comes: for T_{av} and T_a the interval between 0·1 and 0·9 of the full voltage should be inserted.

The distortion of the step-function response can be allowed for by the correction $\sqrt{T^2 - T_{av}^2}$ to the measured front time T.

To enable the cold-cathode oscillograph, which has rendered excellent service in the Brown Boveri high-voltage laboratory in the past, to be used without an amplifier for the calibration of systems for measuring step-function impulses, it was necessary to develop a high-voltage step-function generator for impulses with peak value of about 100 kV. In this respect a completely different approach was adopted to that taken by other laboratories [9, 14]—where pressurized spark-gaps are used to produce h.v. step-function impulses—and a testing unit of simple and expedient design developed. The properties of oil spark-gaps investigated by Burawoy [15] were reverted to which, when energized with a multiple of the breakdown voltage, produced h.v. impulses with the very short front time of about 5 ns [2] and can almost be treated as rectangular.

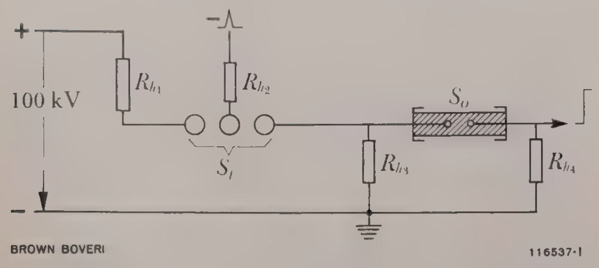

Fig. 23. – Circuit diagram of the 100-kV high-voltage step-function generator

$R_{h1} \ldots R_{h4}$ = High resistances
S_F = Triggering spark-gap
S_O = Oil spark-gap

Fig. 23 shows the circuit diagram of the h.v. step-function generator developed by the Company. The triple-electrode spark-gap S_F is energized with a d.c. potential of about 100 kV. The application of a negative triggering impulse to the centre electrode causes the gap to spark over and a voltage wave, reduced only by the arc drop, flashes across the oil-immersed gap S_O with a multiple of its breakdown voltage.

The two high resistances R_{h1} and R_{h2} of the oil-gap hardly exert any effect on the very rapid phenomena during the formation of the step function. Fig. 24 shows the totally enclosed design of the h.v. step-function generator.

To check the suitability of the two impulse generators, the 0·2-MV measuring system was first calibrated. The first step was to check the low-voltage step function by direct connection to the vertical deflector plates of a "Tektronix 545" oscillograph. Fig. 25a shows the corresponding trace with a sweep rate of 20 ns/cm. The impulse has a very short front time (approx. 1 ns) and can be considered equivalent to a rectangular wave. Fig. 25b shows the trace of the same impulse recorded through the amplifier of the oscillograph. From this curve the front time of the amplifier $T_{av} = 10$ ns.

Fig. 26 shows the schematic layout for the calibration of an impulse measuring system with a step function. When set up ready for operation, an impulse is applied to the h.v. side of the system and the response oscillation, tapped off the l.v. side of the divider, is conducted to the oscillograph by the test lead. The difference between this and the operational layout exists in the slightly different arrangement of the h.v. lead which, instead of being connected to the test object, runs to the lower step-function impulse generator. However, for a h.v. lead of the same length, this deviation has hardly any effect on the step-function response of the system.

---

[2] 1 ns = 10^{-9} s.

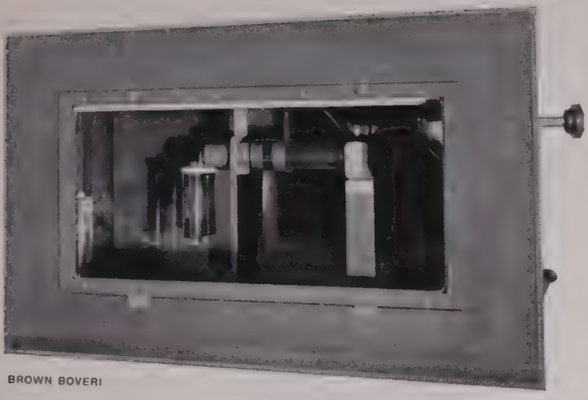

Fig. 24. – Totally enclosed design of 100-kV step-function generator

Top right: Triggering spark-gap
Bottom-left: Oil spark-gap for producing steep-front impulses

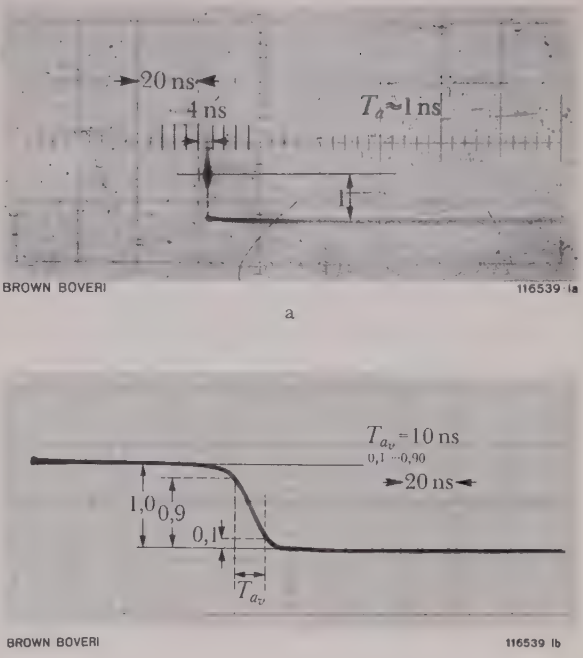

a

b

Fig. 25. – Oscillogram of a low-voltage step-function impulse

a: By direct connection to the deflector plates of the oscillograph
b: Via the amplifier

T_a = Front time of the impulse
T_{av} = Front time of the amplifier

Sweep rate = 20 ns/cm

The low-voltage step-function response of the 0·2-MV measuring system at a sweep rate of 20 ns per cm is illustrated by Fig. 27. From the oscillogram it can be seen that response impulse has a corrected front time of 24 ns and a time constant of $\tau = 15$ ns. Fig. 28a is the oscillogram of the 97-kV step-function response recorded by the fast-sweep oscillograph with a 1·0 μs logarithmic time-base, Fig. 28b shows calibration of the 1 μs time-base with a 5-Mc/s oscillation. In order to obtain a clear trace of such rapid phenomena, a special high-brightness aluminium cathode is used.

The high-voltage step-function response shown in Fig. 28a gives the same front time $T_a = 24$ ns—which does not have to be corrected in this case—and time constant $\tau = 15$ ns. The results of calibrating the 0·2-MV measuring system conclusively prove the suitability of the newly developed high-voltage step-function generator. This generator produces impulses with a very steep front, having a front time of about 5 ns, which can be considered almost rectangular. If the generator were to produce impulses which were less steep—say, with a front time of 10 ns—the response of the 0·2-MV system would be distorted, owing to its short time constant τ.

The low-voltage step-function response of the 0·9-MV system is shown in Fig. 29, using a sweep rate of 40 ns/cm. Here the time constant of the response works out to $\tau = 23$ ns. Fig. 30 shows the l.v. response of the 2·3-MV system with a 7-m h.v. lead. The excellent screening of the voltage divider and the choice of a suitable damping resistor enabled a time constant of only $\tau = 32·6$ ns to be attained by the step-function response, a slight overswing of

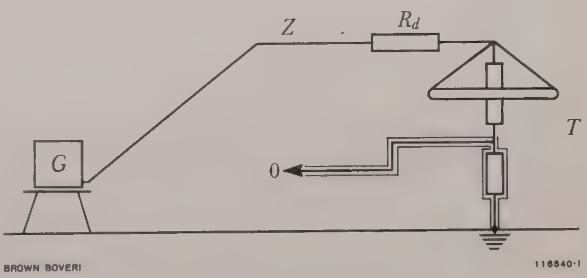

Fig. 26. – Experimental set-up for calibrating an impulse measuring system with a step-function impulse

G = Step-function generator
Z = H.V. lead
R_d = Damping resistance of the measuring system
T = Voltage divider
O = Oscillograph

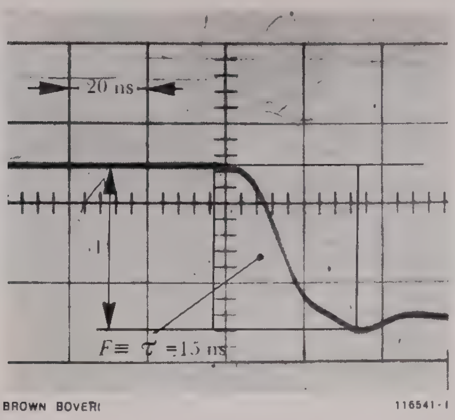

Fig. 27. – Calibrating the 0·2-MV measuring system with a low-voltage step-function impulse

τ = Time constant of 15 ns for the step-function response at a sweep rate of 20 ns/cm

the response curve beyond the final value 1 during the first 160 ns proving advantageous. Fig. 31 a shows the response to a 110-kV step-function impulse with a sweep rate of 0·5 μs/cm; Fig. 31 b showing the calibration with a 10-Mc/s oscillation. From the h.v. response the time constant τ = 33 ns is practically the same as before.

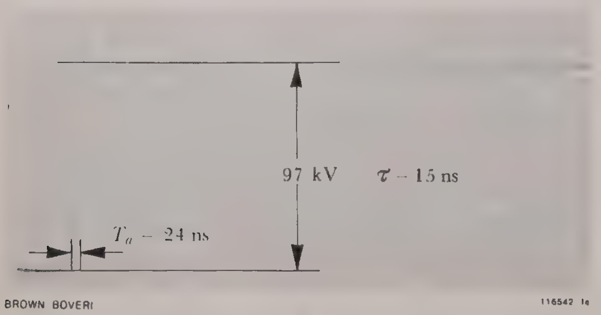

a

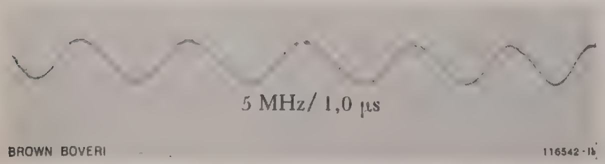

b

Fig. 28. – Calibrating the 0·2-MV measuring system with a high-voltage step-function impulse at 97 kV

a: Step-function response with τ = 15 ns and T_a = 24 ns (front time)

b: Calibrating the logarithmic sweep rate with a 5-Mc/s oscillation

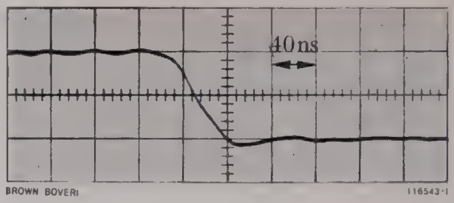

Fig. 29. – Calibrating the 0·9-MV measuring system with a low-voltage step-function impulse

Time constant τ = 23 ns of the response with a sweep rate of 40 ns/cm

The error of the 0·2, 0·9 and 2·3-MV systems is plotted against the chopping time of a linear steep-front impulse in Fig. 32. Even without any correction of the system error, the newly developed systems permit steep-front waves chopped after 0·5 μs to be measured with an inaccuracy not exceeding 6 to 7 %. When allowance is made for the correction determined during calibration, the same impulses can be measured to an accuracy of 2 %, this figure also taking into account the inaccuracy inherent in the evaluation of the oscillograms. The system error for full-wave measurements is so small for all three systems (see equation 19) that it is only necessary to allow for the inaccuracy of the oscillogram in practice.

Owing to the importance of knowing exactly what properties the new measuring systems possess, the error of the 2·3-MV system was also determined from the frequency response, as described on p. 248 to 251. We were accordingly faced with the problem of determining the amplitude and phase angle of two voltages in the proportions 1 : 1000 in the visualized frequency range between 0 and 30 Mc/s, with corresponding accuracy.

Whereas measurement of the amplitude is not particularly difficult and can be performed with the aid of a suitable tube voltmeter or, better still, a broad-band oscillograph, simultaneously calibrating the sensitivity for the various ranges, a sufficiently accurate method of determining the phase displacement in the frequency range 0–30 Mc/s has not been discovered yet. Hence our first attempts at determining the phase displacement from the Lissajous figures obtained with the oscillograph were unsuccessful because the horizontal amplifier of the oscillograph did not possess the necessary bandwidth and determination of the phase angle from the Lissajous figures proved inaccurate. A satisfactory answer could only be obtained when a broad-band differential amplifier was used, which permitted the measurement of an alternating voltage U_1 or U_2, and their vectorial difference $(\overline{U}_1 - \overline{U}_2)$, even when they were very different in magnitude, e.g.

$$\frac{|U_1|}{|U_2|} \approx \frac{1000}{1}$$

The suitability and measuring accuracy of the differential amplifier were checked at frequencies between 0 and 40 Mc/s on systems having a known phase displacement, such as coaxial cables. The inaccuracy of the measurement at frequencies up to 10 Mc/s amounts to about ±1%, above that about ±2%. The higher accuracy at the lower frequencies is, moreover, particularly favourable because the higher frequencies ($f > 10$ Mc/s) only contribute a small share to the system error with steep-front impulses and may therefore be determined with less accuracy.

The angle $\Phi(f)$ can be measured, as in Fig. 33, from the input and output voltages U_A and U_B of a system, as indicated by the oscillograph at a frequency f, and from their vectorial difference $\overline{U}_A - \overline{U}_B$:

$$\Phi(f) = \arc\cos \frac{|U_A|^2 + |U_B|^2 - |\overline{U}_A - \overline{U}_B|^2}{2\,|U_A| \cdot |U_B|} \qquad (86)$$

The known phase displacement Φ_K of the test leads at a corresponding frequency must then be deducted from the phase displacement Φ.

A further advantage of the differential amplifier is that, simultaneously with the phase displacement, it also gives the amplitude, which can be deter-

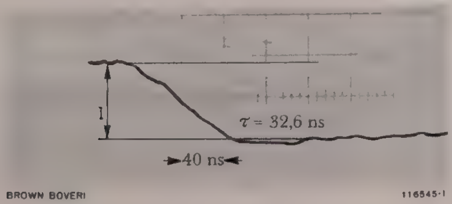

Fig. 30. – Calibrating the 2·3-MV measuring system with a low-voltage step-function impulse

τ = Time constant of the step-function response = 32·6 ns at a sweep rate of 40 ns/cm

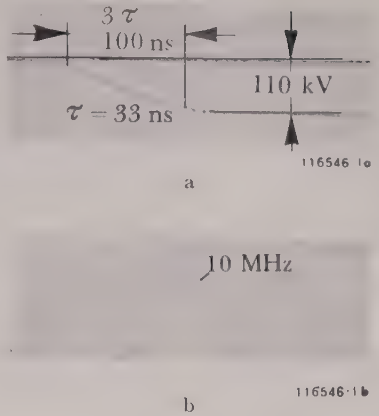

Fig. 31. – Calibrating the 2·3-MV measuring system with a high-voltage step-function impulse at 110 kV

a: Time constant of the step-function response $\tau = 33$ ns

b: Calibrating the logarithmic sweep rate of 0·5 μs with a 10-Mc/s oscillation

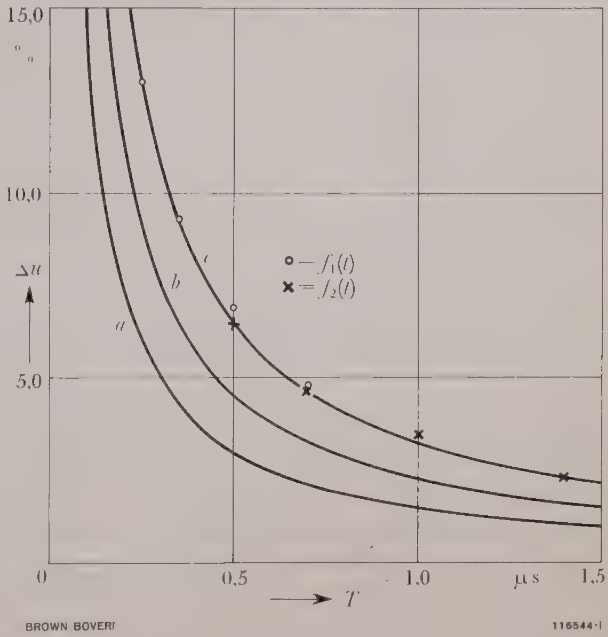

Fig. 32. – System error of the 0·2, 0·9 and 2·3-MV measuring systems with a linear steep-front wave

a = 0·2-MV system

b = 0·9-MV system

c = 2·3-MV system

Δu = Percentage system error

T = Chopping time

The curves drawn were determined from the step-function response

o × = Points obtained by resolving the functions $f_1(t)$ and $f_2(t)$ according to Fourier

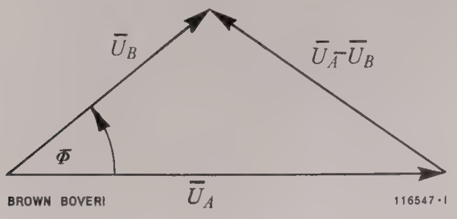

Fig. 33. – Determination of the phase displacement of an impulse measuring system

$\bar{U}_A$ = Voltage applied to the measuring system and conveyed to input '*A*' of the differential amplifier (see Fig. 34)

$\bar{U}_B$ = Voltage tapped off divider, conveyed to input '*B*' of differential amplifier

Φ = Angle between $\bar{U}_A$ and $\bar{U}_B$

mined from the ratio $|U_A|/|U_B|$ when the sensitivity of the oscillograph is suitably calibrated.

Fig. 34 shows the experimental set-up for measuring the frequency response of the 2·3-MV system. In order to obtain in the desired frequency range a voltage of adequate amplitude at the tapping point, a frequency generator with a broad-band (video) amplifier was used from 0–5 Mc/s, above that a 300-W transmitter, 0–10 kV, with interchangeable sets of coils for frequencies up to 30 Mc/s. The output voltage of the frequency generator G_f or the broad-band amplifier was applied to the input '*A*' of the differential amplifier, to which the h.v. lead of the measuring system is also connected. The voltage tapped off the divider was applied through the cable to the input '*B*' of the differential amplifier. The frequency was accurately set by means of a crystal wavemeter *F* and for each series of readings the voltages U_A, U_B and their vectorial difference were oscillographed. The constancy of the applied voltage during a series of measurements at a frequency *f* was supervised with a tube voltmeter *V*. The curves of amplitude $A(f)$ and phase angle $\Phi(f)$ of the frequency response so obtained are reproduced in Fig. 35 and 36. As Fig. 35 shows, the amplitude curve, in addition to exhibiting a weak "resonance frequency" at 3 Mc/s due to the inductance of the h.v. lead and the screen capacitance of the divider, indicates a second, pronounced resonance at 15 Mc/s. This is the resonance frequency of the h.v. lead itself, i.e. of its capacitance to earth C_z with the inductance L_z. The main resonance frequency of the h.v. lead, which is treated as a chain system, is

$$f_{r_z} = \frac{1}{\pi \sqrt{C_z \cdot L_z}} \tag{87}$$

For a 7-m lead with $l_z = 1{\cdot}25$ μH/m and $c_z = 8{\cdot}33$ pF/m

$$f_{r_z} = \frac{1 \cdot 10^9}{\pi \cdot 7{\cdot}0 \sqrt{1{\cdot}25 \cdot 8{\cdot}33}} = 14 \text{ Mc/s}$$

The effect of this resonance frequency on the error of the measuring system, as may be gathered from equations (61) and (63), is only slight. From the amplitude and phase angle characteristics of the frequency response, given by equations (62) and (63), taking into account the correction according to equation (70) to (73), the system error was calculated for different chopping times *T* with a linear steep-front wave and plotted in Fig. 32. As can be seen, the system error thus obtained agrees very well with the corresponding figures from the step-function method.

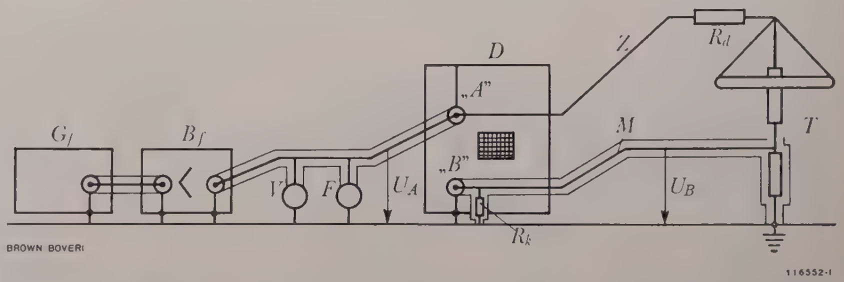

Fig. 34. – Schematic layout of a system for measuring the amplitude and phase angle of the frequency response

G_f = Frequency generator
B_f = Broad-band amplifier
V = Tube voltmeter
F = Wave-meter
D = Differential amplifier with inputs '*A*' and '*B*'
Z = High-voltage lead
R_d = Damping resistance
T = Voltage divider
M = Measuring cable
R_k = Terminating resistance of measuring cable
$\bar{U}_A$ = Applied voltage
$\bar{U}_B$ = Voltage tapped off divider

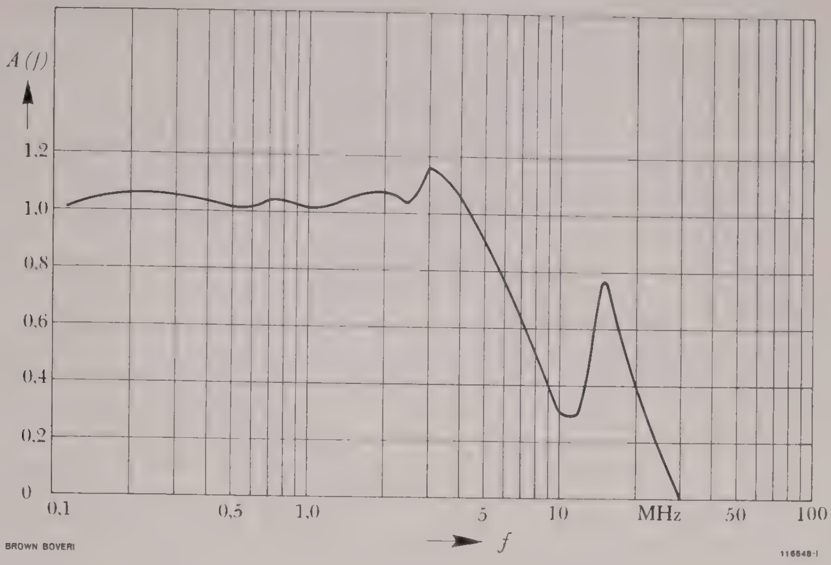

Fig. 35. – Amplitude of the 2·3-MV measuring system

$A(f)$ = Amplitude ratio
f = Frequency

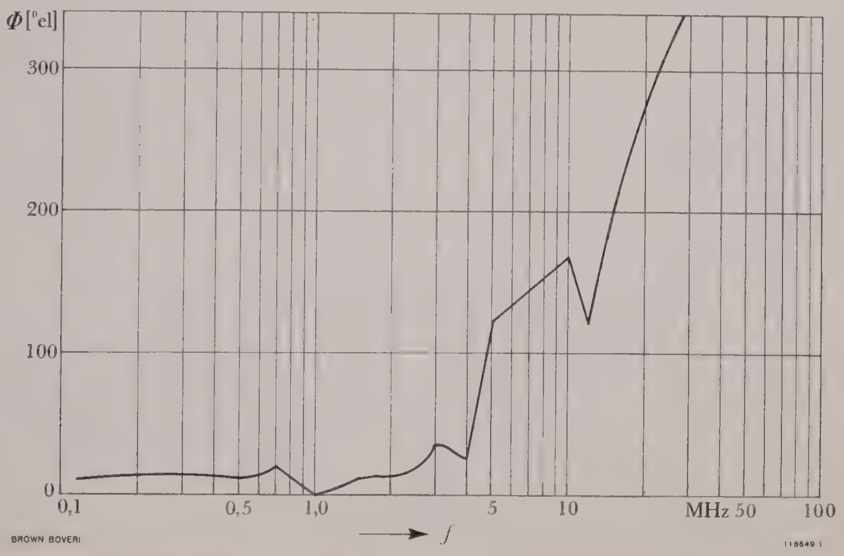

Fig. 36. – Phase angle of the 2·3-MV measuring system

$\Phi(f)$ = Phase displacement
f = Frequency

Finally, the step-function response of the system will be determined from the frequency response by the method described on p. 253–5. The curve of the function $\mathrm{Re}(2\pi f)$ calculated from equation (77) on p. 253 is plotted in Fig. 37. The curve was approximated by 11 straight lines, and for each of these parts the corresponding partial step-function response as in equation (82) was determined with the aid of the inverse function $\eta(f_2 t)$ shown in Fig. 17a and b on p. 254, duly observing that horizontal parts of the curve of $\mathrm{Re}(2\pi f)$ do not render any contribution to the step-function response. The individual parts of the step-function response are

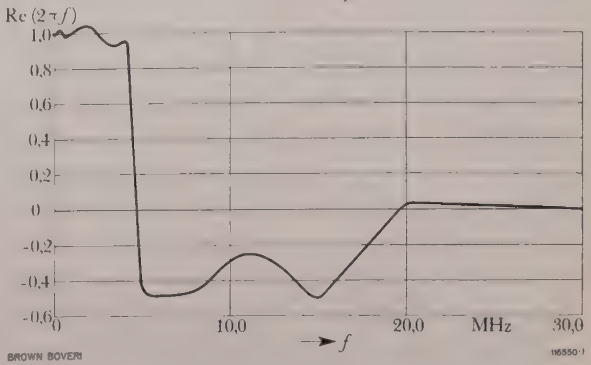

Fig. 37. – Curve of the function Re(2πf) of the 2·3-MV measuring system

f = Frequency

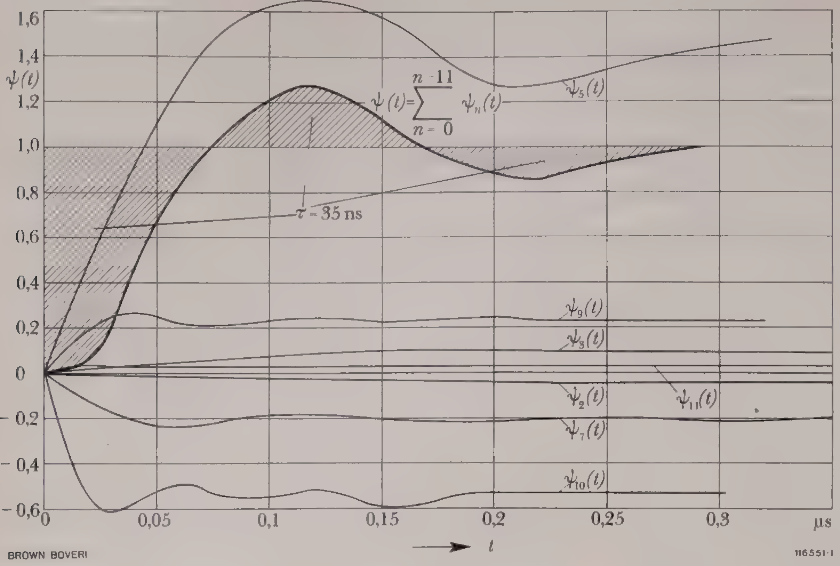

Fig. 38. – Result of the mathematical derivation of the step-function response of the 2·3-MV system from its frequency response

$\psi_1(t) \ldots \psi_{11}(t)$ = Partial step-function responses
$\psi(t)$ = Resultant with time constant $\tau = 35$ ns
t = Time

shown together with the resultant response in Fig. 38. From this curve a time constant of $\tau = 35$ ns can be derived which, allowing for the graphical approximation method used, agrees very well with the directly recorded step-function response of $\tau = 32{\cdot}6$ ns (Fig. 30).

The close agreement between these results also conclusively proves the high accuracy of the 2·3-MV impulse-voltage measuring system, as well as the suitability and correctness of the newly developed method of calibration.

In conclusion, the following statement can be made regarding the application of the two methods of determining the error of a system for measuring impulse voltages:

The low and high-voltage step-function method is without doubt the simpler and leads more quickly to a result; it will therefore prove particularly suitable for checking or proving the accuracy of a laboratory built set-up before impulse tests are commenced. On the other hand the frequency-response method provides a clear picture of the effect which changing individual elements of a measuring system has on the system error, because certain details can be more clearly analysed. This method can therefore prove very helpful, particularly for experiments during development and research work on systems for measuring impulse voltages. Likewise, this method can be recommended as a supplementary means of calibrating measuring systems which may be intended as a replacement for the sphere gap, and whose electrical and spatial layout is more or less fixed (known as sub-standards). The improvement effected and the progress made in the measurement of impulse voltages enable the Company to achieve maximum possible accuracy, not only during research and development, but also during acceptance tests on high-voltage equipment produced in the factory, thereby helping to consolidate the confidence in Brown Boveri products and test methods.

(KME) A. AŠNER

Appendix I

Proof of the Identity of Sine Impulses of the Fourier Series According to Equation (45), p. 249, and the Linear Steep-Front Wave in the Interval 0—T

For the $(2n+1)$th sine impulse the Fourier coefficient $b^*(\omega)$ is

$$b^*(\omega)_{2n+1} = U \cdot \frac{1}{\pi} \cdot (-1)^n \int_0^T \sin\left[(2n+1) \cdot \frac{\pi}{2T} t\right] \sin \omega t \, dt$$

$$= -U \cdot \frac{1}{\pi} \cdot \frac{\omega \cos \omega T}{\left(\omega^2 - \frac{(2n+1)^2 \pi^2}{4T^2}\right)} \qquad (1\text{a})$$

and for the coefficient of the sum of all sine impulses

$$b^*(\omega) =$$

$$= \sum_{n=0}^{n=\infty} -\frac{1}{\pi} \cdot U \cdot \frac{8}{(2n+1)^2\,\pi^2} \cdot \frac{\omega \cos \omega T}{\omega^2 - \dfrac{(2n+1)^2\,\pi^2}{4T^2}} \tag{2a}$$

By substituting

$$K^2 = \frac{\omega^2\, 4T^2}{\pi^2} \tag{3a}$$

and resolving

$$\frac{1}{(2n+1)^2} \cdot \frac{1}{K^2 - (2n+1)^2} =$$

$$= \frac{1}{K^2} \left[\frac{1}{(2n+1)^2} + \frac{1}{K^2 - (2n+1)^2} \right] \tag{4a}$$

equation (2a) becomes

$$b^*(\omega) =$$

$$= \sum_{n=0}^{n=\infty} - U \cdot \frac{1}{\pi} \cdot \frac{8\omega \cos \omega T}{\pi^2\, \omega^2} \left[\overbrace{\frac{1}{(2n+1)^2}}^{\text{I}} + \overbrace{\frac{1}{K^2 - (2n+1)^2}}^{\text{II}} \right] \tag{5a}$$

For part I we find

$$-\sum_{n=0}^{n=\infty} \frac{1}{(2n+1)^2} = -\frac{\pi^2}{8} \tag{6a}$$

$$b_{\text{I}}^*(\omega) = -U \cdot \frac{1}{\pi} \cdot \frac{8\omega \cos \omega T}{\pi^2\, \omega^2} \cdot \frac{\pi^2}{8} =$$

$$= -U \cdot \frac{1}{\pi} \cdot \frac{\cos \omega T}{\omega} \tag{7a}$$

For part II the sum is calculated as follows

$$\sum_{n=0}^{n=\infty} \frac{1}{K^2 - (2n+1)^2}$$

If in equation (51) on page 249 we first substitute $x = 0$, and then $x = \pi$, and subtract the one equation from the other, we obtain

$$f(x)_{x=0} - f(x)_{x=\pi} =$$

$$= \frac{4u \sin \pi u}{\pi} \left(\frac{1}{u^2 - 1} + \frac{1}{u^2 - 3^2} + \frac{1}{u^2 - (2n+1)^2} + \dots \right) \tag{8a}$$

The desired sum is then

$$\sum_{n=0}^{n=\infty} \frac{1}{K^2 - (2n+1)^2} = \frac{(\cos \pi u - 1)}{4u \sin \pi u} \tag{9a}$$

in which

$$u = K = \frac{2T\omega}{\pi} \tag{10a}$$

For $b_{\text{II}}^*(\omega)$ we obtain

$$b_{\text{II}}^*(\omega) =$$

$$= -U \cdot \frac{1}{\pi} \cdot \frac{8\omega \cos \omega T}{\pi^2\, \omega^2} \cdot \frac{\pi^2}{8T\omega} \cdot \frac{-2 \sin^2 \omega T}{2 \sin \omega T \cos \omega T} =$$

$$= \frac{1}{\pi} \cdot U \cdot \frac{\sin \omega T}{T \omega^2} \tag{11a}$$

Summarizing we obtain the following for the coefficient $b^*(\omega)$

$$b^*(\omega) =$$

$$= b_{\text{I}}^*(\omega) + b_{\text{II}}^*(\omega) = U \cdot \frac{1}{\pi} \left[-\frac{\cos \omega T}{\omega} + \frac{\sin \omega T}{T \omega^2} \right] \tag{12a}$$

i.e. the same as in equation (48), page 249. Hence $b(\omega) \equiv b^*(\omega)$.

For the coefficient $a^*(\omega)$ we obtain

$$a^*(\omega) = U \cdot \frac{1}{\pi} \cdot \frac{8}{\pi^2} \sum_{n=0}^{n=\infty} \frac{1}{(2n+1)^2} \cdot$$

$$\cdot \frac{\overbrace{\omega \sin \omega T}^{\text{I}} - \overbrace{(-1)^n (2n+1) \cdot \dfrac{\pi}{2T}}^{\text{II}}}{\omega^2 - (2n+1)^2 \cdot \dfrac{\pi^2}{4T^2}} \tag{13a}$$

Taking equations (4a) and (9a) into account, this works out to

$$a_{\text{I}}^*(\omega) = U \cdot \frac{\omega \sin \omega T}{\pi} \cdot$$

$$\cdot \frac{8}{\pi^2} \cdot \frac{1}{\omega^2} \sum_{n=0}^{n=\infty} \left(\frac{1}{K^2 - (2n+1)^2} + \frac{1}{(2n+1)^2} \right)$$

$$= U \left\{ \frac{1}{\pi} \cdot \frac{1}{\omega^2 T} \left(-\frac{1}{\cos \omega T} + \cos \omega T + \frac{1}{\pi \omega} \sin \omega T \right) \right\} \tag{14a}$$

For the part $a_{\text{II}}^*(\omega)$, identity, i.e.

$$a_{\text{II}}^*(\omega) = U \cdot \frac{1}{\pi} \left[\frac{1}{T \omega^2} \left(\frac{1}{\cos \omega T} - 1 \right) \right] \equiv$$

$$\equiv -U \cdot \frac{1}{\pi} \cdot \frac{8}{\pi^2} \sum_{n=0}^{n=\infty} \frac{(-1)^n \cdot \dfrac{\pi}{2T}}{(2n+1) \left[\omega^2 - \dfrac{(2n+1)^2\,\pi^2}{4T^2} \right]} \tag{15a}$$

can be proved as follows.

The Mittag-Leffler development of the function $\frac{1}{\cos Z}$ is [16]:

$$\frac{1}{\cos Z} = 4\pi \sum_{n=0}^{n=\infty} \frac{(-1)^n (2n+1)}{(2n+1)^2 \pi^2 - 4Z^2} =$$

$$= 4\pi \left(\frac{1}{\pi^2 - 4Z^2} - \frac{3}{9\pi^2 - 4Z^2} + \cdots \right) \quad (16a)$$

When $Z = \omega T$ equation (15a) can be converted as follows:

$$U \cdot \frac{1}{\cos Z} =$$

$$= U \left(1 + 4\pi \sum_{n=0}^{n=\infty} \frac{(-1)^n 4Z^2}{\pi^2 (2n+1) \left[(2n+1)^2 \pi^2 - 4Z^2 \right]} \right) \quad (17a)$$

Following partial resolution

$$U \cdot \frac{1}{\cos Z} =$$

$$= U \left(1 + 4\pi \sum_{n=0}^{n=\infty} \frac{(-1)^n (2n+1)}{(2n+1)^2 \pi^2 - 4Z^2} - 4\pi \sum_{n=0}^{n=\infty} \frac{(-1)^n}{(2n+1)} \right) \quad (18a)$$

with the Leibniz series

$$\sum_{n=0}^{n=\infty} \frac{(-1)^n}{(2n+1)} = 1 - \frac{1}{3} + \frac{1}{5} - \cdots = \frac{\pi}{4} \quad (19a)$$

we obtain equation (16a) from equation (18a), thus proving the identity (15a). By combining equations (14a) and (15a) we obtain

$$a^*(\omega) = a_{\mathrm{I}}^*(\omega) + a_{\mathrm{II}}^*(\omega) =$$

$$= U \cdot \frac{1}{\pi} \left[\frac{1}{\omega} \sin \omega T + \frac{1}{T\omega^2} (\cos \omega T - 1) \right] \quad (20a)$$

This is identical with equation (47) on page 249; hence $a^*(\omega) \equiv a(\omega)$ and the sum of the sinusoidal impulses according to equation (45) in the interval $0 - T$ is identical with the linear steep-front impulse.

Appendix II

Determination of the Inverse Functions $\eta(f_2 t)$ and $\zeta(f_2 t)$ for Derivation of the Step-Function Response from the Frequency Response of the Measuring System

The function $\mathrm{Re}(2\pi f)$ or $\mathrm{Im}(2\pi f)$ is assumed to conform to Fig. 39a. This can then be represented by the two parts in Fig. 39b and c. With the notation corresponding to equations (79) to (81), p. 253, in which

$$a(t) = \frac{1}{\pi} \int_0^\infty \frac{\mathrm{Re}(2\pi f)}{2\pi f} \sin 2\pi f t \, \mathrm{d}(2\pi f) \quad (21a)$$

$$\beta(t) = \frac{1}{\pi} \int_0^\infty \frac{\mathrm{Im}(2\pi f)}{2\pi f} \cos 2\pi f t \, \mathrm{d}(2\pi f) \quad (22a)$$

the shape of $\mathrm{Re}(2\pi f)$ or $\mathrm{Im}(2\pi f)$ in Fig. 39a is given by

$$a(t) =$$

$$= \frac{1}{\pi} \left(\int_0^{f_1} \frac{1}{2\pi f} \sin 2\pi f t \, \mathrm{d}(2\pi f) - \int_0^{f_1} \frac{\sin 2\pi f t}{2\pi f_1} \mathrm{d}(2\pi f) \right) =$$

$$= \frac{1}{\pi} \left(\mathrm{Si}(2\pi f_1 t) - \frac{1 - \cos 2\pi f_1 t}{2\pi f_1 t} \right) \quad (23a)$$

$$\beta(t) =$$

$$= \frac{1}{\pi} \left(\int_0^{f_1} \frac{1}{2\pi f} \cos 2\pi f t \, \mathrm{d}(2\pi f) - \int_0^{f_1} \frac{\cos 2\pi f t}{2\pi f_1} \mathrm{d}(2\pi f) \right) =$$

$$= \frac{1}{\pi} \left(\mathrm{Ci}(2\pi f_1 t) - \frac{\sin 2\pi f_1 t}{2\pi f_1 t} \right) \quad (24a)$$

For a shape of $\mathrm{Re}_0(2\pi f)$ or $\mathrm{Im}_0(2\pi f)$ as in Fig. 40a, which may be treated as a superposition of the two functions $\mathrm{Re}_1(2\pi f)$ and $\mathrm{Re}_2(2\pi f)$, or $\mathrm{Im}_1(2\pi f)$ and $\mathrm{Im}_2(2\pi f)$ as in Fig. 40b and 40c, with the limiting frequencies f_1 and f_2, and the part of the function $\mathrm{Re}(2\pi f)$ or $\mathrm{Im}(2\pi f)$ approximated by a straight line to correspond with Fig. 16

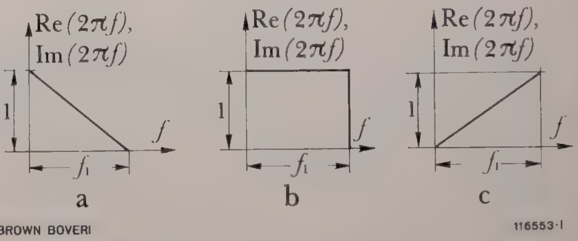

Fig. 39. – For the mathematical derivation of the inverse functions for a linearly decreasing curve of Re (2πf) or Im (2πf)

f = Frequency

f_1 = Limiting frequency

The curve 'a' is obtained as the difference between 'b' and 'c'.

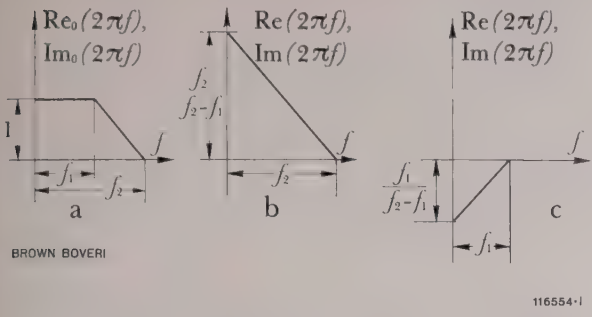
$\mathrm{Re}_0(2\pi f)$, $\mathrm{Im}_0(2\pi f)$
1
f_1
f_2
f
a
$\mathrm{Re}(2\pi f)$, $\mathrm{Im}(2\pi f)$
$\frac{f_2}{f_2-f_1}$
f_2
f
b
$\mathrm{Re}(2\pi f)$, $\mathrm{Im}(2\pi f)$
$\frac{f_1}{f_2-f_1}$
f_1
f
c
BROWN BOVERI
116554·I

Fig. 40. – For the mathematical derivation of the inverse functions for the part of the function Re $(2\pi f)$ or Im $(2\pi f)$ approximated by a straight line

f = Frequency
f_1 and f_2 = Limiting frequencies

The function 'a' is obtained by superposing 'b' on 'c'.

$$\eta(t) = \frac{f_2}{f_2 - f_1} \cdot \frac{1}{\pi} \left(\mathrm{Si}(2\pi f_2 t) - \frac{1 - \cos 2\pi f_2 t}{2\pi f_2 t} \right) - \\ - \frac{f_1}{f_2 - f_1} \cdot \frac{1}{\pi} \left(\mathrm{Si}(2\pi f_1 t) - \frac{1 - \cos 2\pi f_1 t}{2\pi f_1 t} \right) \quad (25\,\mathrm{a})$$

Following conversion we obtain

$$\eta(t) = \eta(f_2 t) = \\ = \frac{1}{\pi} \left\{ \frac{1}{1 - \frac{f_1}{f_2}} \left[\mathrm{Si}(2\pi f_2 t) - \frac{1 - \cos 2\pi f_2 t}{2\pi f_2 t} \right] - \right. \\ \left. - \frac{\frac{f_1}{f_2}}{1 - \frac{f_1}{f_2}} \left(\mathrm{Si}\left(\frac{f_1}{f_2} 2\pi f_2 t \right) - \frac{1 - \cos \frac{f_1}{f_2} 2\pi f_2 t}{\frac{f_1}{f_2} 2\pi f_2 t} \right) \right\} \quad (26\mathrm{a})$$

With similar notation the inverse function $\zeta(f_2 t)$ is given by

$$\zeta(t) = \zeta(f_2 t) = \\ = \frac{1}{\pi} \left\{ \frac{1}{1 - \frac{f_1}{f_2}} \left[\mathrm{Ci}(2\pi f_2 t) - \frac{\sin 2\pi f_2 t}{2\pi f_2 t} \right] - \right. \\ \left. - \frac{\frac{f_1}{f_2}}{1 - \frac{f_1}{f_2}} \left[\mathrm{Ci}\left(\frac{f_1}{f_2} 2\pi f_2 t \right) - \frac{\sin \frac{f_1}{f_2} 2\pi f_2 t}{\frac{f_1}{f_2} 2\pi f_2 t} \right] \right\} \quad (27\mathrm{a})$$

The inverse functions were calculated for different values of $f_2 t$ with f_1/f_2 as parameter with the help of the function tables of Jahnke and Emde [17] and plotted in Fig. 18a–d. The partial step-function responses of the curve of $\mathrm{Re}(2\pi f)$ or $\mathrm{Im}(2\pi f)$ represented by a straight line in Fig. 16 can be determined with the aid of the above functions.

Bibliography

[1] K. Berger: Comparative Tests on Spark-Gaps. Report on the work of Study Committee No. 8. CIGRE Report No. 326, 1956.

[2] R. Elsner: Die Messung steiler Hochspannungsstösse mittels Spannungsteiler. Arch. Elektrotech. 1939, Vol. 33, No. 1.

[3] P. R. Howard: Errors in Recording Surge Voltages. Proc. Inst. Elect. Engrs, 1952, Vol. 99, II/70, p. 371–83.

[4] J. Hagenguth: Short-time spark-over of gaps. Elect. Engng, 1937, Vol. 56, p. 67.

[5] Goossens and Provost: Fehlerquellen bei der Registrierung hoher Stossspannungen mit dem Kathodenstrahl-Oszillographen. Bull. schweiz. elektrotech. Ver. 1946, Vol. 37, No. 7, p. 175–84.

[6] A. Liechti: Spannungsteiler in Stossanlagen. Micafil-Nachr. 1945.

[7] P. L. Bellaschi: The Measuring of High-Surge Voltages. Trans. Amer. Inst. Elect. Engrs, 1933, Vol. 52, p. 545.

[8] A. F. Rohlfs, J. S. Kresge, F. A. Fisher: The Response of Resistance Voltage Dividers to Steep-Front Impulse Waves. Trans. Amer. Inst. Elect. Engrs, 1957, Vol. 76/I, p. 634–46.

[9] M. Oeszkaya: Über Messfehler bei der Stossspannungsmessung mit Spannungsteiler und Oszillographen. Techn. Ber. No. 186 of the Studiengesellschaft für Höchstspannungsanlagen dated 30 June 1958.

[10] I. H. Park: Surge Measurement Errors Introduced by Coaxial Cables. Trans. Amer. Inst. Elect. Engrs, 1958, Vol. 77/I, p. 343–50.

[11] C. J. Miller and J. F. Wittibschlager: Measurements of Steep-Front Impulse Waves with an Isolated Screen Room Installation. Trans. Amer. Inst. Elect. Engrs, 1958, Vol. 77/I, p. 262–71.

[12] A. Ašner: Neue Erkenntnisse über die Messung sehr hoher, rasch veränderlicher Stossspannungen mittels Spannungsteiler. Thesis ETH, Zurich, No. 2975, 1960.

[13] K. W. Wagner: Operatorenrechnung und Laplacesche Transformation. Barth-Verlag, Leipzig 1950.

[14] C. F. Creed: The measurement of impulse waves chopped on the front. CIGRE Report No. 320, 1958.

[15] O. Burawoy: Funkenverzögerung bei Spannungsstössen von sehr kurzer Dauer. Arch. Elektrotech., 1926, Vol. 16, No. 3, p. 186–219.

[16] E. T. Whittacker and G. N. Watson: A Course of Modern Analysis. 4th Ed. Cambridge 1946, p. 136.

[17] E. Jahnke and F. Emde: Tables and Functions with Formulae and Curves. Dover Publications, New York 1945.

MEASURING THE ACTIVE POWER LOSSES OF LARGE REACTORS

621.317.384:621.318.43

The usual methods for measuring the active power at high voltage fail with reactors, because the errors inherent in the test circuit falsify the results. For this reason a bridge circuit of higher accuracy was developed. The new process is generally applicable for the measurement of impedance, phase displacement, active and apparent power at high voltage and very small inductive power factors ($0{\cdot}001 < \cos\varphi < 0{\cdot}1$).

FOR MEASURING the active and apparent power with high voltage it is usual to employ ammeters, voltmeters and wattmeters which are connected through current and voltage transformers. The measuring accuracy depends on the accuracies of the five above-mentioned elements; for exacting demands, apparatus of the class 0·1 (i.e. 0·1% error at full reading) is used, with known error curves which have to be taken into consideration during the evaluation of the measurements.

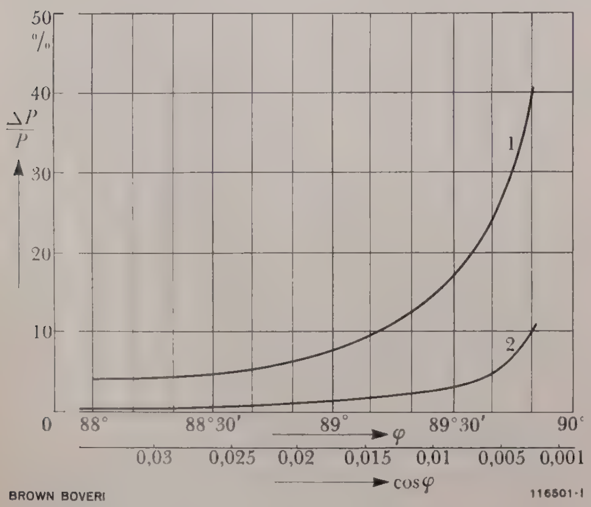

Fig. 1. – Percentage error $\frac{\Delta P}{P} \cdot 100$ in the measurement of active power in function of the phase angle φ between current and voltage

at constant transformation errors of the measuring circuit $\Delta\varphi = 5'$ (curve 1) and $\Delta\varphi = 1'$ (curve 2), respectively.

With very small power factors, e.g. at almost 90° lagging current, limits are imposed on this process. As is well known, the measured effective power is burdened with a systematic error, which grows with increasing phase displacement. The following consideration furnishes the magnitude of this error. The wattmeter indication is proportional to the product of the currents (i, $k \cdot u$) in its current and voltage coils, and the cosine of the phase angle φ' between currents, i.e.

$$P = C \cdot k \cdot u \cdot i \cdot \cos\varphi' \tag{1}$$

The currents in the wattmeter do not correspond exactly to those in the system, but differ from them by Δi and $k \,.\, \Delta u$, respectively; the phase angle between the wattmeter currents is also different from the phase angle between the current and voltage of the system by the error angle $\Delta\varphi$. These errors are caused mainly by the deviations of the values of the instrument transformers from the true values.

The absolute error of the active power measurement, by considering the individual errors Δu, Δi and $\Delta\varphi$ is

$$\begin{aligned}\Delta P &= \frac{\partial P}{\partial u}\Delta u + \frac{\partial P}{\partial i}\Delta i + \frac{\partial P}{\partial \varphi}\Delta\varphi = \\ &= C \cdot k\,(i\cos\varphi\,\Delta u + u\cos\varphi\,\Delta i - u\,i\sin\varphi\,\Delta\varphi) \qquad (2)\end{aligned}$$

and the relative error, expressed in percent

$$\frac{\Delta P}{P} \cdot 100 = 100\left(\frac{\Delta i}{i} + \frac{\Delta u}{u} - \tan\varphi\,\Delta\varphi\right) \tag{3}$$

The first two terms in equation (3) for the percentage error are independent of the phase angle φ between current and voltage; e.g. by using instrument transformers of the class 0·1 the error produced by both of them cannot be more than 0·2%. Therefore equation (3) becomes approximately

$$\left|\frac{\Delta P}{P}\right| \cdot 100 \approx 100\tan\varphi\,\Delta\varphi \tag{3a}$$

Equation (3) is represented in Fig. 1 by curves for $\Delta\varphi = 5'$ and $\Delta\varphi = 1'$, respectively, where $\Delta\varphi$ is the transformation error of the measuring circuit. It can be seen that, at phase angles of more than $\varphi = 85°$, an angular error of a few minutes in the measuring system causes considerable errors in measurement. The problem of the measurement of active power at very low power factors ($0{\cdot}001 < < \cos\varphi < 0{\cdot}1$, see also Fig. 1), is of practical significance in connection with the measurement of the active losses of large reactors, which are being used more and more as parallel inductances for stabilizing long extra-high-voltage transmission lines. Similar conditions also exist during short-circuit tests on large high-voltage transformers.

In order to take the errors discussed above into consideration, the complete measuring circuit, i.e. the instrument transformers with the instruments connected and the leads already laid out, must be calibrated at rated conditions with an accuracy of at least $\pm 1'$. This would lead to intolerable complications; before every measurement the calibrating instrument transformer and the test apparatus would have to be transported to the place of measurement and set up.

In addition to the transformation error already mentioned, there are the errors inherent in the wattmeter itself. As a result of the inductance of the voltage coil, the current lags the voltage by at least $1'$. Besides, the error in the reading of the wattmeter could be considerable, for although modern instruments can be heavily overloaded, the maximum wattmeter deflection at power factors of the order of $\cos\varphi = 0{\cdot}001$ amounts to only a small fraction of the full deflection.

These difficulties led to the search for another principally different method for measuring the active power at high voltages, heavy currents and very small lagging power factors.

Different Methods of Measurement

Classical Bridge Connections

In principle, the phase displacement φ between current and voltage can be measured in a bridge circuit. Multiplying the power factor so obtained by the apparent power, which can be easily measured, gives the active power. There are a number of a.c. bridges which can be employed to measure the inductances, e.g. the Wien, Maxwell and Hay bridges. None of the classical bridge connections, however, is suited for the present conditions—heavy current and at the same time high voltage. The Maxwell bridge connection can be seen in Fig. 2. Here the total test current flows through the resistance R_3. This resistance must be non-inductive (time constant $L/R < 10^{-7}$ s), otherwise the voltage drop in it will not be in phase with the test current. A few volts are necessary for balancing the bridge, i.e. with a current of say 100 A there would be a resistance of

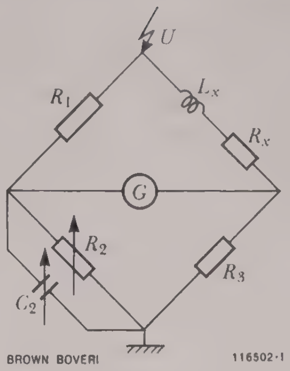

Fig. 2. – The Maxwell bridge

L_x, R_x = Test object, G = Galvanometer.

Note: the whole current in the object flows through R_3; the voltage drops across the divider R_1, R_2.

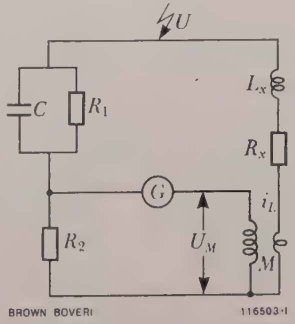

Fig. 3. – The Wilkinson-Carter bridge for the measurement of the active power of reactors

L_x, R_x = Test object.

Note: The secondary voltage U_M of the mutual inductance M is proportional to the reactor current i_L; the voltage U drops across the ohmic divider R_1, R_2. C can be used to displace the phase of the voltage appearing across R_2.

a few hundredths of an ohm. To fulfil these three requirements together ($I = 100$ A, $R = 0{\cdot}01$ Ω, $L/R < 10^{-7}$, from which $L < 0{\cdot}001$ μH results) is extremely difficult and most probably impossible. The conditions in the other classical bridges are quite similar.

The Wilkinson and Carter Method[1]

The Wilkinson and Carter connection avoids the disadvantage of connecting the resistance in series with the object and uses a mutual inductance M (Fig. 3) instead. The mutual inductance transforms the object current i_L to a voltage U_M leading by 90°. With a lossless reactor L_x (with $R_x = 0$), this voltage is in phase with the applied voltage U and is compared with it by means of an ohmic divider R_1, R_2. If the reactor is not lossless, the phase of the voltage on R_2 is displaced by means of a capacitance C till a balance of the bridge is obtained. From these balancing conditions, which have not been thoroughly discussed here, the power factor can be determined

$$\cos\varphi = \frac{R_1^2\,\omega\,C}{R_1 + R_2} \qquad (4)$$

The main disadvantage of the Wilkinson and Carter circuit is the ohmic divider R_1, R_2. As can be easily seen, the high voltage cannot be coupled exactly according to phase by an ohmic divider. Considering, for example, an ohmic divider for 200 kV and limiting the power developed in it to 1000 W, the resultant value for the resistance R would be 40 MΩ. Since the impedance of the stray capacitance, which is in parallel, is of the same order of magnitude, such a divider is completely useless. These conditions could perhaps be improved by means of a controlled ohmic divider; it is, however, doubtful if it would be possible to construct a divider whose angular error is less than 1′.

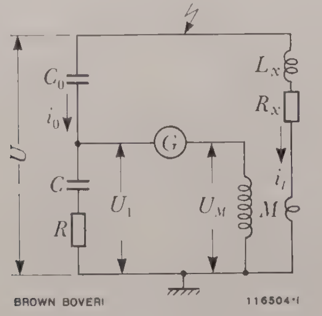

Fig. 4. – Bridge circuit with a capacitive divider C_0, C and a mutual inductance M for the measurement of the active losses of reactors

Note: Secondary voltage U_M of the mutual inductance M is proportional to the reactor current i_L; the voltage U drops across the capacitive divider C_0, C; R displaces the phase of the voltage U_1.

Bridge with Mutual Inductance and Standard Capacitor

A circuit which has been used for experimental purposes, avoids the ohmic divider and uses instead a capacitive divider (Fig. 4). C_0 is a lossless screened standard capacitor, as normally used for measurements with the Schering bridge, C a precision capacitance decade. The resistance R is used to displace the phase of the voltage across C till the bridge is balanced. As with the Wilkinson-Carter bridge, the reactor current i_L is transformed to a voltage U_M leading by 90° by means of a mutual inductance M. Fig. 5 shows the vector diagram of this bridge which, for the sake of clarity, has been divided into two parts. The balance conditions give the following with the notations from Fig. 4 and Fig. 5:

$$U_1 = i_0\left(R + \frac{1}{\mathrm{j}\,\omega\,C}\right) \approx U\,\mathrm{j}\,\omega\,C_0\left(R + \frac{1}{\mathrm{j}\,\omega\,C}\right) =$$

$$= U\left(\mathrm{j}\,\omega\,C_0\,R + \frac{C_0}{C}\right)$$

$$\cos\varphi \approx \tan\delta = \frac{\mathrm{Im}\,(U_1)}{\mathrm{Re}\,(U_1)} = \frac{\omega\,C_0\,R}{C_0/C} = \omega\,C\,R \qquad (5)$$

$$U_M = i_L\,.\,\mathrm{j}\,\omega\,M =$$

$$= \frac{U}{R_x + \mathrm{j}\,\omega\,L_x}\cdot\mathrm{j}\,\omega\,M = \frac{U}{R_x^2 + \omega^2\,L_x^2}\,(R_x - \mathrm{j}\,\omega\,L_x)\,\mathrm{j}\,\omega\,M \approx$$

$$\approx \frac{U}{\omega^2\,L_x^2}\,(\mathrm{j}\,\omega\,M\,R_x + \omega^2\,L_x\,M)$$

Comparison of the real parts of U_1 and U_M gives the expression for ωL_x

$$\frac{U}{\omega^2\,L_x^2}\,\omega^2\,L_x\,M = U\,\frac{C_0}{C}$$

$$\omega\,L_x = M\,\frac{C}{C_0} \qquad (6)$$

and further

$$R_x = \cos\varphi\,.\,\omega\,L_x = M\,\frac{\omega\,R\,C^2}{C_0} \qquad (7)$$

---

[1] K. J. R. Wilkinson and G. W. Carter: A method of measuring losses in reactors at low power factor. BEAMA Journ. 1939, Vol. 44, p. 145-50.

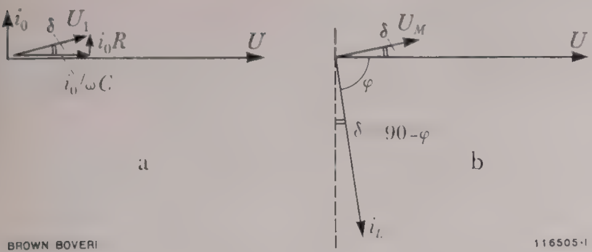

Fig. 5. – Vector diagram of the bridge with a capacitive divider and a mutual inductance

a: For the left-hand portion of the bridge
b: For the right-hand portion of the bridge
Notation as in Fig. 4.

The measurement with this bridge was in principle possible, but for present requirements it is not sufficiently accurate. The main reason for this was the transformation error of the phase angle of the mutual inductance, which is of the order of magnitude of 10′–30′. It may be possible to construct an air-cored mutual inductance which has a transformation error of less than 1′. Another disadvantage is the sensitivity of the mutual inductance to disturbances by external magnetic fields. This characteristic quality makes itself perceptible during measurements in test bays or power stations, where, in contrast to laboratory measurements, conductors carrying heavy currents may be in the vicinity. Further errors in measuring could arise as a result of a bad insulation resistance R_i of the screened cable (C_0-C). This resistance is in parallel to the capacitance C and causes a phase displacement $1/\omega R_iC$, thereby causing an error in the measurement. In order to keep the phase displacement due to the insulation resistance less than 1′, there must be an insulation resistance $R_i > 10^8\ \Omega$ for a capacitance $C = 0{\cdot}1\ \mu$F. This requirement is not always fulfilled by long test leads which are not quite new and could therefore lead to unmanageable errors in measurement.

A new bridge circuit has been found which avoids the disadvantages described above. This bridge will now be discussed.

The L_xR_x-Bridge with Current Transformer

Measuring Circuit and Vector Diagram

It appears almost natural, on the one hand, to apply the high voltage to the bridge by means of a compressed-gas capacitor and, on the other, the current by means of a current transformer, and compare them with each other according to their magnitude and phase.

The compressed-gas capacitor, as well as the current transformer, are extremely reliable elements and can be used for the most exact measurements. The dielectric of the capacitor consists only of gas and is therefore, for all practical purposes, free of losses. Its current leads the applied voltage by 90° minus less than 2″. By careful screening it is possible to obtain an exactly defined capacitance. Furthermore, the advantage of using the compressed-gas capacitor is borne out by the fact that it is a standard item of equipment of all high-voltage laboratories.

Today there are current transformers of great accuracy on the market which, for example, in a range of 5–200 % of the rated current, have a transformation error of less than 0·001 % and a phase angle error of less than 0·2′. Unlike the mutual inductance, as used in the circuits described under the previous two headings, the current transformer with its closed iron circuit is not exposed to the disturbing influences of external magnetic fields.

The advantages of the proposed coupling elements are pronounced. But considering that the phase angles of the currents i_0 and i_L are displaced from each other by almost 180° (Fig. 6b), it would at first seem impossible to balance the bridge. The L_xR_x bridge circuit in Fig. 7 with a current trans-

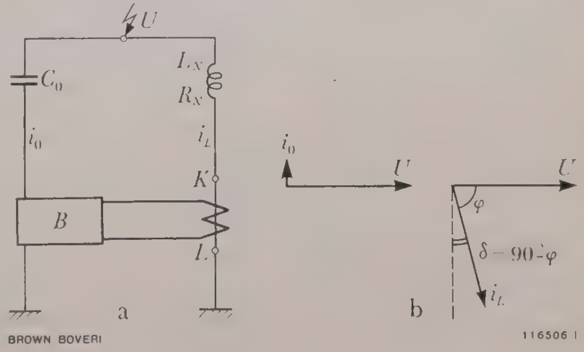

Fig. 6. – Bridge circuit with

a: voltage U coupled through the standard capacitor C_0 and the reactor current through a current transformer

L_x, R_x = Test object
B = Bridge

b: Vector diagram of ‘a’

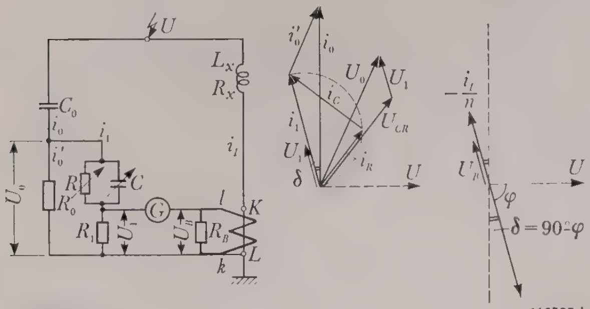

BROWN BOVERI 116507·I

Fig. 7. – L_xR_x bridge with current transformer

a: Circuit diagram
L_xR_x = Test object
$K-L$, $l-k$ = Current transformer with a transformation ratio n
R_B = Non-inductive resistance (burden)
R_0, R_1, R = Precision resistances
C = Precision capacitance
C_0 = Standard capacitor
G = Null galvanometer
i = Currents
U = Voltages

b: Vector diagram of 'a'

former shows, however, that by means of an artifice and a definite RC circuit, it is possible to make both vectors coincide.

The primary winding $K-L$ of a precision current transformer is in series with the reactor L_xR_x under test. The secondary winding of the current transformer is connected in such a way that the voltage appearing on its purely ohmic burden R_B is in phase opposition to the primary current i_L (see vector diagram Fig. 7b, right). The circuit R_0, R, R_1, C in the left-hand portion of the bridge results in the fact that the voltage U_1 appearing across the resistance R_1 leads the current flowing through the compressed-gas capacitor. The same effect would be obtained if the galvanometer were connected to a series-connected inductance-resistance in series with C_0. This apparently simple connection, however, is unfavourable from the measuring aspect, because an inductive element cannot be constructed so purely as resistive and capacitive elements and therefore its use as a comparison element in precision measurements is generally avoided. Since the impedance of the compressed-gas capacitor, i.e. about $3 \times 10^7\ \Omega$ ($C_0 = 100$ pF, frequency = 50 c/s) is several orders of magnitude greater than the impedance of the R_0, R, C, R_1 circuit (maximum 1000 Ω) the capacitor current i_0 leads the applied voltage U very accurately by 90°. The bridge is in balance when, by suitably adjusting the R, C values, the voltage U_1 leads the current i_0 by an angle δ. It is then possible to determine the angle $\delta = 90° - \varphi$, as well as the unknown quantities ω, L_x and R_x from the bridge data. These data, together with the reactor current i_L, found in a separate measurement, preferably with the same current transformer, supply the desired values of the active and reactive powers as well as the exact voltage during the measurement. That is:

Voltage $U = i_L \sqrt{R_x^2 + \omega^2 L_x^2} \approx i_L \omega L_x$

Reactive power ≈
≈ apparent power $Q = i_L^2 \sqrt{R_x^2 + \omega^2 L_x^2} \approx i_L^2 \omega L_x$

Active power $P = Q \cos\varphi$

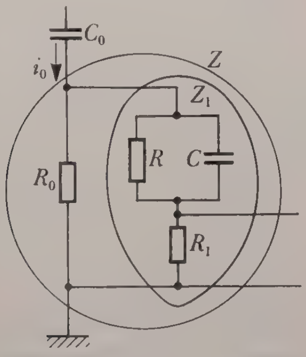

BROWN BOVERI 116508·I

Fig. 8. – Left-hand portion of the bridge in Fig. 7

Equivalent impedances Z_1 and Z. Other notation as in Fig. 7.

Requirements for a Balance

With the notation in Fig. 7 and Fig. 8 and by assuming $i_0 = U \cdot \mathrm{j}\omega C_0$, which is justified since $\frac{1}{\omega C_0} \gg Z$ for $C_0 < 1000$ pF, it follows that

$$U_1 = i_1 R_1 = \frac{i_0 Z}{Z_1} R_1 = U \mathrm{j} \omega C_0 \frac{Z}{Z_1} R_1$$

$$Z_1 = R_1 + \frac{R \dfrac{1}{\mathrm{j}\omega C}}{R + \dfrac{1}{\mathrm{j}\omega C}} = \frac{R_1 + R + \mathrm{j}\omega R R_1 C}{1 + \mathrm{j}\omega R C}$$

$$Z = \frac{R_0 Z_1}{R_0 + Z_1};$$

$$\frac{Z}{Z_1} = \frac{R_0}{R_0 + Z_1} = \frac{R_0 (1 + \mathrm{j}\omega R C)}{(R_0 + R_1 + R) + \mathrm{j}\omega C R (R_0 + R_1)}$$

$$U_1 = U \mathrm{j}\omega C_0 R_1 R_0 \frac{1 + \mathrm{j}\,\omega\, R\, C}{(R_0 + R_1 + R) + \mathrm{j}\,\omega\, C\, R\, (R_0 + R_1)}$$

The above expression, after a few transformations, yields:

$$U_1 = U \omega C_0 R_1 R_0 \frac{-\omega C R^2 + \mathrm{j}\,[(R_0 + R_1 + R) + \omega^2 C^2 R^2 (R_0 + R_1)]}{(R_0 + R_1 + R)^2 + \omega^2 C^2 R^2 (R_0 + R_1)^2} \tag{8}$$

When the bridge is balanced we have (see vector diagram Fig. 7b)

$$\frac{-\operatorname{Re}(U_1)}{\operatorname{Im}(U_1)} = \tan\delta =$$

$$= \omega\, R\, C \frac{R}{(R_0 + R_1)\,(1 + \omega^2 C^2 R^2) + R} \tag{9}$$

Since mostly $\omega^2 R^2 C^2 \ll 1$ (e.g. $\omega^2 R^2 C^2 < 0{\cdot}03$ for 50 c/s, $R < 500\ \Omega$ and $C < 1\ \mu\mathrm{F}$), we have in the majority of cases the approximate formula

$$\tan\delta \approx \omega\, R\, C \frac{R}{R_0 + R_1 + R} \tag{9a}$$

Since for small angles the approximation $\tan\delta \approx$ $\approx \sin\delta = \cos\varphi$ is valid, formula (9a) at the same time gives the power factor $\cos\varphi$. The relative error with this formula remains less than 1% up to about $\tan\delta \approx \cos\varphi = 0{\cdot}14$.

With larger values of $\tan\delta$, $\cos\varphi$ must be calculated according to formula (10).

$$\cos\varphi = \sin\delta = \frac{\tan\delta}{\sqrt{1 + \tan^2\delta}} \tag{10}$$

By considering the phase of U_1, the expression (9) was obtained for the power factor $\cos\varphi$. Further relationships can be derived from the identity of U_1 and U_B (when the bridge is balanced). With the notation in Fig. 7 we have

$$U_B = U_1$$

$$U_B = -\frac{i_L}{n} R_B = -\frac{U}{R_x + \mathrm{j}\,\omega\, L_x} \cdot \frac{1}{n} \cdot R_B$$

and with equation (8) for U_1:

$$-\frac{U}{R_x^2 + \omega^2 L_x^2}\,(R_x - \mathrm{j}\,\omega\, L_x)\,\frac{R_B}{n} =$$

$$= U\,\omega\, C_0\, R_1\, R_0 \frac{-\omega C R^2 + \mathrm{j}\,[(R_0 + R_1 + R) + \omega^2\, C^2 R^2\, (R_0 + R_1)]}{(R_0 + R_1 + R)^2 + \omega^2\, C^2\, R^2\, (R_0 + R_1)^2}$$

Equating the imaginary parts of both sides we get:

$$\frac{\omega\, L_x}{R_x^2 + \omega^2 L_x^2} \cdot \frac{R_B}{n} =$$

$$= \omega\, C_0\, R_1\, R_0 \frac{R_0 + R_1 + R + \omega^2\, C^2\, R^2\, (R_0 + R_1)}{(R_0 + R_1 + R)^2 + \omega^2\, C^2\, R^2\, (R_0 + R_1)^2}$$

By assuming $R_x \ll \omega L_x$ which for $\cos\varphi = 0{\cdot}1$ causes an error of less than 1%, and for $\cos\varphi = 0{\cdot}01$ an error of less than 0·01%, and with $\omega^2 C^2 R^2 \ll 1$ [according to equation (9)], we have

$$\omega\, L_x = \frac{R_B}{n} \cdot \frac{1}{\omega\, C_0} \cdot \frac{R_0 + R_1 + R}{R_0\, R_1} \tag{11}$$

The apparent resistance R_x can be calculated from equations (9a) and (11)

$$R_x = \omega L_x \cos\varphi \tag{12}$$

Further quantities in which we are interested can be derived from knowledge of the current i_L, which was obtained from a separate measurement:

Voltage $\quad U = i_L \sqrt{R_x^2 + \omega^2 L_x^2} \approx i_L \omega L_x \quad (13)$

Reactive power $\quad Q = i_L^2 \cdot \omega L_x \quad (14)$

Apparent power $\quad S = i_L^2 \sqrt{R_x^2 + \omega^2 L_x^2} \approx i_L^2 \omega L_x \quad (15)$

Active power $\quad P = S \cos\varphi = i_L^2 \omega L_x \cos\varphi \quad (16)$

Discussion of the Requirements for Balance

Considering the requirements for a balance—i.e. equations (9a) and (11)—it can be seen that, for given values of $\cos\varphi$ and L_x, the bridge can be balanced for infinite combinations of the triplet R_0, R_1, R. There are however minimum values for R_0 and R_1, as will be understood from the following. From equation (11) for a definite test object L_x and for definite current transformer data with the transformation ratio n, the burden R_B and the standard capacitor C_0, we have

$$\frac{R_0\, R_1}{R_0 + R_1 + R} = \frac{R_B}{n} \cdot \frac{1}{\omega\, C_0} \cdot \frac{1}{\omega\, L_x} = K = \text{const.} \tag{11a}$$

and further $\quad R = R_0 \left(\frac{R_1}{K} - 1\right) - R_1 \quad (17)$

Since R is a real, ohmic resistance and cannot be negative, two requirements follow from equation (17), namely

$$\frac{R_1}{K} > 1, \qquad \text{i.e.} \quad R_1 > K \tag{18}$$

and

$$R_0 \left(\frac{R_1}{K} - 1\right) > R_1 \quad \text{i.e.} \quad R_0 > \frac{R_1}{\frac{R_1}{K} - 1} = \frac{1}{\frac{1}{K} - \frac{1}{R_1}}$$

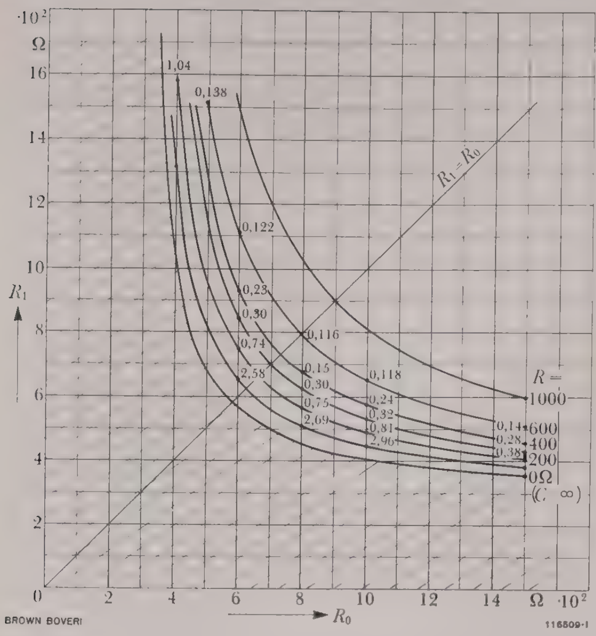

Fig. 9. – Family of curves illustrating the requirements for balancing the bridge in accordance with equation (17) for a reactor with the following data:

Reactive power $Q = 8000$ kVar, rated voltage $U = 275/\sqrt{3}$ kV. Bridge data with the notation in Fig. 7: $C_0 = 107{\cdot}6$ pF, $n = 10$, $R_B = 0{\cdot}3\ \Omega$. In the hatched portion, balance is not possible. The values noted are capacitances in μF as they would appear at bridge balance for $\cos\varphi = 0{\cdot}006$.

For $R_1 \rightarrow \infty$, R_0 tends towards a low limiting value, i.e.

$$\lim_{R_1 \rightarrow \infty} R_0 = K \tag{19}$$

Thus R_0, as well as R, must be greater than K, which was defined by equation (11a), otherwise the bridge cannot be balanced. Fig. 9 shows a family of curves which represent equation (17) for R as a function of R_0 and R_1. These curves were calculated for a special case with $K = 290\ \Omega$. It can be seen that the curves, for constant R, are equilateral hyperbolas and are displaced in the directions of abscissa and ordinate by K. Also plotted in the same graph are the relevant values for C as they would appear at bridge balance for $\cos\varphi = 6 \times 10^{-3}$. A customary capacitance decade with its condition $0{\cdot}1 < C < 1{\cdot}0$ μF, considerably reduces the range of selection of R_0 and R_1. Also, for practical reasons, R_0 as well as R_1 should be as low as possible, since only then is the influence of the parasitic capacitances negligibly small.

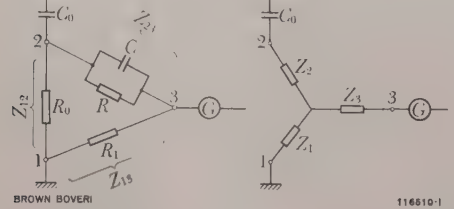

Fig. 10. – L_xR_x bridge with a current transformer

a: Left-hand portion with notation as in Fig. 7

b: Equivalent star connection of 'a'

Equivalent Bridge Circuit

The left-hand side of the bridge circuit in Fig. 7a represents in reality a delta connection of R_0, R_1, R, C. Let us now consider this delta connection transformed into an equivalent star connection (Fig. 10).

The general formulae for the delta/star transformation are (notation from Fig. 10):

$$Z_1 = \frac{Z_{12}\,Z_{13}}{Z_{12} + Z_{23} + Z_{13}}\ ; \qquad Z_2 = \frac{Z_{23}\,Z_{12}}{Z_{12} + Z_{23} + Z_{13}}\ ;$$

$$Z_3 = \frac{Z_{23}\,Z_{13}}{Z_{12} + Z_{23} + Z_{13}}$$

In the present case the impedances Z_{12}, Z_{23} and Z_{13} may be expressed as follows:

$$Z_{12} = R_0\ ; \qquad Z_{23} = \frac{R}{1 + \mathrm{j}\,\omega\,C\,R}\ ; \qquad Z_{13} = R_1$$

The insertion of these values in the general formulae, after a long calculation, finally gives:

$$Z_1 = \frac{R_0\,R_1}{R + R_0 + R_1} + \mathrm{j}\,\omega\,\frac{C\,R^2\,R_0\,R_1}{(R + R_0 + R_1)^2} = R' + \mathrm{j}\,\omega\,L' \tag{20}$$

$$Z_2 = \frac{R_0\,R}{R + R_0 + R_1} + \frac{1}{\mathrm{j}\,\omega\,\dfrac{(R_0 + R_1 + R)^2}{\omega^2\,C\,R\,(R_0 + R_1)\,R_0\,R}} = R'' + \frac{1}{\mathrm{j}\,\omega\,C''} \tag{21}$$

$$Z_3 = \frac{R_1\,R}{R + R_0 + R_1} + \frac{1}{\mathrm{j}\,\omega\,\dfrac{(R_0 + R_1 + R)^2}{\omega^2\,C\,R\,(R_0 + R_1)\,R_1\,R}} = R''' + \frac{1}{\mathrm{j}\,\omega\,C'''} \tag{22}$$

It can be seen that Z_1 represents the series connection of an ohmic resistance with an inductance, whilst Z_2 and Z_3 constitute the series connection of an ohmic resistance with a capacitance. Further, the current transformer, which is on the right-hand side of the bridge in Fig. 7a, is connected in such a way that across the burden R_B a voltage drop occurs which is in phase opposition to its primary current. The current transformer with its burden R_B can be treated mathematically as a negative resistance amounting to $-\frac{R_B}{n}$.

When the delta/star transformation is considered and the current transformer with its burden R_B is replaced by the negative resistance $-\frac{R_B}{n}$, the bridge circuit in Fig. 7a is transformed into the equivalent bridge circuit in Fig. 11. Further neglecting R'', $1/j\omega C''$ and $1/j\omega C'''$ which are several orders of magnitude smaller than the impedances connected in series with them, we obtain the simplified circuit diagram in Fig. 12. It can now be seen that the delta connection of the resistive and capacitive elements R_0, R_1, R, C exercises the same function as the series connection L', R' in the equivalent circuit. The advantages of resistances and capacitances as measurement elements in this way are so significant compared with inductances, that it would not be worth while to use an LR circuit in reality. The series resistance R''' reduces the sensitivity of the bridge galvanometer and therefore should be kept as small as possible. Besides, considering that

$$R' = \frac{R_0\,R_1}{R_0 + R_1 + R} = K = \text{constant} \qquad (11a)$$

the condition $R''' =$ minimum becomes synonymous with $\frac{R'''}{R'} =$ minimum. But R'''/R' is given by

$$\frac{R'''}{R'} = \frac{R_1\,R}{R_0 + R_1 + R} \cdot \frac{R_0 + R_1 + R}{R_0\,R_1} = \frac{R}{R_0} \qquad (23)$$

At a definite value of R, the value of R_0 should be large, that is it should lie in the right-hand portion of the curves in Fig. 9.

Measuring Errors and Correction Formulae

Measuring errors with earthed bridge screen

In order to eliminate the influence of the earth capacitances, the lead between the standard capacitor and the bridge is screened and the screen brought to the potential of the bridge corner. This is attained, as usual with other bridges, either by means of a voltage regulator or with an auxiliary bridge composed of R, L, C elements. Under certain circumstances, however, it is permissible to earth the bridge screen. This has the advantage of producing a balance much more quickly, since the process of alter-

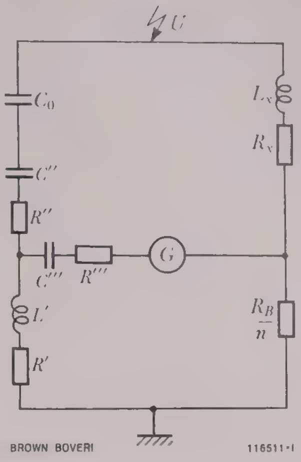

Fig. 11. – Equivalent circuit of the L_xR_x bridge with a current transformer

The primed quantities are equivalent impedances resulting from the delta/star transformation of the left-hand portion of the bridge according to Fig. 8; R_B/n is the transformed resistance of the current transformer.

L_x, R_x = Test object
C_0 = Standard capacitor
G = Null galvanometer

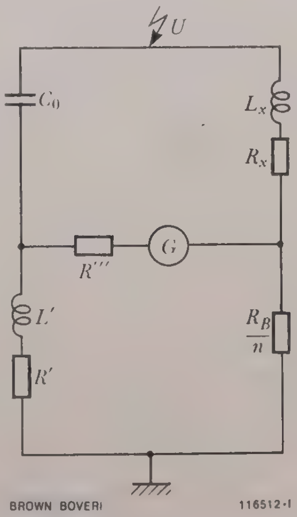

Fig. 12. – Simplified equivalent circuit of the bridge in Fig. 11

Notation as in Fig. 11.

nately balancing the bridge–screen–bridge–screen and so on, is eliminated. The earthed screen is particularly favourable with small capacitances between high voltage and screen, where this is particularly unstable. With an earthed screen the errors are consciously accepted. Their magnitude can be calculated, and with particularly accurate measurements they can be taken into consideration.

The error with an earthed shield will now be calculated. A method will also be shown for keeping this error small.

The phase relationship between the voltage U_1 and the voltage U is $180° - \varphi$ (Fig. 7b); further below, U_1 is calculated and the result compared with formulae (8) and (9a), respectively. The parasitic capacitance of the bridge corner (lead) is denoted by C'.

With the notation in Fig. 13 we have

$$U_1 = U \mathrm{j} \omega C_0 \frac{Z_2}{Z_1 + Z_2} R_1 =$$

$$= U \mathrm{j} \omega C_0 R_1 \frac{\dfrac{R_0}{1 + \mathrm{j} \omega C' R_0}}{\dfrac{R_0}{1 + \mathrm{j} \omega C' R_0} + \dfrac{R_1 + R + \mathrm{j} \omega R R_1 C}{1 + \mathrm{j} \omega C R}}$$

After a few conversions and with A denoting a real constant, it follows that

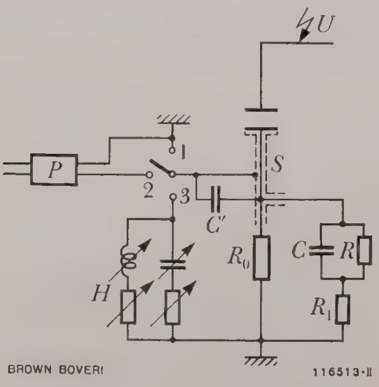

Fig. 13. – Left-hand portion of the bridge with different screening conditions

Switch position 1: Screen (S) earthed
Position 2: Screen regulated by a voltage regulator (P)
Position 3: Screen regulated by an auxiliary bridge (H) according to Beldi[2]
C' = Capacitance between the lead (bridge corner) and screen
C_0, C, R, R_0, R_1 = Bridge elements

$$U_1 =$$

$$= A \mathrm{j} \left[R_0 + R_1 + R + \omega^2 C R (C R R_0 + C R R_1 + C' R_0 R_1 + C' R_0 R) + \right.$$

$$\left. + \mathrm{j} \omega C R (R_0 + R_1 + R) - \mathrm{j} \omega (C R R_0 + C R R_1 + C' R_0 R_1 + C' R_0 R)\right]$$

and for $\tan \delta = \cos \varphi$

$$\cos \varphi = \frac{-\operatorname{Re}(U_1)}{\operatorname{Im}(U_1)} =$$

$$= \frac{\omega C R^2 - \omega C' R_0 (R_1 + R)}{R + (R_0 + R_1)(1 + \omega^2 C^2 R^2) + \omega^2 C C' R R_0 (R_1 + R)} \tag{24}$$

By assuming $\omega^2 C^2 R^2 \ll 1$, $\omega^2 C C' R R_0 \ll 1$, expression (24) simplifies itself to

$$\cos \varphi = \frac{\omega C R^2}{R_0 + R_1 + R} - \frac{\omega C' R_0 (R_0 + R)}{R_0 + R_1 + R} =$$

$$= (\cos \varphi)' - \frac{\omega C' R_0 (R_0 + R)}{R_0 + R_1 + R} \tag{25}$$

Therefore the use of the formula

$$(\cos \varphi)' = \frac{\omega C R^2}{R_0 + R_1 + R} \tag{9a}$$

gives too large a value, so that the second term of (25) has to be subtracted in order to arrive at the correct value of $\cos \varphi$.

The relative error of the measurement with an earthed screen is accordingly

$$\Delta = \frac{\cos \varphi - (\cos \varphi)'}{(\cos \varphi)'} =$$

$$= - \frac{\omega C' R_0 (R_0 + R)}{R_0 + R_1 + R} \cdot \frac{R_0 + R_1 + R}{\omega C R^2}$$

With $\omega C R^2 = (R_0 + R_1 + R)(\cos \varphi)'$ from equation (9a), and the notation $K = \dfrac{R_0 R_1}{R_0 + R_1 + R}$ used earlier, we finally arrive at

$$\Delta = - \frac{\omega C' (R_0 R_1 + R_0 R)}{(R_0 + R_1 + R)(\cos \varphi)'} =$$

$$= - \frac{\omega C'}{(\cos \varphi)'} \cdot \frac{R_0 R_1}{(R_0 + R_1 + R)} \left(1 + \frac{R}{R_1}\right) =$$

$$= - \frac{\omega C'}{(\cos \varphi)'} \cdot K \left(1 + \frac{R}{R_1}\right) \tag{26}$$

The formula (26) is very important. With its help it is possible to determine whether to measure with the screen earthed or to regulate its potential.

---

[2] See F. BELDI: Eine Hochspannungsbrücke für Verlustmessungen an Isolierstoffen. Bull. schweiz. elektrotech. Ver. 1930, Vol. 21, p. 197.

Example of the application of formula (26)

The bridge data are $K = 300\ \Omega$, $R = 300\ \Omega$, $R_1 = 600\ \Omega$; the expected power factor $\cos\varphi = 5 \times 10^{-3}$, and the capacitance lead-to-screen $C' = 4500$ pF, which corresponds to a normal cable between the standard capacitor and the bridge.

The relative error to be expected with these data is

$$\Delta = -\frac{\omega C'}{(\cos\varphi)'} \cdot K\left(1 + \frac{R}{R_1}\right) = \\ = \frac{314 . 4{\cdot}5 . 10^{-9}}{5 . 10^{-3}} \cdot 300\left(1 + \frac{300}{600}\right) = \\ = 0{\cdot}125 \text{ or } 12{\cdot}5\,\%$$

Thus in this case, either the corrected formula (25) for the calculation of $\cos\varphi$ must be used or the potential of the screen must be regulated.

On order that the screen may be solidly earthed, and to attain the advantages resulting from it in the majority of cases, a special low-capacitance lead was made from polyethylene insulated high-frequency cable and used during the measurement. The screen capacitance for a length of 6 metres amounts to only 600 pF.

Exact formula for cos φ with a large capacitance C_0 of the standard capacitor

A compressed-gas capacitor of 100 pF is mostly used as C_0 (Fig. 7a). Its impedance of $3 \times 10^7\ \Omega$ at 50 c/s is several orders of magnitude higher than the resistance of a few hundred ohms connected in series with it, so that the current flowing through this series connection leads the main voltage U by exactly 90°. The formula (9) for the measured power factor $\cos\varphi$ was derived from this supposition. If, however, C_0 is much larger (e.g. when using a standard capacitor of 10 000 pF), errors arise from the formulae (9) and (9a), respectively. This error is now calculated.

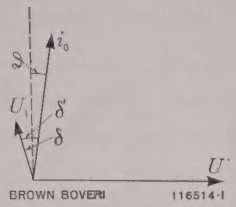

Fig. 14. – Vector diagram taking into consideration the phase angle of i_0

δ' = Measured angle
δ = Desired angle
ϑ = Error angle

Other notation as in Fig. 7.

With the notation in Fig. 7a we obtain the vector diagram in Fig. 14, where the phase angle of the current through C_0 has been taken into consideration. The formula (9a)

$$\tan\delta' = \omega R C \frac{R}{R_0 + R_1 + R}$$

gives us the angle δ' between i_0 and U_1; ϑ denotes the deviation of the angle of the current i_0 from a current which leads the voltage U by 90°. The phase angle wanted is δ, or $90 - \delta = \varphi$ (see also vector diagram in Fig. 6b right). From Fig. 14 we find $\delta = \delta' - \vartheta$ and for small angles of δ, δ', ϑ with sufficient accuracy

$$\cos\varphi = \tan\delta = \tan\delta' - \tan\vartheta \qquad (27)$$

Considering the formulae (9a) and

$$\tan\vartheta = \omega C_0 \frac{R_0 (R_1 + R)}{R_0 + R_1 + R} \qquad (28)$$

we obtain

$$\cos\varphi = \omega C R \frac{R}{R_0 + R_1 + R} - \omega C_0 \frac{R_0 (R_1 + R)}{R_0 + R_1 + R} = \\ = \frac{\omega C R^2}{R_0 + R_1 + R}\left(1 - \frac{C_0 R_0 (R_1 + R)}{C R^2}\right) \qquad (29)$$

The relative error, consequent upon assuming that the current i_0 leads the voltage U by exactly 90°, i.e. when the formula (9a) is used, is accordingly

$$\Delta = \frac{C_0 R_0 (R_1 + R_2)}{C R^2} \approx \frac{C_0}{C} \qquad (30)$$

since R_0, R_1, R are of the same order of magnitude. In order to minimize the effect of the stray capacitances, C is made more than 0·1 μF. Then

$$\Delta\,\% < \frac{C_0}{10^{-7}} \cdot 10^2 = C_0 \cdot 10^9 \qquad (30a)$$

Therefore with

$C_0 =$ 100 pF $\quad \Delta <$ 0·1%
$C_0 =$ 1 000 pF $\quad \Delta <$ 1 %
$C_0 =$ 10 000 pF $\quad \Delta <$ 10 %

Conclusion: If the capacitance of the standard capacitor $C_0 > 1000$ pF, the formula (29) must be used instead of formula (9a).

Measured Results

The active losses of different objects were measured by means of the new bridge circuit. The current transformer used for these measurements was a portable precision transformer type 4731 from the firm Tettex, Zurich, with an angular error of less than 1′, while the purely ohmic burden R_B was a precision resistance of 0·3 Ω. A vibration galvanometer served as the detector.

The measured results for a 275-kV shunt reactor with a reactive power rating of 8000 kVar is given here as an example. At the highest measuring voltage of 157·4 kV, the current was 51·6 A; from this we obtain a reactive power of 8120 kVar. The bridge data at balance were $R_0 = 800\ \Omega$, $R = 283\ \Omega$, $R_1 = 620\ \Omega$, and $C = 0{\cdot}37\ \mu F$. From these data the power factor $\cos\varphi$ is calculated according to formula (9a) as follows:

$$\cos\varphi = \omega R C \frac{R}{R_0 + R_1 + R} =$$

$$= 314 \,.\, 283 \,.\, 0{\cdot}37 \,.\, 10^{-6} \frac{283}{1703} = 0{\cdot}00545$$

The use of the formula (9a) instead of the complicated formula (9) is permissible, since

$$\omega^2 R^2 C^2 = (314)^2 \times (0{\cdot}37 \times 10^{-6})^2 (283)^2 \approx 10^{-3} \ll 1.$$

The error caused by the earthed screen of the bridge is calculated according to formula (26):

$$\Delta = \frac{\omega C'}{(\cos\varphi)'} \cdot K \left(1 + \frac{R}{R_1}\right) =$$

$$= \frac{314 \,.\, 0{\cdot}6 \,.\, 10^{-9}}{5{\cdot}45 \,.\, 10^{-3}} \cdot 290 \left(1 + \frac{283}{620}\right) =$$

$$= 1{\cdot}4 \,.\, 10^{-2}, \text{ that is } 1{\cdot}4\%$$

Included in the above calculation is the screen capacity C' of 600 pF and the factor K where

$$K = \frac{R_0 R_1}{R_0 + R_1 + R} = \frac{800 \,.\, 620}{800 + 620 + 283} = 290$$

The corrected value for $\cos\varphi$ is thus

$$\cos\varphi = 0{\cdot}00545 (1 - \Delta) = 0{\cdot}00538$$

The active losses are consequently

$$P = S \,.\, \cos\varphi = 8120 \,.\, 0{\cdot}00538 = 43{\cdot}7 \text{ kW}$$

The impedance of the reactor, according to formula (11) (with $n = 10$ and $C_0 = 107{\cdot}6$ pF) is:

$$\omega L_x = \frac{R_B}{n} \cdot \frac{1}{\omega C_0} \cdot \frac{R_0 + R_1 + R}{R_0 R_1} =$$

$$= \frac{0{\cdot}3}{10} \cdot \frac{10^{12}}{314 \,.\, 107{\cdot}6} \cdot \frac{1}{290} = 3050\ \Omega$$

The influence of the earthed screen on the results was examined experimentally by means of previous measurements at reduced voltage. In the process, the screen capacitance was artificially altered by means of capacitors connected in parallel. The results corresponded exactly to the theoretically derived formula (26). The time necessary to balance the bridge with earthed screen amounted to only 50 seconds.

Conclusion

The new process described here allows the active power to be precisely measured in cases where the usual wattmeter method fails. This method can be used with available elements up to highest known service voltages and the heaviest currents (e.g. 500 kV and 150 A or more). The $L_x R_x$ bridge with a current transformer was developed expressly for the measurement of the active losses of reactors. But it can also be used advantageously for the measurement of impedance, phase displacement and active power at very small inductive power factors $(0{\cdot}001 < \cos\varphi < 0{\cdot}1)$.

(CR) F. DEUTSCH

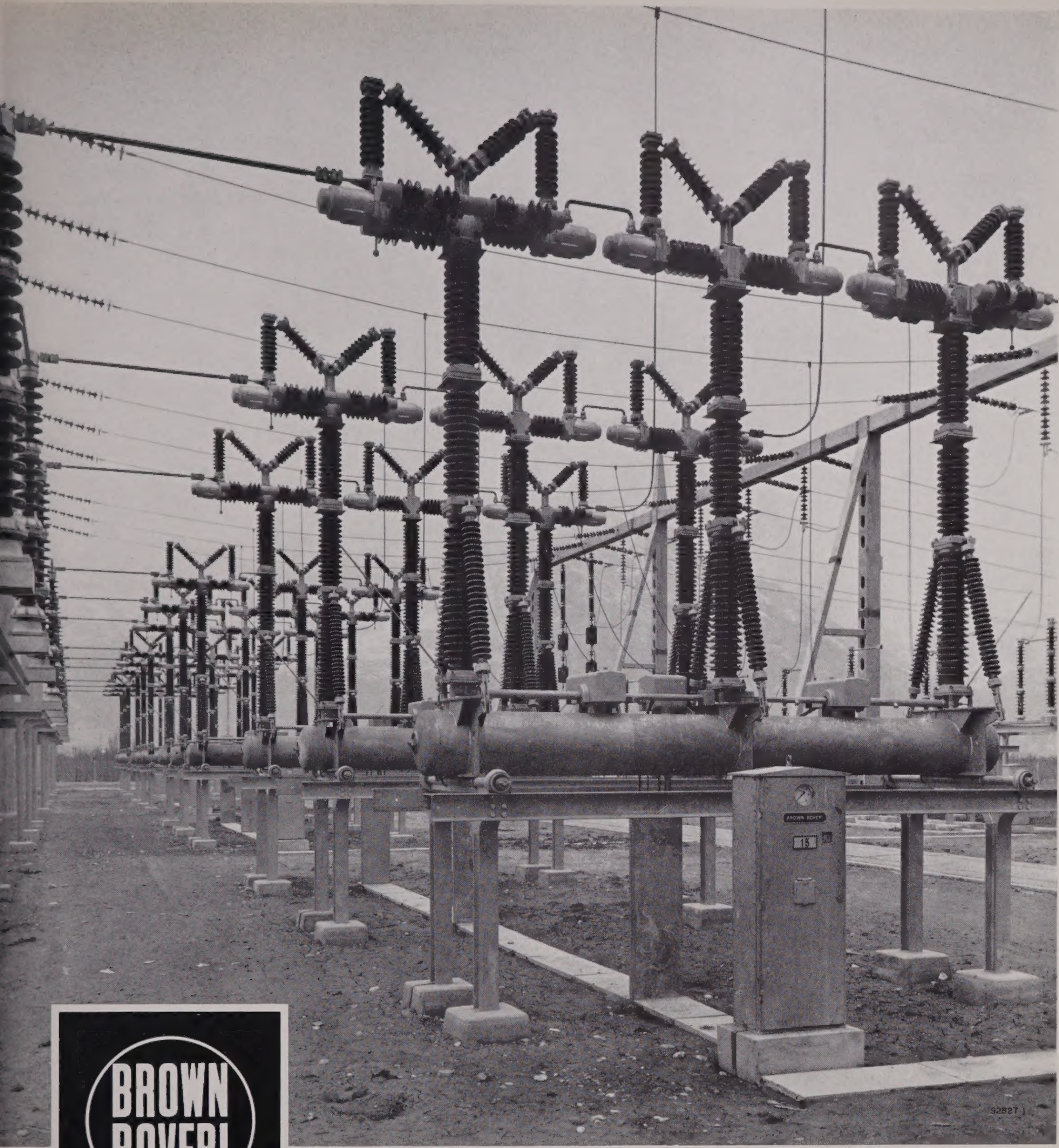

220-kV airblast breakers in the switchyard at Riddes of the Mauvoisin Power Co., Sion (Switzerland)

BROWN BOVERI

AIRBLAST CIRCUIT-BREAKERS

in conjunction with our dependable quick-acting relays protect power systems against breakdowns and atmospheric disturbances. They are noteworthy for their freedom from restriking when interrupting lines at no-load and capacitive currents.

BROWN
BOVERI

Published by Brown, Boveri & Company, Limited, Baden, Switzerland. Printed by Kreis & Co. AG., Basle, Switzerland
Obtainable direct from the publishers